Master Thesis in Geosciences

Geodetic mass balance of Svalbard glaciers: 1936 – 2004

Christopher Nuth

UNIVERSITY OF OSLO

FACULTY OF MATHEMATICS AND NATURAL SCIENCES

Blank page, for double side paper print.

Remove for digital publishing

Geodetic mass balance of Svalbard glaciers: 1936 – 2004

Christopher Nuth

Master Thesis in Geosciences

Discipline: Physical Geography, Hydrology, and Geomatics

Department of Geosciences

Faculty of Mathematics and Natural Sciences

UNIVERSITY OF OSLO

December 1, 2006

Tutor(s): Jack Kohler (Norsk Polarinstitutt) & Jon Ove Hagen (UiO)

This work is published digitally through DUO – Digitale Utgivelser ved UiO

http://www.duo.uio.no

It is also catalogued in BIBSYS (http://www.bibsys.no/english)

Cover picture: The front of Hansbreen, taken in April, 2006.

Table of Contents

Abstract

Glaciers and ice masses are very important components of the earth system both in terms of global water storage and as climate indicators. The amount of water tied up in glaciers and ice caps is equivalent to about 69 meters of sea-level (Church and others, 2001). Recent predictions from global climate models indicate the arctic will experience enhanced changes as compared to the lower latitudes linked to the rise of greenhouse gases in the next 100 years (ACIA report, 2005). Svalbard glaciers and ice masses may therefore experience a rapid response to a change in climate (Hagen and others, 2003a). It is thus beneficial to document both present and the long term past glacier fluctuations to increase the comprehension of climatic changes.

Svalbard is a high arctic archipelago, located in a climatically sensitive area at the northern extremity of the warm North Atlantic ocean current. Approximately 36000 km^2 is covered by glaciers consisting of ice caps, tidewater, outlet, and smaller cirque and piedmont glaciers (Hagen and others, 1993). In this study, a 54 year geodetic balance of Svalbard glaciers is derived by comparing the oldest topographic map series of Svalbard (1936/38) to modern digital elevation models (DEM) from 1990. The errors of the older maps are assessed where precision is limited, but accuracy is sufficient for glacier studies. Elevation changes are analyzed for 7 regions in Svalbard (~5000 km^2), where significant thinning was found at glacier fronts, and elevation increases in the upper parts of the accumulation areas. All regions experience volume losses and negative geodetic balances, although regional variability exists relating to both climate and topography. Many surges are apparent within the elevation change maps. Estimated volume change for the regions is -1.59±0.07 km^3a^{-1} (ice eq.) for a geodetic annual balance of -0.30 m a^{-1} (w. eq.), and the glaciated area has decreased by 16% in the 54 year time interval.

For recent balance estimations, differential GPS (2004) and laser altimetry (1996 & 2002) measurements are compared to the 1990 DEM over four glaciers in northwest Svalbard, and along two 60 km profiles in southern Svalbard. For both regions, the rate of frontal thinning has increased dramatically. The annual geodetic balances have become twice as negative for two smaller glaciers, Midtre and Austre Lovenbreen, while becoming more than three times more negative on the larger Kongsvegen. In southern Svalbard, while the glacier fronts are thinning faster in these recent measurements, complex dynamic behavior is occurring at higher altitudes, which complicate the elevation change signal. A number of dynamical events occurred in Wedel Jarlsberg Land between 1990 and 1996.

The glaciers of Svalbard are losing ice volume at a faster rate more recently which can be attributed to a changing climate. The large scale synoptic patterns in atmospheric and oceanic circulation, and possibly temporal changes associate with them, is leading to increased thinning at the glacier fronts and slight increases at higher altitudes. Climate change is not only affecting glacier surface change in the form of temperature, but also in the form of precipitation. These changes progress through the glacier creating complicated dynamic patterns. Nonetheless, the present glacial-climate signal is that of increased volume loss.

Chapter 1

Introduction and background

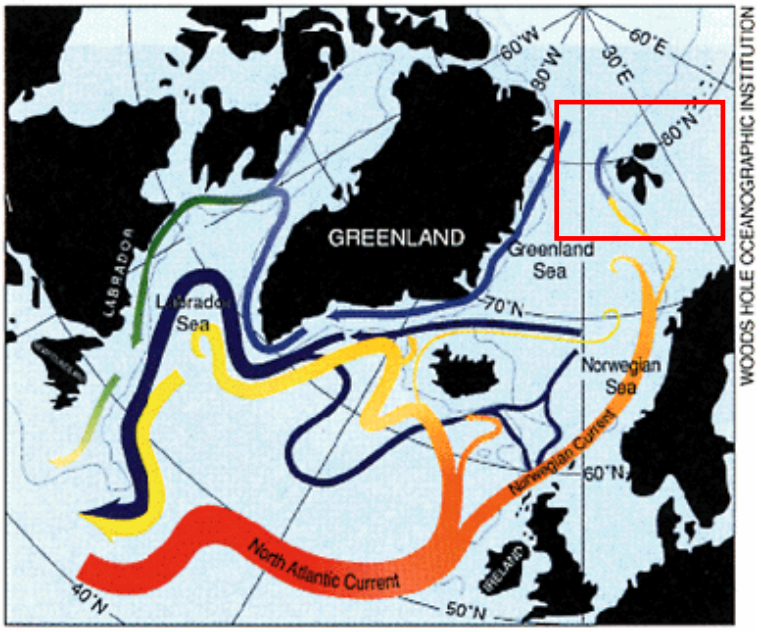

Cover Picture: Location of Svalbard (red box) showing the major ocean currents responsible for transport of energy and heat to the arctic. (© Woods Hole Oceanographic Institute)

Introduction

Ice covers approximately 10% of the earth's surface (Paterson, 1994) where 2 million km^2 of glaciers are located in the northern hemisphere arctic, 275000 km^2 excluding Greenland (Dowdeswell and others, 1997). The amount of water tied up in glaciers and ice caps is equivalent to about 69 meters of sea-level (Church and others, 2001). While Antarctica and Greenland represent the majority of this water reservoir (61.1 and 7.2 m sea level, respectively), the smaller glaciers and ice caps represent only 0.5 meters (Dyurgerov and Meier, 1997a). Nonetheless, it is the small glaciers and ice caps that are becoming increasingly important to sea-level rise in shorter time scales (Church and others, 2001). Global climate models predict that the Arctic will experience enhanced changes as compared to lower latitudes in response to increasing greenhouse gas concentrations (ACIA report, 2005). Arctic ice masses are therefore expected to show a rapid response, and present an early indication, of climate change (Hagen and others, 2003a).

Glaciers are long term indicators of climate as their presence is a function of both precipitation and temperature (i.e. accumulation and ablation). The mass balance is the change in water storage of a glacier reservoir, typically measured on an annual or seasonal interval. A long term variation of the mass balance is a signal of the immediate climate over the particular time period for which measurements are available. The response of a glacier terminus to a change in climate, however, is not instantaneous as is the mass balance; a time lag exists while surface changes are transferred through to the glacier front (Johannesson and others, 1989). The terminus position of a glacier thus represents a weighted mean of the longer term past climate over a defined time length, past which no memory of a former climate exists (Johannesson and others, 1989). Glacial advance and retreat are reactions to the long term climatic trends of the geographic locality whereas the mass balance is the short term climatic forcing upon the glacier.

Glacier mass balance, in addition to being a present-day indicator of climate, is a method in determining the present glacial contributions to sea-level rise. Mass balance measurements measure the seasonal and/or annual changes in the water equivalent mass of a glacier. Mass balance measurement programs exist on only a handful of glaciers that are biased towards the smaller ice masses (<20 km^2). Few records exist longer than 20 years (Dowdeswell and others, 1997). Therefore, to estimate the contribution of glaciers to sea level rise, Dyurgerov and Meier (1997a, 1997b) were forced to spatially extrapolated the limited dataset of mass balances over the area composed of smaller glaciers (all areas excluding Greenland and Antarctica). Recently, with increased technological advancements in the realms of remote sensing and aerial altimetry, the extent of glacier change has been more easily documented through elevation changes. To fill in the missing data associated with Alaska glaciers (Dyurgerov and Meier, 1997a), Arendt and others (2002) estimated the mass change of Alaska glaciers through elevation changes from 67 glaciers. In addition, the uncertainty in the mass balance of the Greenland ice sheet is decreasing as elevation change studies over the entire ice sheet are becoming more prevalent through aerial and satellite altimetry (i.e. Davis and others, 1998; Krabill and others, 1999, 2000; Paterson and Reeh, 2001);

The relevance of glacier elevation change studies lies in the increased ability to extract mass balance data over large areas and to provide a greater spatial assessment of glacier changes from the recent past climate. This chapter will introduce some basic glaciology and terminology relevant for elevation change studies, and further describe the mass balance as determined *in situ*

(the *traditional* balance), and determined by elevation comparison (the *geodetic* balance). The objectives, located at the end of this chapter, present an overview of the theme and goals of the manuscript.

Basic glaciology and definitions

Glaciers are commonly classified into three basic types, *temperate, sub-polar,* and *polar*, but numerous variations within these classes exist (Paterson, 1994). A glacier generally consists of two zones, ablation and accumulation. The *ablation* (melting) zone is the area where all of the previous winters' snowfall plus underlying ice is eliminated by summer melting. The *accumulation* area occurs at higher elevations where snow survives through the summer season. In some regions, the accumulation zone contains an additional two zones, the *percolation* zone and the *wet snow* zone. Surface melting occurs in the percolation zone when the temperature of the upper layers is raised above 0°C. Melt-water produced percolates to deeper layers where it can refreeze (called internal accumulation), intensifying the densification of snow and firn. The refreezing of water releases enough energy to increase the temperature of the surrounding snow pack. The wet snow zone begins at a point where the temperature of all the snow deposited from the previous winter has been raised above 0°C. Many arctic glaciers, especially in Svalbard, have a region where the refrozen meltwater creates *superimposed ice*, which occurs between the wet snow zone and the ablation area.

The division between the accumulation and the ablation zone is determined by the snow line at the end of the summer, commonly referred to as the equilibrium line altitude (ELA). The ELA in glaciers that contain superimposed ice is defined by the division between the superimposed ice zone and the ablation area. If the ELA can be determined, the accumulation area ratio (AAR) (the accumulation area divided by the total glacier area) is a useful ratio for indicating mass balance variation (Paterson, 1994).

The state of a glacier is inferred through the mass balance or the change in the ice reservoir through the balance year (typically denoted by the end of the summer season). The *traditional* approach estimates the seasonal or annual ice mass or loss through stake and snow-pit measurements in the field. Summer and winter balances combine to form the annual net balance, which summed through time, creates the cumulative net balance (Paterson, 1994). The *geodetic* approach towards mass balance estimation involves determining the elevation and area changes

of a glacier (from maps and profiles) over a longer time scale resulting in an estimate of the three dimensional volume change. The *traditional* cumulative mass balance theoretically is equivalent to the *geodetic* balance if the time periods are identical.

Traditional mass balance

The *traditional* mass balance, sometimes called the *glaciological* balance, is defined as the budget of inputs (accumulation) and outputs (ablation) in the ice storage of a glacier reservoir. Generally, a stake network is drilled into the glacier where ablation is measured in late summer by the additional length of the exposed stake compared to the previous year. Accumulation is similarly measured at the end of the winter season from snow probing and stake heights. The specific mass balance ($\dot{b}$) refers to an individual point balance on the glacier (Hagen and Reeh, 2004). The specific net mass balance is the sum of accumulation and ablation at a point (or area) throughout the balance year, typically 1 year,

$$\dot{b}_n = \dot{b}_s + \dot{b}_w \qquad [1]$$

where b_n, b_s, and b_w is the net, summer, and winter balances, respectively. A relationship often exists between balance and altitude, such that summer, winter, and net specific mass balance terms can be plotted as a curve (Oerlemans and Hoogendorrn, 1989; Østrem and Brugman, 1991). In many instances, regression curves can be fit to the data to increase the sample size (Lliboutry, 1974; Fountain and Vecchia, 1999).

The total net balance (V) refers to the integration (or summation) of the specific mass balances over the glacier surface (Paterson, 1994; Hagen and Reeh, 2004) and results in a volume mass change of the glacier.

$$\Delta V = \sum_i (\dot{b}_i \cdot A_i) \qquad [2]$$

where $\dot{b}$ is the point measurements, A is glacier area (relative to the previous summer surface (Paterson, 1994)), and i is the representative elevation bin. As this term is much confused in the literature, the total net balance will be referred to as a volume change since it is the three-dimensional quantity of the mass balance. The average net balance is then the change in mass per unit area (Paterson, 1994):

$$B = \frac{\Delta V}{A} \qquad [3]$$

The area should be defined as the area at the end of the balance year (Paterson, 1994), though an average of the areas (if available) is a more representative quantity (Elseberg and others, 2001).

The number of stakes required for mass balance estimation depends upon the particular glacier although much debate exists. In cases such as Storglaciären in northern Sweden, an elaborate stake network exists providing full spatial representation of the glacier surface (Jansson, 1999). However, this type of program requires a great deal of time and money to maintain, and thus stake networks have been generally limited to the centre line. Some studies infer that the amount of stakes can be limited to less than five (Fountain and Vecchia, 1999) where even one stake located at the ELA may be sufficient enough for regional extrapolation of mass balances (Rasmussen, 2004; Rasmussen and Andreassen, 2005).

The relationship between the specific mass balance and an elevation change is the important link between mass balance and dynamics in relation to climate. The elevation change at the surface is a function of the mass balance plus the emergence/submergence ice fluxes:

$$\frac{dh}{dt} = \dot{b} + \frac{dq_x}{dx} + \frac{dq_y}{dy} \qquad [4]$$

where h is elevation, $\dot{b}$ is the net specific mass balance, q_i are the ice fluxes in the x and y directions (Paterson, 1994). Assuming steady state, the flux terms theoretically cancel when integrated over the glacier surface. Glaciers are rarely in steady state where the magnitude of the terms is important. This relationship is the foundation for deriving mass balances through a geodetic approach, and further, for better understanding mass balances and dynamics in a climatic context.

Geodetic mass balance

An alternative to the *traditional* approach in determining the total net mass balance of a glacier or glacier area is through elevation changes. A *geodetic* approach measures the cumulative ice volume change from topographic area and elevation data (map comparison). The geodetic approach has recently evolved with the advancement of digital technologies, photogrammetric methods, satellites, aerial altimetry, global positioning systems, and geo-information systems. Automatic photogrammetric methods decrease the time required for map creation from photographs and increase the accuracy and precision of the data. A greater number of maps can be produced, over a larger area, in a shorter amount of time. In addition, the

acquisition of glacier elevations via satellite and laser altimetry has significantly increased the spatial and temporal coverage of elevation changes. Therefore, the geodetic approach is used to create a larger spatial scale estimate of glacier mass balances (i.e. Krabill and others, 2000; Arendt and others, 2002), confirm traditional mass balance estimates (Haakenson, 1986; Krimmel, 1989; Cox and March, 2004), and generate a greater understanding of glacier stability, dynamics, and response times in relation to climate (Harrison and others, 2001; Elseberg and others, 2001; Melvold and Hagen, 1998; Hagen and others, 2005).

The method of geodetic balance estimation was introduced in the early fifties by Finsterwalder (1954) who translated the decrease in area between adjacent contours into average elevation changes through trigonometry. The approach inherently contained a hypsometric (area-elevation distribution) averaging scheme and provided the original basis for determining volume changes and mass balances from map comparison. More recently, while repeated glacier mapping was being incorporated for hydrological water power management (Østrem, 1986), Haakensen (1986) introduced the gridded geodetic method. A grid of elevation change points created through linear interpolation, converted into volume changes by simply multiplying the elevation changes by the grid size and summing over the glacier surface. Good agreement existed between estimates using Finsterwalder's hypsometric area method and the gridding method while little variation was found between the geodetic balance and the traditional balance confirming the actual mass balance as estimated from the two independent approaches (Haakensen, 1986).

Krimmel (1989) compared the traditional balance to the geodetic balance using similar methods as Haakensen (1986). Discrepancies were found where the geodetic balance was more negative than the traditional balance due to the use of assuming constant density for the geodetic volume changes, or from a systematic error in the traditional balances. Later, Krimmel (1999) performed a similar study using five re-created DEMs where the same systematic difference between the geodetic and traditional balances occurred. Krimmel concluded that errors in the traditional mass balance could be systematic, and errors with the geodetic method could result from either poor photogrammetry and/or the use of a constant density for water equivalence conversion. Andreassen (1999) similarly found that the geodetic mass balance was more negative than the traditional balance which was attributed to either faulty maps in the accumulation area, or systematic errors within the traditional balance. A larger study of 7 glaciers on the mainland Norway found good coherency between geodetic and traditional

balances although variations existed from glacier to glacier (Andreassen and others, 2002). Østrem and Haakensen (1999) found large discrepancy in a comparison of one maritime glacier, where greater emphasis was placed into the systematic errors associated with the traditional approach rather than the geodetic approach as systematic errors were easier to control in map comparison.

More recently, on the same glacier as in the studies by Krimmel (1989, 1999), Elseberg and others (2001) proposed that using outdated maps for area integration in the traditional balance calculation will lead to a systematic error that increases with time. Thus, the geodetic method was used to adjust the cumulative traditional balance. Cox and March (2004) emphasized that the traditional method is ideal for annual measurements, while the geodetic method is more appropriate for the long-term. The errors for a geodetic balance are less time-dependent; i.e the errors do not systematically accumulate through time as is the case with annual traditional measurements.

Converting elevation changes to volume and mass balance depend upon the type of data sets used as well as the method chosen. The *hypsometric* method is defined by the conversion of altitudinal average elevation changes (*dz*) into volume changes through multiplication by the corresponding altitude bin areas (*A*) and summation over the glacier surface:

$$dV = \sum_i dz_i \cdot A_i \qquad [5]$$

Finsterwalder (1954) determined *dz* through contour and area change comparison though more recently *dz* is determined by averaging elevation change points or pixels over a given altitude bin (Sapiano and others, 1998; Arendt and others, 2002). The area used in the volume change estimate must be that of the largest glacier area (Finsterwalder, 1954; Echelmeyer and others, 1996; Arendt and others, 2002). This method, similar to the traditional balance method, assumes a point, or collection of points, is representative for a given altitude bin.

An alternative approach, the *grid* method has evolved with increased availability of DEMs. The gridding method is defined mathematically through pixel summation (Etzelmüller and others, 1993):

$$dV = {l_p}^2 \sum_A (h_{i1} - h_{i2}) \qquad [6]$$

Here, the volume change is determined by summation of elevation changes for each pixel (h_{i1}-h_{i2}) over the glacier surface multiplied by the pixel area (l_p^2).

In both methods, the volume changes are converted into mean elevation changes ($\overline{dh}/dt$) for the whole glacier, or the geodetic balance (*B*), by division of the average area ($\overline{A}$) from the two map dates (Finsterwalder, 1954; Echelmeyer and others, 1996; Arendt and others, 2002):

$$\frac{\overline{dh}}{dt} = B = \frac{dV}{\overline{A}} \qquad [7]$$

When presented in water equivalent units, the *geodetic* balance has been empirically shown to be similar to the traditional mass balance (Haakensen, 1986: Krimmel 1989, 1999: Andreassen, 1999; Andreassen and others, 2002; Cox and March, 2004).

The conversion from ice to water equivalent is essential if geodetic balances are to be compared to traditional balances. Assuming a density equivalent to ice (0.9 kg m^{-2}) requires that the density profile of the firn remain constant through time (Bader, 1954). The assumption is generally true for the ablation area but is much weaker for the transition area between the accumulation and ablation zones where the transient ELA is significantly different in the two map dates. Krimmel (1989) used varying densities for firn and ice weighted by the percentage of area associated with both, although difficulty arises as the variable density relies on the traditional measurements resulting in an inter-dependency of the two methods (Krimmel, 1999). Sapiano and others (1998) used a smaller density (0.85 kg m^{-2}) derived by weighting the percentage of areas associated with ablation, accumulation, and firn. The effect of that conversion factor was found smaller then the effect of error within the seasonal correction (explained below), and thus has little influence on the overall elevation changes measured.

A seasonal adjustment parameter is used to account for the fact that elevation maps are created on different dates, not exactly corresponding with the end of the summer season. Between these two dates, additional elevation changes can occur due to ablation or emergence. Generally, these adjustments are dependent upon the traditional mass balance measurements (Cox and March, 2004) which create an additional inter dependency between the methods. An adjustment for ablation has been defined through analysis of snowdepths (Sapiano and others, 1998), through temperature/ablation models (Andreassen, 1999), or through degree day modelling (Cox and March, 2004). Emergence corrections do not affect the cumulative geodetic balance greatly (Cox and March, 2004) as it simply is a redistribution of mass through the glacier, however, may be useful when comparing DEMs with laser and GPS profiles over a short time interval (i.e. <5 years).

Svalbard climate and glaciers

Svalbard is a high arctic archipelago located between 74° - 81° N latitude and 10° - 35° E longitude (cover picture, pg 1). The climate is warmer than other areas at the same latitude due to general air circulation patterns as well as being located at the tail end of the North Atlantic Drift where one part of the warm water current flows into the Fram Strait between West Svalbard and East Greenland (Hagen and others, 1993). Weather in the arctic is dominated by semi-permanent patterns of high and low pressures (Serreze and Barry, 1988; Serreze and others, 1993) that are typically more dominant in winter on Svalbard (Humlum and others, 2003). Climate on Svalbard is variable, with winter rain and summer snow not uncommon. The dominant weather patters are low pressures from the southwest bringing warm air or high pressures from the northeast with cold dry air (Hagen and others, 1993; Humlum and others, 2003).

Svalbard has been ascribed with a high climatic sensitivity (Houghton and others, 2001), probably due to the intense coupling between climate and sea-ice extent, as well as with atmospheric and oceanic circulation systems (Humlum, 2002, 2003). Temperature has been generally warming since the early 1900s (Nordli and Kohler, 2003). Precipitation gradients exist across Svalbard, with maritime climatic conditions on the coasts leading to thicker snow packs than the central regions (Winther and others, 1998; Sand and others, 2003). Generally, the east coast experiences 40% more winter precipitation than the west coasts while accumulation rates in the south are twice as high as those in the north (Sand and others, 2003).

Svalbard has a land area of ~63,000 km^2 with about 60% (36600 km^2) covered by glaciers (Hagen and others, 1993). The majority of glaciers on Svalbard consist of larger ice masses divided into individual outlet glaciers by mountain ridges, but there are also several ice caps, and numerous cirque and piedmont glaciers (Hagen and others, 1993). Svalbard glaciers are generally polythermal (sub-polar), that is, characterized by a cold ice layer overlying a warm ice layer. The majority of glaciers in Svalbard have been retreating the past 100 years, with occasional surge advances (Liestøl, 1988; Hagen and others, 2003b).

Two small glaciers near Ny Ålesund (78°55'N, 11°56'E), Midtre Lovenbreen and Austre Brøggerbreen (~5 km^2), are the sites of the longest high-arctic mass balance data series (*traditional*) starting from 1967 and 1968, respectively. Both glaciers have experienced, almost exclusively, negative mass balances through the record (Hagen and Liestøl, 1990). Winter

precipitation and summer temperature show the greatest correlation to the net mass balance (Lefauconnier and Hagen, 1990; Lefauconnier and others, 1999). In 1987, a mass balance program was initiated on the larger Kongsvegen, a more representative glacier in size for the rest of Svalbard (Hagen and others, 1999). In addition, mass balance has been measured on ten other glaciers for different periods within the last 50 years (Hagen and others, 2003a). By combining all these records together with mean annual accumulation rates derived through ice cores on the major ice caps of Spitsbergen (Pinglot and others, 1999; 2003), and Austfonna (Pinglot and others, 2003), the mass balance for the entire archipelago was estimated to be between -0.12 (Hagen and other 2003a) and -0.27 ma^{-1} w. eq. (Hagen and other 2003b).

Many glaciers on Svalbard are categorized as being of the surge-type (Liestøl, 1969) although the exact percentage estimate varies from 13% (Jiskoot and others, 1998) to 36% (Hamilton and Dowdeswell, 1996), to as high as 90% (Lefauconnier and Hagen, 1991). In a non-surge glacier, accumulation is balanced by the ice flux to the ablation area, maintaining a steady-state surface profile (see Eq. 4). In a surging glacier, however, the ice flux is too low to maintain a steady-state surface profile, such that the slope of the glacier surface increases with time (Lefauconnier and Hagen, 1991). Glacier surge is then characterised by sudden increases of ice velocity (up to 10 times the normal speed) resulting in a shift of ice from the accumulation area to the ablation area followed by an advance of the front (Lefauconnier and Hagen, 1991). The relatively short surge phase (~1-10 years) is followed by a long quiescent phase (~30-100 years) where the glacier remains dormant with minimal ice fluxes while it rebuilds the surface profile. While surging is thought to be independent of climatic variations, the length of the quiescent phase and the frequency of glacier surging may be climatically controlled (Dowdeswell and others, 1995; Hagen and others, 2003b)

The controls and mechanisms of glacier surging is not completely understood, but a few different mechanisms have been proposed. A pioneer study of Variegated glacier in Alaska led Kamb (1987) to link the surge event to changes in the basal hydrology of the glacier. The proposed model explains the surge phenomenon by a hydrological switch from separated tunnel conduit systems to a linked-cavity conduit system (Kamb, 1987). Icelandic glaciers are preferentially fed with basal water through subglacier eruptions. These events significantly correlate to surge events emphasizing the role of increased basal water in glacier surging in Iceland (Björnsson, 1998).

Surging on Svalbard, however, has different characteristics than surges from Alaska and Iceland (Murray and others, 2003). Hamilton and Dowdeswell (1996) infer that a non-random geographical distribution exists within the populations of surging glaciers which may be a 'local reflection of a global pattern'. The incidence of surging in Svalbard has been tied statistically to geometric parameters (i.e. length, slope, AAR), lithological parameters (i.e. the underlying bedrock consistence), and to the presence of internal reflection horizons (which infer polythermal layering) (Hamilton and Dowdeswell, 1996; Jiskoot and others, 2000). In general though, climate is not thought to influence the incidence of surging on Svalbard. Only Dowdeswell and others (1995) propose that negative mass balances may be decreasing the frequency of surging and lengthening the quiescent phase time interval.

Objectives

Svalbard is affected from both the warm north Atlantic current and cold arctic high pressure systems. For this reason, Svalbard may be an important indicator for future climate change, and while present glacier changes should be described, it is also important to document glacier change as far back in time as possible. Although Svalbard contains a small amount of water in the global perspective, it is thought that these smaller glaciers will be the greatest contributor to sea level rise in the next hundred years (ACIA Report, 2005).

In this study, glacier elevation changes are estimated by comparing the oldest topographic map series of Svalbard from 1936/38(Norsk Polarinstitutt), modern DEMs (1990 and 1995), differential GPS profiles (2005), and NASA altimetry profiles (Bamber and others, 2005). Methods are assessed to show the strength of a geodetic approach and advantages of using it to understand glacier mass balance and volume change in relation to climate.

The Norwegian Polar Institute mapped Svalbard after the war through high oblique aerial photographs from 1936/38 resulting in 100 meter contour maps at a scale of 1:100000. A major effort to re-map Svalbard is ongoing since 1995 where Digital Elevation Models (20 meter pixel resolution) are being created from 1990 vertical photographs (1:50000). These two data forms provide the baseline datasets from which glacier changes are derived in this study.

The objectives of this study are to:

- Assess the feasibility of using high oblique aerial photographs for glacier elevation change studies, and quantify the accuracy of the 1936/38 topographic map series of Svalbard (*Chapter 2*).
- Estimate long term volume changes over northwest, central, and south Svalbard and provide an estimate of the recent contribution of the relevant regions to sea level change. (*Chapter 3*)
- Estimate modern elevation and volume changes in context of the long term changes and further assess the climatic and dynamic influences which complicate the glacier surface history (*Chapter 4*).
- Provide a general understanding of the methods, accuracies, and assumptions associated with geodetically derived elevation and volume changes and discuss implications in the understanding of climate and glacier dynamics on Svalbard.

Chapter 2:

The 1936/38 topographical map series of Svalbard: accuracy and errors

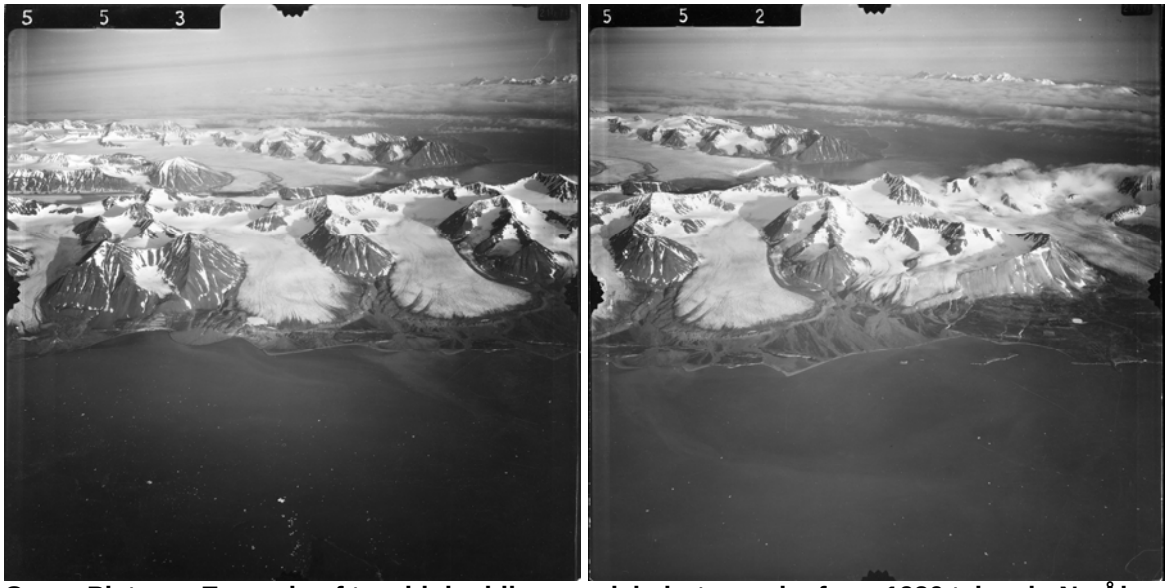

Cover Picture: **Example of two high oblique aerial photographs from 1936 taken in Ny Ålesund. Midtre Lovenbreen is shown from two angles. (©Norsk Polarinstitutt)**

Introduction

Pre 1950s topographical maps were typically created from oblique aerial photographs analyzed manually on a photogrammetric workstation. Oblique aerial photographs are of two types: *high-oblique* where the horizon is visible and *low-oblique* which does not have a visible horizon (Cambell, 2002). High-oblique photography was popular for the time as large areas could be mapped easily with satisfactory precision (Wolf, 1983). However, the drastic scale changes from foreground to background in oblique images complicates measurements of distances, areas, and elevations (Cambell, 2002). Additionally, a considerable amount of reliability is dependent upon the skill of the photogrammetrist when assembling topographic maps through manual photogrammetry.

The accuracy of older topographic maps is highly dependent upon the quality and quantity of ground control points (GCP). Before the launch of the global positioning system (GPS), GCPs were difficult to acquire; the accuracy of each individual point was dependent upon its neighbors due to the triangulation procedure used for positioning. Inaccurate GCPs are probably the single most detrimental factor for older topographic maps in glacier elevation

change studies. Generally, the large scale biases affecting old topographic maps derive from GCP errors.

Increases in computing power and digital technology have evolved photogrammety into an automated process. The ease of acquiring aerial surveys decreased flying heights for photography increasing the resolution of imagery. Additionally, the use of vertical photography limited scale distortion inherent within oblique photography. Nonetheless, the accuracy in modern photogrammetry is still dependent upon the number and accuracy of GCPs though this is aided by precision and efficiency of the Global Positioning System (GPS). Modern photogrammetry brings about an alternative to analyzing older maps, whereby images can be re-compiled within an automatic workstation. Through LIDAR altimetry, the number of ground control points can be exponentially increased (James et al, 2006) removing the problem of datum coherency. Nonetheless, over large spatial areas, the photogrammetry is still time-consuming, and as in the case of the 1936/38 topographic maps, would take years to complete.

The accuracy and error of a volume change estimate is similar to the accuracies of the maps used and the coherency between their geodetic referencing systems. Similarly, it is dependent upon the quality (i.e. clarity of the atmosphere) and scale (flying height) of the photographs, the contrast available within the images (i.e. whether fresh snow is present), the precision and quantity of GCPs, and skill of the photogrammetrist (Østrem and Haakensen, 1999; Andreassen, 1999). The best alternative in using older photos is to re-create maps using modern digital systems (Krimmel, 1999; Cox and March, 2004; James and others, 2006), although the accuracy through manual photogrammetry (old topographic maps) is usually sufficient enough for glacier studies (Østrem, 1986; Echelmeyer and others, 1996; Arendt and others, 2002).

An essential criterion for map comparison is that the datums and reference systems be consistent. Many methods exist for transforming the reference systems of maps; most result in accuracies greater than ±5-10 meters in the horizontal (Appendix A.1). However, in some instances the datums contain orthogonal plane differences that are difficult to recognize (Cox and March, 2004). One technique to assure datum coherency is to examine the surrounding land topography, assuming the land has not changed elevation. It may be necessary to only compare bedrock (non-glacier) elevations with similar slopes to the glacier (Echelmeyer and others, 1996).

Approach

The accuracy of the 1936/38 topographic map series of Svalbard is assessed by comparing non-glacier land area to a modern DEM from 1990. We assume that the majority of errors derive from the 1936/38 map, since it is based on high oblique photography with lower quality and the higher flying height, and therefore take the 1990 DEM as the more reliable of the two epochs. When analyzing non-glacier point elevation differences for deriving glacier error estimates, the non-glacier point statistics must properly represent elevation data over glaciers. Point populations of non-glacier elevation differences is abbreviated as ΔZ_L throughout the text and refers to the vertical error associated between the maps.

The goals of this chapter are to:

- Analyze potential variables affecting elevation accuracy.
- Quantify random and systematic errors associated with the 1936/38 topographic map series of Svalbard.
- Statistically represent glacial elevation accuracy through the population of non-glacier elevation difference points (ΔZ_L)

Independent Variables

The first step in understanding map elevation errors is to analyze potential variables that contribute to these errors using the population of non-glacier elevation difference points (ΔZ_L). The 1990 DEM is taken as truth (although errors do exist, unrelated to the 1936/38 map errors); all errors are assumed to derive from the 1936/38 map. The independent variables chosen correspond to both the surface topography and aerial photography:

- *Elevation* –To determine if a bias exists between the errors and 1990 elevations.
- *Slope* – Geolocation (horizontal) errors translate into elevation errors where the magnitude of the elevation error depends on the tangent of the surface slope.
- *Aspect* – To determine if any translational errors exist between the maps. Translation refers to the existence of a spatial shift between the maps; related to errors in the ground control. This variable, however, may be influence by the flight lines and look directions of the photographs.

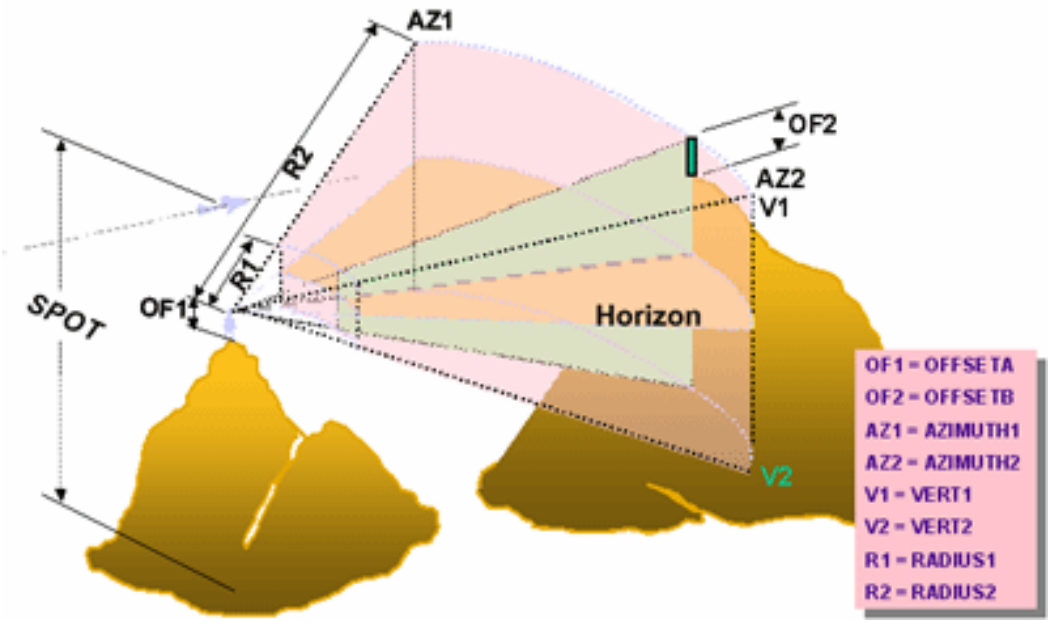

Fig. 1: Visual display of the Viewshed function and required parameters (©Esri ArcGIS).

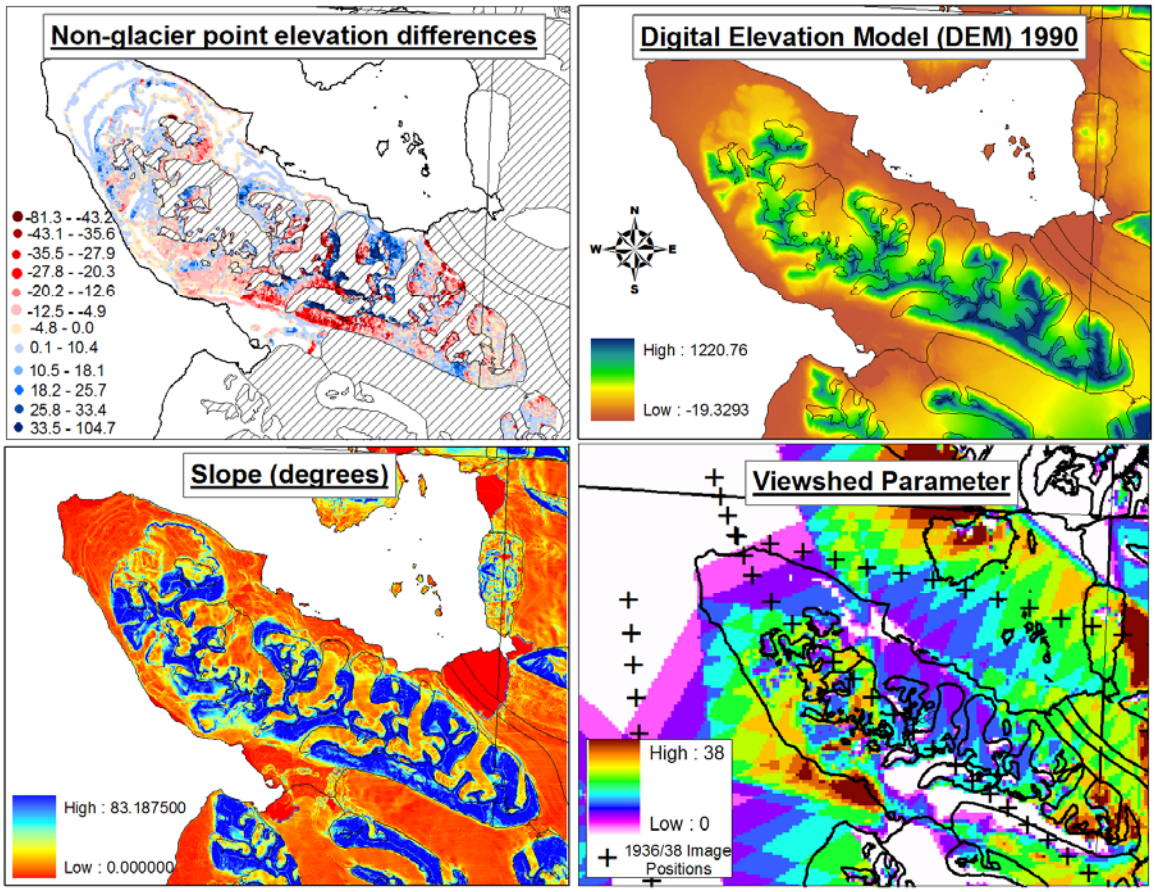

Fig. 2: Subset of the sample error population (ΔZ_L) chosen for the statistical analysis (top left), along with three of the predictor variables: 1990 DEM elevation (top right), slope (bottom left), and Viewshed (bottom right).

- *Distance to 1936/38 oblique photograph positions* – To determine whether the varying spatial scale inherent in high-oblique aerial photographs has an affect on elevation accuracy since precision deceases with pixel resolution.
- *Viewshed* – (Esri ArcGIS) is a function that takes a DEM and a number of 'observer' points to create a map in which pixels represent the number of observer points that are viewable. The importance of viewshed is that at least 2 images are required to derive accurate elevations from oblique aerial photographs where mountain shadowing becomes a significant component. A viewshed analysis of the 1936 aerial survey is created by digitizing the 1936(38) image positions and analyzing them against the 1990 DEM. Seven parameters are associated with each point describing the area each image can view (Fig. 1). *Azimuth1* and *Azimuth2* are the horizontal viewing angles (0-360 degrees) of the image, set to a width of 40 degrees. *Vert1* and *Vert2* describe the vertical angles of the image, determined to be 0 and -35 degrees for the oblique aerial photographs. A search *Radius* of 15 km is used; i.e. the function will not analyze areas outside a 15 km radius from the viewpoint. This parameter was decided by visual inspection of the images where areas further than 15 km are thought to contain a resolution incapable of resolving accurate topography (also found through comparison with known non-visible areas). Lastly, *offset A* is the flying height set at 3000 m.a.s.l. A visual description of the parameters is shown in Fig. 1, where results of the Viewshed analysis on the 1936/38 aerial survey of Svalbard is shown in Fig. 2 and in Fig. 1 of chapter 3.

A subset of non-glacier elevation difference points (ΔZ_L) were selected to analyze the predictor variables: elevation, slope, aspect, viewshed, distance to photo. The sample population is from northwest Svalbard (Fig. 2) as this region consists of photos from numerous directions, giving a reasonable representation of the aerial survey coverage of Svalbard.

To identify which predictor variables require further analysis, a matrix scatter plot of all variables is provided in Fig. 3. Vertical errors (ΔZ_L) show slight relations with elevation, slope, and viewshed. Complex patterns are present between ΔZ_L with distance to photo and aspect. However, a fundamental statistical assumption of homoscedasticity is not satisfied within the populations of ΔZ_L, and collinearity exists between the independent variables, making multivariate statistics, regression analysis, and interpretation difficult.

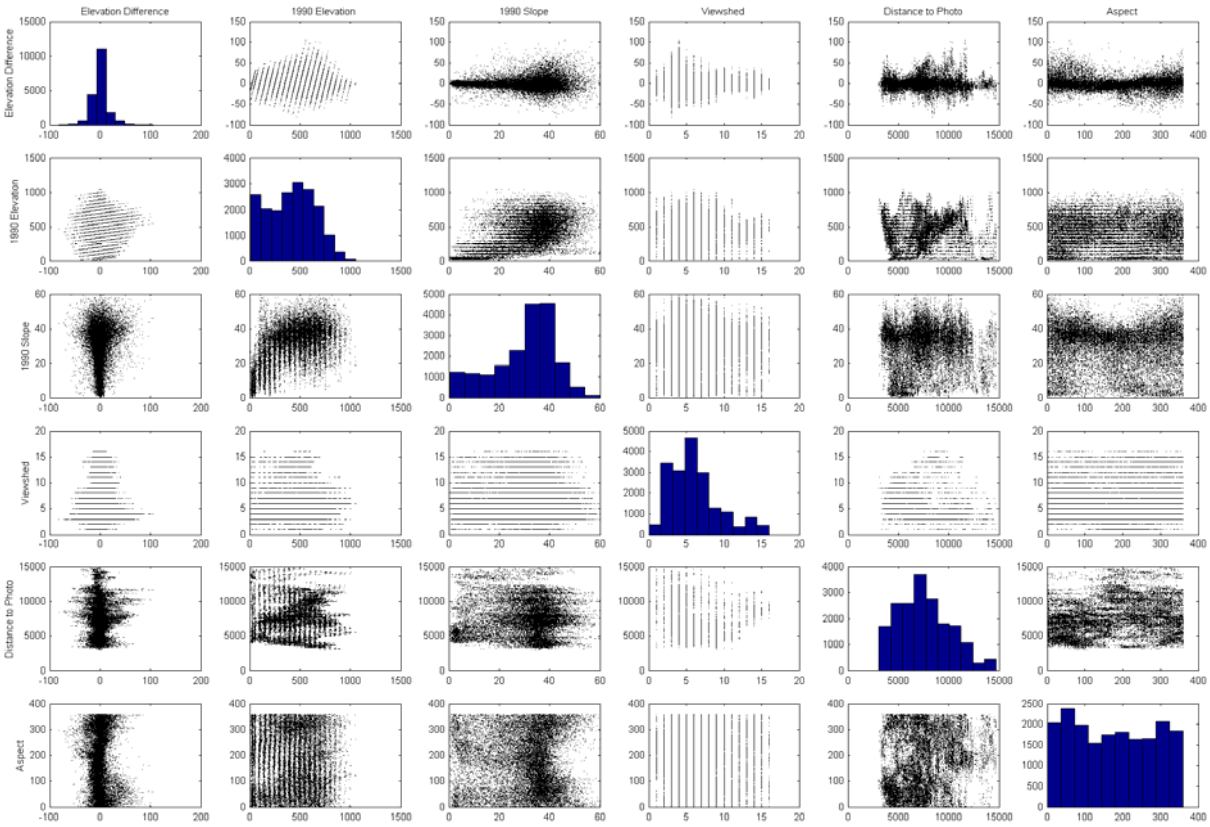

Fig. 3: Matrix scatter plot for ΔZ_L, 1990 elevation, 1990 slope, viewshed, distance to photo, and aspect.

The assumption of *Homoscedasicity* states that the variance of the dependent variable is the same for all independent variables (Kleinbaum and others, 1998). Heteroscedasticity is a characteristic of the dependent variable, elevation error (ΔZ_L), as it inherently contains a distribution centered about a mean of zero. Any relation between ΔZ_L and an independent variable will be slightly masked, and only apparent through a changing variance of ΔZ_L with the independent variable. A clear example is the plots of ΔZ_L vs. slope and viewshed (Fig. 4) where the variance of the errors increases with slope and decreases for the viewshed parameter. Biases are present if the means of ΔZ_L differs greatly from zero.

Collinearity describes the relationships of the independent variables to each other (Kleinbaum and others, 1998) and makes the relation between the independent variables with ΔZ_L difficult to determine. For example, slope shows a slight relation with elevation whereby low elevations generally contain slopes less than 20 degrees and high elevations contain slopes greater than 20 degrees (Fig. 3). It is apparent that the DEM and the slope maps are visually similar (Fig. 2). In addition, points visible in 10 images or more (viewshed)

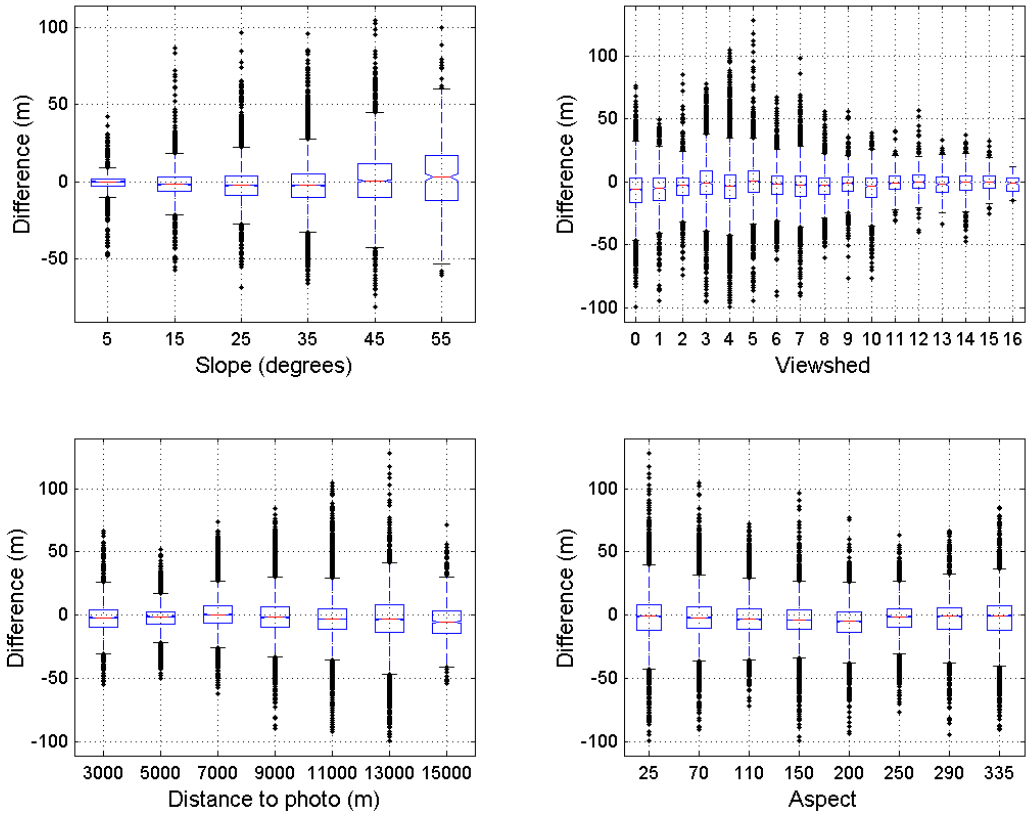

Fig. 4: Box and whisker plots of the elevation difference ΔZ_L (y-axis) against four independent variables (x-axis): slope (top-left), Viewshed (top right), Distance to photograph (bottom left), and aspect (bottom right). The box has lines at the lower quartile, median, and upper quartile values which represent 50% of the data. The whiskers display the extent of the rest of the data. Outliers are plotted as points. The notches represent the uncertainty about the means.

are restricted to elevations lower than ~500 meters altitude (Fig. 3). Therefore, the slight relation between ΔZ_L and 1990 elevation is probably an artifact of the relation between ΔZ_L with slope and the viewshed parameter.

Fig. 4 shows more detailed box and whisker plots of ΔZ_L vs the independent variables: slope, viewshed, distance to photo, and aspect. As mentioned earlier, the relation between ΔZ_L with slope is apparent as the boxes (inter quartile range: IQR) and whiskers (2x the standard deviation) increase with increasing slope. Similarly, the boxes and whiskers for ΔZ_L decrease with increasing viewshed. The entire IQR for viewshed values of zero and one are negative inferring a bias for ΔZ_L where less than 2 images are visible; i.e. the 1936 map is too high. The predictor variables "distance to photo" and aspect show little relation with ΔZ_L although small trends exist. Aspect seems to be a random component of ΔZ_L though a small bias exists for aspects between 150 and 200 degrees. This pattern is probably the result of the direction of the particular flight lines and is difficult to account for due to the large number of

outliers. A complex pattern exists between ΔZ_L and distance to photo; no specific relation can be discerned. It seems a negative bias exists for points at a distance of ~15 km from the photograph position although the point population is spatially limited.

In summary, two predictor variables, slope and viewshed, are related to the non-glacial point elevation differences, ΔZ_L. Geolocation errors, or horizontal errors, translate into vertical errors by multiplying by the tangent of the slope and thus elevation error increases with increasing slope. A result of the viewshed analysis is that areas with greater aerial coverage (viewshed>10) are associated with the smallest ΔZ_L inferring the greatest accuracy. In addition, ΔZ_L with viewshed values equal to 0 - 2 experience negative biases. The spatial distribution of areas with large ΔZ_L and areas where viewshed is zero correspond significantly (Fig. 2). Areas not visible in any of the 1936/38 images are clearly covered by contour points that were 'schematically' placed simply for the completion of the map.

Large random variability exists in the population of ΔZ_L between the 1936/38 and 1990 maps. Small biases are apparent within certain error subset populations of the independent variables (i.e. Viewshed<2). Most of these biases can be accounted for through data filtering, while others are difficult to account for due to large random variation. Slope can be used to filter non-glacial elevation change points to make the population set more representative for glacial areas. Similarly, viewshed should also be used for filtering non-glacial points, but also glacial points that are not visible by at least 2 images.

Data Filtering and Systematic Bias

Data filtering is performed on the populations of ΔZ_L to create representative sample sets for error quantification of glacial areas. It seems reasonable to filter ΔZ_L for slopes less than 20 degrees, as glaciers do not contain slopes greater than that. The viewshed parameter is used to filter out points not visible in at least 2 images as photogrammetry requires at least 2 images to resolve topography. The results of the filtering decreased the means (bias) significantly (Table 1). Most importantly, the standard deviations decreased by 25% to 40% for the individual regions (Table 1). The slope and viewshed filters are used on ΔZ_L to properly represent the map bias and to estimate elevation error for glacier areas. A viewshed filter is used for removing 'schematic' contours from glacial areas.

Fig. 5 shows box and whisker plots of the original and filtered population sets versus elevation for each region. A negative bias that increases with elevation is apparent in the un-filtered error points. However, slope and viewshed create confounding relationships that lead to wrong identification of an elevational bias. After filtering, the altitudinal bias is mainly removed for Brøggerhalvøya/Oscar W, Prins Karls Forland, and Nordenskiöld West. The bias is only minimized for Nordenskiöld Central, Heerland, Nathorst Land, and Wedel Jarlsberg Land. It is difficult to accurately quantify a potential altitudinal bias due to the fact that the filtered data sets are not spatially representative at higher altitudes (i.e. a minimal number of points exist at higher altitudes). For all regions, a negative bias exists in the means (Table 1) implying that the 1936 map surface is systematically higher than the 1990 surface. The northwest and west regions (Brøggerhalvøya, Prins Karls Forland, and Nordenskiöld West) have biases less than 2 meters while the other regions contain significant biases greater than 2 meters (see Fig. 6e).

Table 1: Non-glacier point (ΔZ_L) statistics of the various population sets for the regions analyzed in this study. The filter chosen is bold italicized.

Brøgger-Halvøya/OscarW

Parameters	Count	Mean	St. Dev.	Min	Max
All Points	47143	-3.05	17.19	-99.8	128.5
Slope<40&Vshed>1	25475	-1.49	14.42	-96.3	96.6
Slope<30&Vshed>1	11526	-1.03	11.92	-96.3	96.6
Slope<20&Vshed>1	***5980***	***-0.24***	***8.23***	***-57.4***	***86.3***
Slope<30&Vshed>2	10343	-1.07	12.15	-96.3	96.6
Slope<30&Vshed>3	7980	-1.05	11.52	-54.1	96.6
Slope<30&Vshed>5	3305	-2.39	10.06	-52.7	40.56

Prins Karls Forland

Parameters	Count	Mean	St. Dev.	Min	Max
All Points	41608	-9.75	21.75	-99.7	103.5
Slope<40&Vshed>1	29405	-6.62	17.53	-97.4	87.9
Slope<30&Vshed>1	16679	-3.30	13.56	-91.7	87.9
Slope<20&Vshed>1	***9561***	***-1.66***	***9.87***	***-89.2***	***87.9***
Slope<30&Vshed>2	16370	-3.37	13.60	-91.7	87.9
Slope<30&Vshed>3	15057	-3.55	13.62	-91.7	87.9
Slope<30&Vshed>5	11731	-2.59	13.25	-81.3	87.9

Nordenskiöld West

Parameters	Count	Mean	St. Dev.	Min	Max
All Points	58225	-3.53	19.60	-132.9	126.2
Slope<40&Vshed>1	47865	-2.33	17.23	-132.9	126.2
Slope<30&Vshed>1	35250	-0.96	14.23	-132.9	126.2
Slope<20&Vshed>1	***19996***	***0.46***	***11.93***	***-94.5***	***126.2***
Slope<30&Vshed>2	31474	-0.83	14.09	-132.9	91.6
Slope<30&Vshed>3	26453	-0.96	14.10	-132.9	91.6
Slope<30&Vshed>5	17258	-1.09	14.38	-132.9	91.6

Nordenskiöld Central

Parameters	Count	Mean	St. Dev.	Min	Max
All Points	113117	-7.68	19.13	-146.3	122.1
Slope<40&Vshed>1	84368	-6.82	17.51	-146.3	84.6
Slope<30&Vshed>1	56590	-5.97	15.77	-146.3	70.5
Slope<20&Vshed>1	***28426***	***-4.67***	***13.17***	***-121***	***54.7***
Slope<30&Vshed>2	50484	-5.97	15.91	-146.3	70.5
Slope<30&Vshed>3	40986	-5.63	16.15	-146.3	70.5
Slope<30&Vshed>5	25217	-4.28	15.18	-146.3	62.6

Heerland

Parameters	Count	Mean	St. Dev.	Min	Max
All Points	61207	-7.10	18.43	-99.2	80.9
Slope<40&Vshed>1	42985	-7.01	17.94	-97.1	79.4
Slope<30&Vshed>1	22467	-5.91	15.52	-77.9	79.4
Slope<20&Vshed>1	***9623***	***-4.83***	***11.61***	***-69.1***	***79.4***
Slope<30&Vshed>2	19235	-5.58	15.05	-77.9	79.4
Slope<30&Vshed>3	14344	-5.88	14.98	-77.9	65.3
Slope<30&Vshed>5	7391	-6.51	15.02	-77.9	65.3

Nathorst

Parameters	Count	Mean	St. Dev.	Min	Max
All Points	55490	-3.11	17.89	-85.3	106.8
Slope<40&Vshed>1	43748	-3.60	16.61	-85.3	93.8
Slope<30&Vshed>1	29471	-3.82	15.05	-85.3	93.8
Slope<20&Vshed>1	***12713***	***-2.87***	***11.60***	***-74.6***	***73***
Slope<30&Vshed>2	26305	-3.74	14.95	-80.1	93.8
Slope<30&Vshed>3	21272	-3.35	14.74	-80.1	93.8
Slope<30&Vshed>5	10752	-1.04	14.85	-74.1	93.8

Wedel Jarlsberg Land

Parameters	Count	Mean	St. Dev.	Min	Max
All Points	106224	-12.82	24.53	-347.2	110.6
Slope<40&Vshed>1	66619	-10.47	20.28	-320.6	99.2
Slope<30&Vshed>1	38535	-9.35	17.51	-152.2	69.8
Slope<20&Vshed>1	***18913***	***-6.50***	***12.49***	***-128***	***63.6***
Slope<30&Vshed>2	34787	-9.22	17.31	-152.2	69.8
Slope<30&Vshed>3	29256	-9.26	17.24	-152.2	69.8
Slope<30&Vshed>5	15295	-9.84	17.39	-152.2	66.1

All Points (10% points of 496209)

Parameters	Count	Mean	St. Dev.	Min	Max
All Points	49621	-7.39	20.65	-320.6	119.3
Slope<40&Vshed>1	34085	-6.08	18.16	-320.6	108
Slope<30&Vshed>1	21127	-4.96	15.74	-128.7	78.55
Slope<20&Vshed>1	***16435***	***-3.13***	***12.22***	***-127***	***78.6***
Slope<30&Vshed>2	18958	-4.86	15.67	-128.7	78.55
Slope<30&Vshed>3	15588	-4.79	15.75	-128.7	68.54
Slope<30&Vshed>5	9080	-4.04	15.56	-128.7	68.54

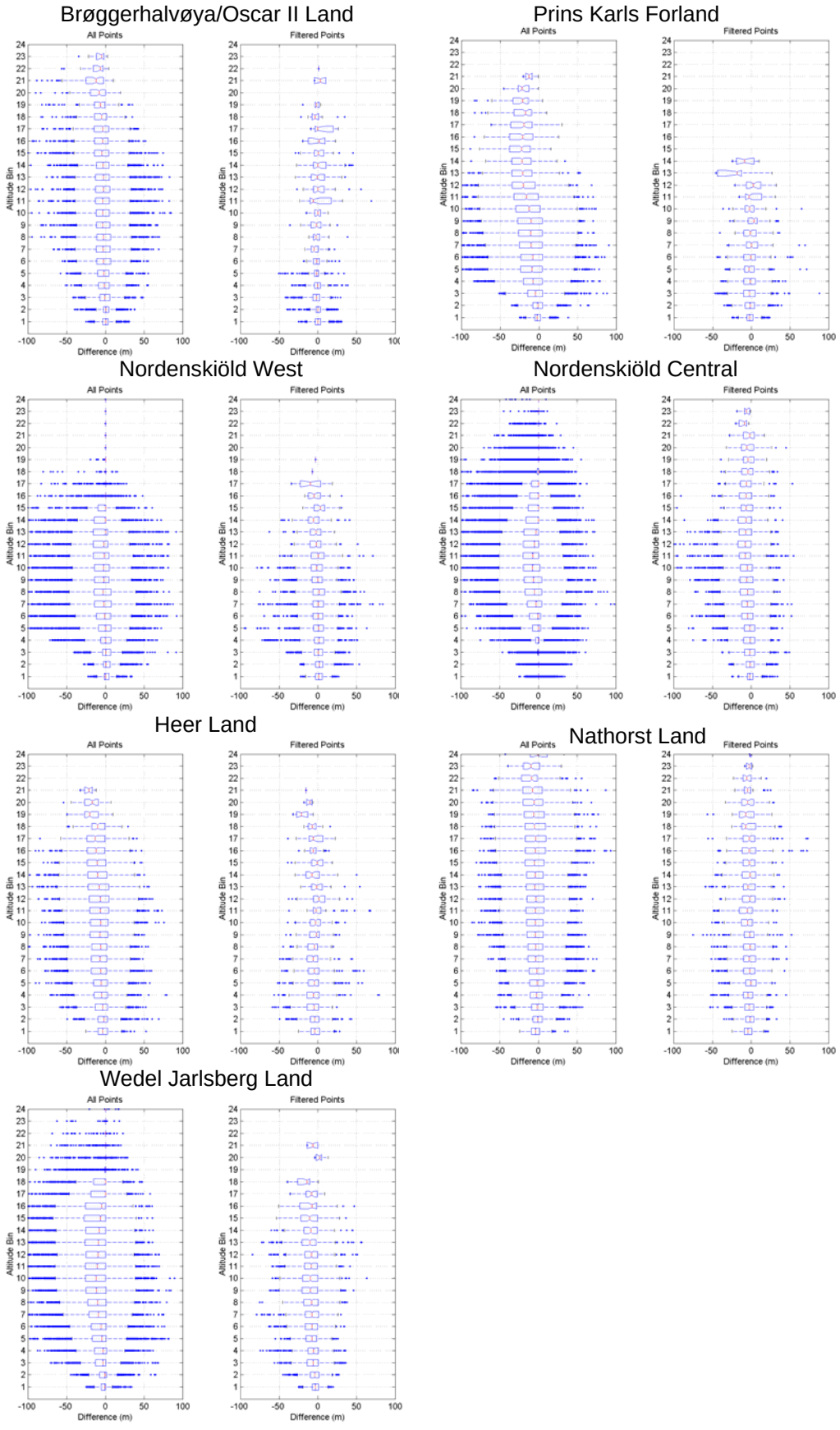

<u>Fig. 5:</u> Box and whisker plots for the error (x-axis) against altitude (y-axis). A description of box and whisker plots is found in the caption of Fig 4.

Understanding the systematic bias

To better understand the spatial distribution of systematic bias within the population of ΔZ_L (the error), the means of the point differences are calculated in a moving window of varying resolutions (Fig. 6). The increasing window resolutions are thought to aid in the understanding of the spatial autocorrelation in the errors. In a perfect world with no errors, it could be expected that a random pattern of pixel values would result for all moving window sizes.

For window resolutions less than 20 km^2 (Fig 6a-d), the bias varies spatially and at different spatial scales. The patterns of the 1 km^2 window size imply a type of spatial autocorrelation that exists within small local areas. With increasing window size, the autocorrelation is smoothed over larger areas. If no bias was present, spatial autocorrelation would be expected to disappear by increasing the moving window resolution, clearly not apparent in Fig 6. To remove the small scale spatial autocorrelation, the moving window size is increased to 100 by 100 km (Fig. 6e) revealing the underlying northwest-southeast bias trend.

The large spatial scale biases associated with the 1936/38 topographic maps is thought to be caused by from errors in GCPs. Fig. 6e can be used as a moving window adjustment to remove systematic error from the population of glacier elevation change points. Due to the limited populations of non-glacier points, especially over Wedel Jarlsberg Land (southern Svalbard), and to the uncertainty in the bias quantification produced by the moving window averaging scheme, the filtered mean differences (Table 1) are used as a constant bias to adjust glacial elevation changes of the particular regions. (See Chapter 3 for a detailed explanation).

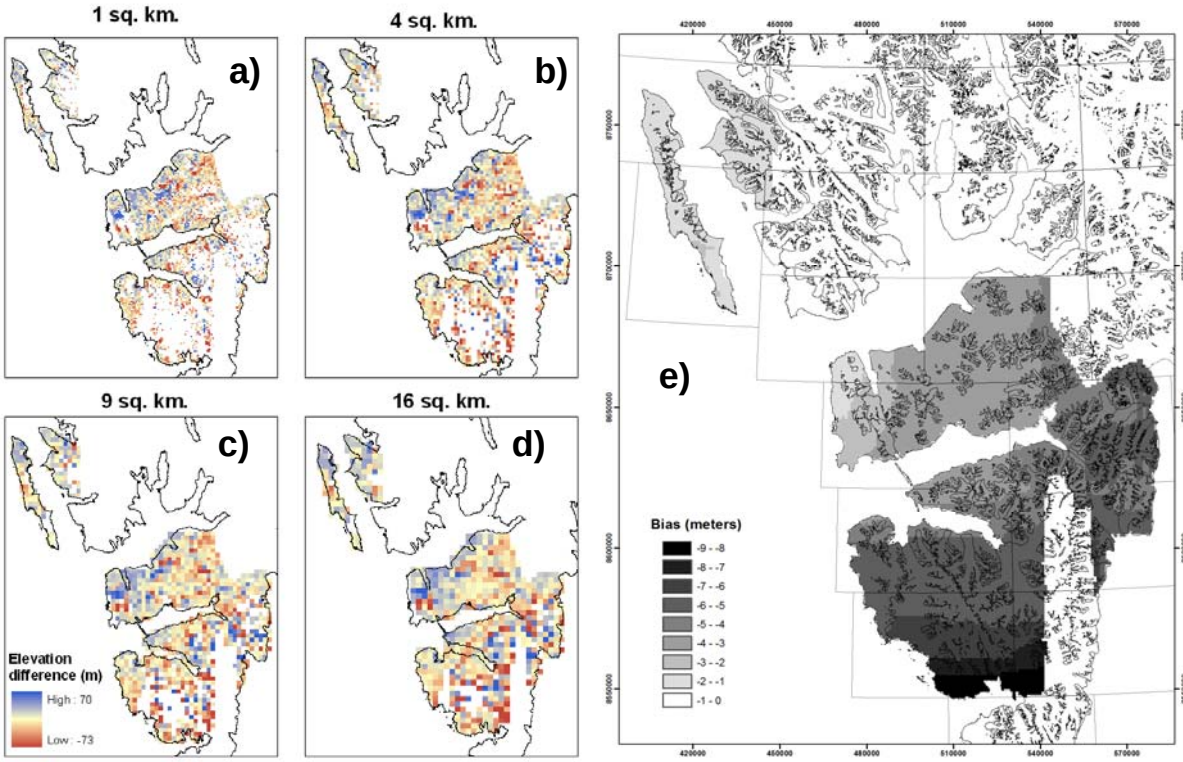

Fig. 6: The means of errors through window (pixel) resolutions of 1 km^2 (a), 4 km^2 (b), 9 km^2 (c), 16 km^2 (d), and 100 km^2 (e).

Spatial Autocorrelation

Spatial autocorrelation is the relationship of features in space. It derives from a standard geographic law (Tobler's Law) which states, "Everything is related to everything else, but near things are more related than distant things" (Tobler, 1970). Points derived from contours are inherently spatially autocorrelated since each neighbor represents the same elevation. Spatial autocorrelation within the population of ΔZ_L is inferred through Fig 6a. The question is to what degree spatial autocorrelation exists, such that a proper statistical standard error can be determined for glacier volume changes. The use of a standard error approach to quantifying glacier volume change errors is explained in Chapter 3.

To explore spatial autocorrelation, semi-variograms are created by examining pairs of points with the distance between them on the *x-axis* and the error difference squared on the *y-axis* (Davis, 2002). If spatial autocorrelation exists, *x* will increase with *y* until leveling off to a threshold of constant *y*, generally referred to as the sill. The distance region between zero and the sill, called the range, defines the neighborhood within which locations are related to one another (Davis, 2002). It is the end value of the range that is particularly important in accounting for spatial autocorrelation within standard errors.

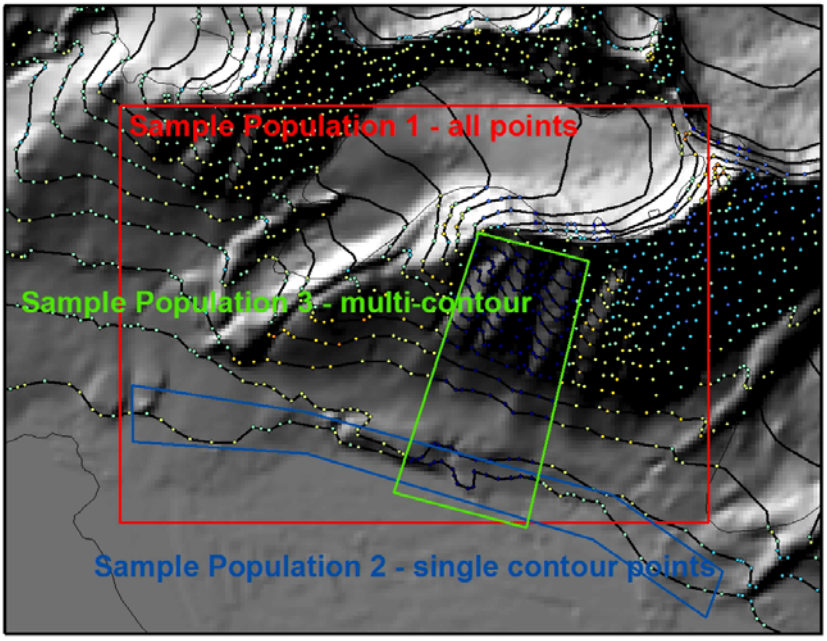

Fig. 7: Map of the various sub populations created for spatial autocorrelation analysis. Sample Population 1 is the isotropic set while Sample Population 2 and 3 are the inter-contour and cross-contour sets, respectively.

In most cases, spatial autocorrelation may only be a function of distance. This is known as isotropic autocorrelation. However, the presence of anisotropy, or the fact that spatial autocorrelation can vary in different directions, is quite common in spatial data. Topographic contours naturally contain a local directional influence by way of inter-contour and cross-contour directions. Inter-contour refers to points along the same contour. Cross-contour is a sequence of elevation contours.

To explore spatial autocorrelation within the population of errors points, three sample populations are created to analyze the potential of both isotropic and anisotropic spatial autocorrelation (Fig 7). Sample population 1 is the anisotropic case with a larger area for analysis. Sample population 2 is used to analyze the inter-contour spatial autocorrelation. Sample population 3 is the cross-contour population set in which the spatial width is dependent upon the range determined from the inter-contour analysis.

In semi-variogram analysis, a model or function is applied to fit a curved line to the data that generally increases with distance until the sill is approached . As stated in the *Predictor Variables* section, the inherent random distribution of the errors about a zero mean complicates the analysis and semi-variogram plots (Fig 8). A function fit to these diagrams will generally consist of a flat line on the x-axis along zero. Nonetheless, one can visualize a sill threshold in this data by visually inspecting where the spread of the squared differences levels off (becomes constant).

In the isotropic case (Fig. 8a), the spread of the squared differences increases greatly as distance increases to 125 meters, and slowly levels off to a threshold at a distance of 500 meters. This implies that the spatial autocorrelation is greatest between points below a distance of 125 meters, and slowly diminishes between 125 and 500 meters distance. This two stepped leveling is thought to be a result of the presence of anisotropic spatial autocorrelation. For the inter-contour population (Fig. 8b), the variance of the squared differences levels off at a distance between 300-400 meters. The points of a single contour are therefore spatially autocorrelated up to a distance of ~400 meters. This threshold is used to determine the width of the sample population 3 such that inter-contour autocorrelation is controlled within the analysis. In the cross-contour population (Fig. 8c), the spread of the distance with respect to the squared error difference increases faster with distance where it levels off at a distance of ~250-300 meters.

In summary, anisotropic spatial autocorrelation exists with the non-point elevation difference population. The anisotropy is inherent within the contour point data, where 2 directions, inter-contour and cross contour can be defined. In order to best determine a distance threshold that defines spatial autocorrelation within the entire dataset, these directional influences can be grouped into the isotropic sample. Although a model cannot be fit to the data (due to the nature of errors being normally distributed about zero), a sill threshold is visually identified by where the spread of the squared differences level off. In this manner, spatial autocorrelation for this dataset is conservatively determined to occur below a distance of 500 meters. The smaller threshold for the cross-contour sill than the inter-contour sill implies that progression of elevation error from one elevation contour to the next elevation contour diminishes faster than the progression of error along one contour. The importance of spatial autocorrelation lies in the standard error estimation of glacier volume changes from non-glacier elevation changes explained in Chapter 3.

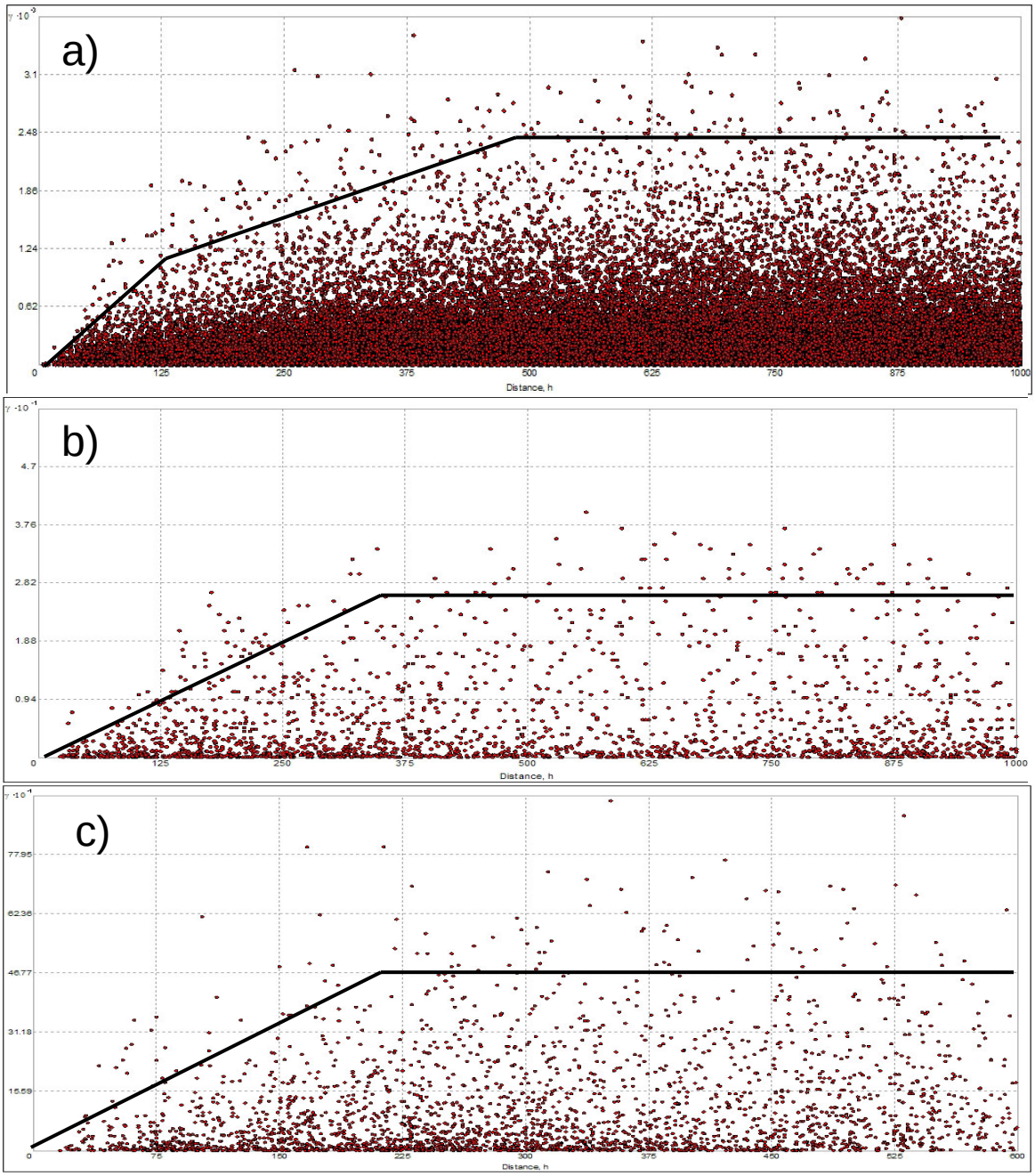

Fig. 8: Semi-variograms for a) Sample Population 1 (isotropic), b) Sample Population 2 (inter-contour anisotropic), c) sample population 3 (cross-contour anisotropic). The black lines are "eyeballed" models fit to the dataset. The y-axis is the error difference squared between a pair of points. The x-axis is the distance between that pair of points. Note the x-axis varies for each graph.

Chapter Summary

In this chapter, the accuracy of the 1936/38 topographic maps is assessed by comparing non-glacier contour points to the 1990 DEM. Variables related to topography and the aerial photographs are analyzed statistically to help differentiate systematic from random errors. The analysis is made complicated by the inherent nature of random errors to be centered around zero creating heteroscedasticity. Nonetheless, relations exist with both slope and viewshed as seen in the changing variances of the errors (Fig. 4). Slope is used to filter the non-glacier point elevation differences (ΔZ_L) to make representative population sets for quantifying glacier elevation change errors. Viewshed is used to filter both the non-glacier and glacier point elevation changes as contours are 'schematically' drawn over these areas simply to complete the maps. Large scale biases exist within the topographic maps as seen in Fig. 6. The regional mean differences (in Table 1) are used to adjust the glacier elevation differences where the bias is attributed to systematic errors in the ground control of the old maps. Spatial autocorrelation is apparent within the population of errors but ceases to exist at a distance of ~500 meters as determined through semi-variogram analysis. This minimum threshold is used when deriving standard error estimates for glacier volume changes (Chapter 3).

Chapter 3

Glacier geometry and elevation changes on Svalbard (1936 – 1990): a baseline dataset

Submitted to *Annals of Glaciology* **45**: proceedings from the IGS symposium on cryospheric indicators of climate change, August 2006.

Christopher Nuth[1,2]

Jack Kohler[1]
Harald Fast Aas[1]
Ola Brandt[1]
Jon Ove Hagen[2].

[1] Norwegian Polar Institute, Polar Environmental Centre, NO-9296 Tromsø, Norway
[2] Department of Geosciences, Section of Physical Geography, Faculty of Mathematics and Natural Sciences, University of Oslo, PO Box 1047, Blindern, NO-0316, Norway

Abstract

This study uses older topographic maps made from high-oblique aerial photographs for glacier elevation change studies. We compare the 1936/38 topographic map series of Svalbard (Norwegian Polar Institute) to a modern Digital Elevation Model (DEM) from 1990. Both systematic and random components of elevation error are quantified through non-glacier elevation difference points. The 1936/38 photographic aerial survey is examined to identify areas with poor data coverage over glaciers. Elevation changes are analyzed for 7 regions in Svalbard (~5000 km^2), where significant thinning was found at glacier fronts, and elevation increases in the upper parts of the accumulation areas. All regions experience volume losses and negative geodetic balances, although regional variability exists relating to both climate and topography. Many surges are apparent within the elevation change maps. Estimated volume change for the regions is -1.59±0.07 km^3a^{-1} (ice eq.) for a geodetic annual balance of -0.30 m a^{-1} (w. eq.), and the glaciated area has decreased by 16% in the 54 year time interval. The 1936-1990 data are compared to modern elevation change estimates in the southern regions, to show that the rate of thinning has increased dramatically since 1990.

Introduction

The geodetic mass balance is the change in net mass of a glacier or glaciated region determined through elevation comparisons. There are many studies outlining the approach of using elevation data to estimate mass balances (Finsterwalder, 1954; Echelmeyer and others, 1996; Andreassen and others, 2002; Cox and March, 2004). Comparisons of geodetic and traditional mass balances on the same glacier have demonstrated that the two methods can lead to different values (Krimmel, 1999; Østrem and Haakensen, 1999). However, errors associated with the traditional mass balance tend to be systematic, making a geodetic balance more accurate over longer time periods (Cox and March, 2004), and in some studies (Elseberg and others, 2001) the geodetic balance is used to adjust the traditional balances.

The use of elevation changes to determine glacier and ice cap mass balance has become more prevalent with the increasing number of available altimetry measurements, made either from aircraft or satellites (Arendt and others, 2002; Bamber and others, 2005). However, the time periods for these recent measurements is restricted to the past few decades, at most, while longer term comparisons are needed for relating glacier change to climate variation. Often, the only recourse is to analyze elevation changes from older maps, despite their relatively poor precision compared to more recent products. Nonetheless, they remain the only possible data source for shedding light on previous glacier geometries without re-performing the original photogrammetry, a significant undertaking.

Svalbard has about 36,000 km^2 of glaciers of various types (ice fields, outlet, tidewater, and smaller cirque glaciers), the majority of which are polythermal (Hagen and others, 1993). Climate on Svalbard varies spatially (Hagen and others, 1993, 2003), with an interior characterized by lower precipitation amounts compared to the coastal regions (Winther and others, 1997; Humlum, 2002). The instrumental climate record for Svalbard, from Longyearbyen, is relatively short, extending not much earlier than 1911 (Nordli and Kohler, 2003). During the 20^{th} century, temperatures have been gradually rising, and the retreat of Svalbard glaciers from their last glacial maximum position occurred sometime after about 1920 (Nordli and Kohler, 2003).

The net mass balance for the whole of Svalbard has recently been assessed using two different methods (Hagen and others, 2003a, 2003b), yielding estimates between -0.27 and -0.12 m a^{-1} w. eq. Bamber and others (2005) have suggested an increased thinning rate in recent years based on repeat aerial surveys in 1996 and 2002. However, there is at present no long-term baseline

reference for these elevation change comparisons. In this study, we compare older maps of Svalbard to modern Digital Elevation Models (DEMs) to derive average elevation changes over a significantly long time interval (1936/38-1990).

Data

The oblique photographic aerial surveys of 1936/38 made by the Norwegian Polar Institute (NPI) were the basis for the first accurate topographic maps of Svalbard. Contour maps were created at a scale of 1:100000 with 50 m contour intervals from the oblique aerial photographs, which were taken at approximately 3000 m a.s.l.. During the 1990s, NPI hand-digitized the older maps, such that the contours are stored digitally as a series of northing and easting points at the measured 1936/38 elevations.

The accuracy and precision of the 1936/38 maps is limited, due to the technology available at the time and to the relatively high flying height. The accuracy of glacier contours varies by elevation, with upper elevation contours less accurate than for the lower elevations. This is due in part to the flight plan, which was preferentially around the coast looking inland, such that the distance to the image point of the higher elevation areas was typically greater, and to the lower contrast in the upper regions of glaciers.

The most recent complete aerial survey over Svalbard was carried out by NPI in late summer 1990, and comprises vertical aerial photographs at a scale of 1:50000. A DEM based on these aerial photos is in the process of being created by NPI using a modern digital photogrammetric workstation. The DEM is incomplete at this writing, however, so the study region is restricted to those areas for which the photogrammetric work is completed. The resolution of the DEM is 20 m and it has a horizontal accuracy of ±2-3 m.

Method

The early maps were created using the European Datum 1950 (ED50), and therefore had to be converted to WGS84, the datum for the 1990 DEM. We use a regional transformation available in Esri ArcGIS; while more accurate local conversion is available based on comparing older NPI ED50 control point coordinates to newer WGS84 positions (obtained through differential GPS), the ArcGIS conversion is adequate and does not lead to appreciable errors.

Each digitized point of the 1936/38 contours is then interpolated into the pixels of the 1990 DEM using bilinear interpolation. This yields a database of irregularly spaced points with two elevation attributes which are differenced and spatially interpolated (Hutchinson, 1989) to create two dimensional maps of elevation change. Elevation changes are converted into volume changes through a hypsometric approach, similar to the traditional mass balance calculation in which balances are assumed to be functions of elevation (Oerlemans and Hoogendoorn, 1989; Østrem and Brugman, 1991). Mean elevation changes are determined for each elevation bin by averaging interpolated pixels.

The relationship between elevation changes and traditional balance at a point is defined by:

$$\frac{dh}{dt} = \dot{b} + \frac{dq_x}{dx} + \frac{dq_y}{dy}, \qquad [1]$$

where h is elevation, $\dot{b}$ is the net specific mass balance, q_i are the ice fluxes in the x and y directions (Paterson, 1994). Integration of equation 1 over the entire glacier surface results in the flux terms canceling (assuming steady state), and thus elevation changes can be converted into geodetic balances independent of dynamics. Although an ice mass is rarely in steady state, it is feasible to assume this condition as the magnitudes of the elevation changes are much larger than the derivitives of the ice fluxes (Paterson, 1994). The integrated term on the left hand side (equation 1) is the geodetic balance, $\overline{dh}/dt$, and is then equivalent to the traditional mass balance on the right hand side.

The geodetic balance, $\overline{dh}/dt$, is obtained by first calculating the total volume change by summation of the average elevation changes weighted by the glacier hypsometry (area-elevation distribution):

$$\Delta V = \sum_i (A_i \cdot \Delta h_i) \qquad [2]$$

where Δh_i is the average elevation change, A_i is the area, and i is the corresponding altitude interval. The hypsometry from the map with the larger glacier area should be used. The cumulative net geodetic balance is then derived by dividing the volume changes by the average of both areas (Finsterwalder R., 1954; Echelmeyer and others, 1996; Arendt and others, 2002) to account for glacial retreat or growth.

The 1936/38 and 1990 aerial surveys were completed in late summer, although the exact timing varies by area. Some workers apply a correction to account for ablation and emergence

during the period between the photographic dates (Krimmel,1989 & 1999; Echelmeyer and others, 1996; Andreassen and others, 2002; Cox and March, 2004). In our case, the relatively large magnitude of the elevation changes over the 54 year time interval and the low mass turnover of Svalbard glaciers (Hagen and others, 2003a) implies that the correction factor will be negligible in light of the overall changes.

Another adjustment commonly included in geodetic balance calculation is for changes in the firn density profile (Krimmel, 1989; Sapiano, 1998). We assume that in steady-state conditions the density profile from the surface to the firn/ice transition is constant through time (Bader, 1954) such that the elevation changes are composed completely of ice, and a single density of 0.9 kg/m^3 can be used. This assumption is weakest in the transition area between the accumulation and ablation zones, for cases in which either the mean or transient equilibrium line altitude (ELA) are significantly different in the two epochs. However, given that no measurements of firn density are available for the older epoch, and the relatively long baseline, we prefer to assume constant density rather than introduce artificial assumptions about its temporal and spatial fluctuations. The results in this study will all be in ice equivalent units, unless otherwise stated.

Errors

The error of an elevation change determined from two maps depends on a number of factors, including the quality of the original photography, spatial and geodetic transformations, the scale of the imagery (related to the flying height), accuracy of the geodetic referencing network, and of course, the skill of the photogrammetrist (Andreassen, 1999).

We use point elevation differences over non-glacier land areas to quantify the elevation errors associated with glacier changes. We assume that the majority of errors derive from the 1936/38 map, since it is based on high oblique photography with lower quality and the higher flying height, and therefore take the 1990 DEM as the more reliable of the two epochs. Elevation differences over non-glacier areas can be explained by a geolocation (horizontal) error in either or both of the two maps. The elevation error that results from geolocation errors is the product of the horizontal error and the tangent of the slope angle (Echelmeyer and others, 1996); the greater the slope of the surface, the greater the apparent elevation error.

A further consideration is to ascertain whether the 1936/38 contours are actually determined from the aerial photography, for in some areas it is apparent that contours are hand-drawn with no

reference to actual photogrammetric measurements. These infilling contours are simply crude estimates made for the sake completing the map, and cannot be used to determine elevation changes. The Esri ArcGIS "Viewshed" function uses a DEM and a vector of observer or camera location points to determine the number of such observer points visible in a particular pixel. A viewshed analysis was performed on the 1936/38 aerial survey by digitizing the approximate x- and y-coordinates for each of the photograph points in the 1936/38 imagery. Seven parameters are required to for the Viewshed function, including the locations, viewing angles, and elevations of the observer points (Esri ArcGIS).

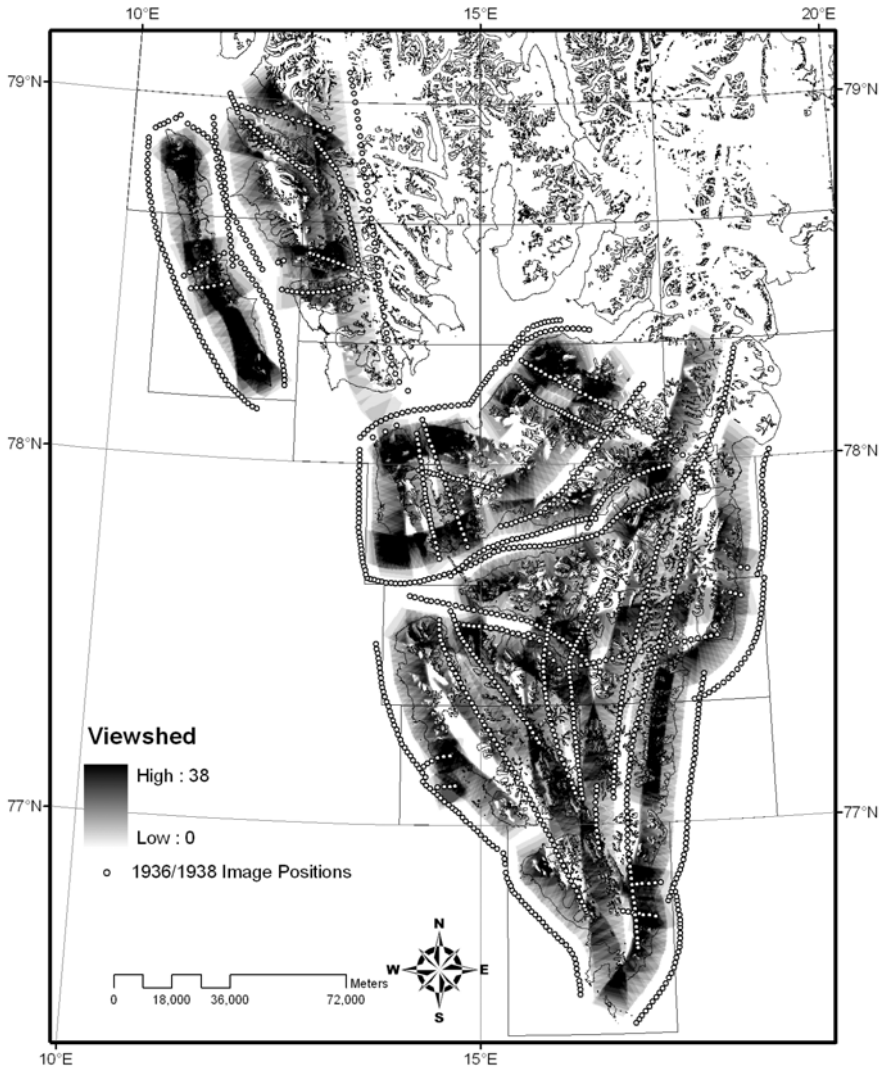

Fig. 1: Viewshed map for the 1936/38 images. The grey scale represents the viewshed parameter, the number of aerial photographs (points) which can see individual pixels in the DEM. The darker the pixels, the better aerial coverage from the photographs.

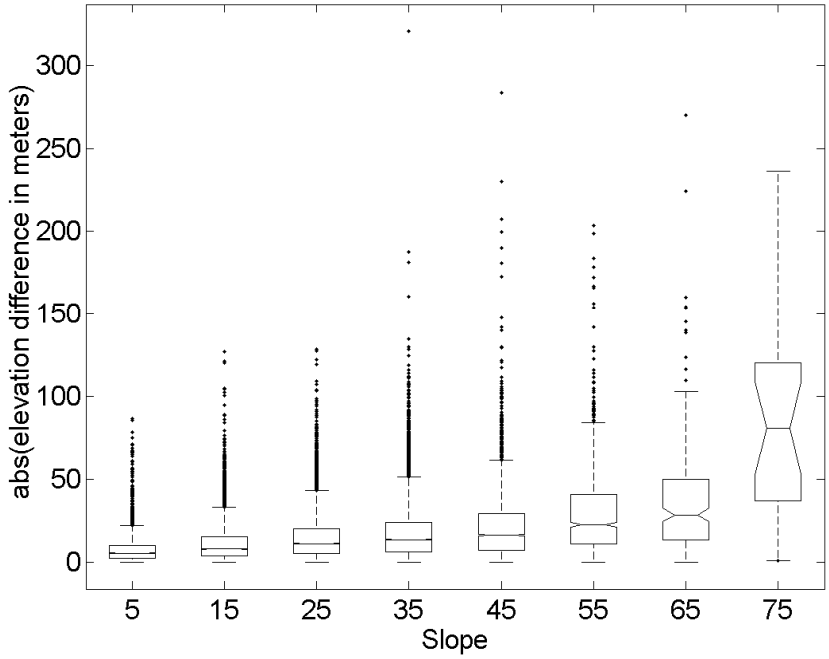

a)

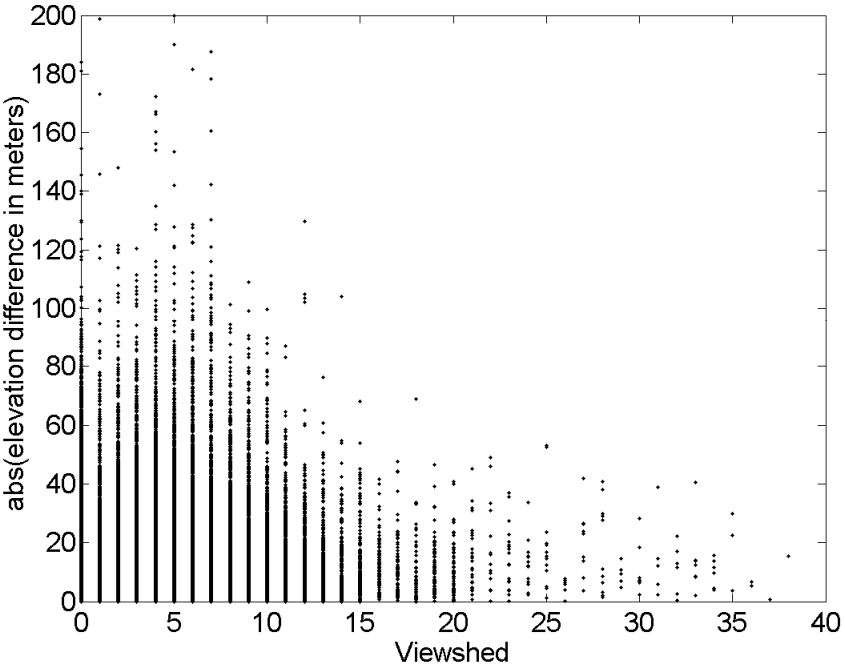

b)

<u>Fig. 2</u>: The relationship between absolute value of the non-glacier elevation differences as a function of a) DEM slope in degrees and b) viewshed parameter. Fig. 2a is a box and whisker plot. The box has lines at the lower quartile, median, and upper quartile values which represent 50% of the data. The whiskers display the extent of the rest of the data. Outliers are plotted as points. The notches represent the uncertainty about the means.

The resulting viewshed image (Fig. 1) assesses the relative quality of the aerial survey; the greater the viewshed parameter, the better the photographic coverage of the area. The viewshed grid is then used to filter out pixels that are not visible from the photographs. There are apparently a number of non-visible areas, some the result of mountain shadowing, but some due to the search radius parameter chosen, which limits the distance from each observer point that the function searches. A larger search radius decreases the non-visible areas significantly; experimentation in test areas revealed that 15 km was a reasonable radius choice.

Fig. 2 shows the relation between the non-glacier elevation differences (errors) with both slope and viewshed. There is a distinct pattern of decreasing means and standard deviations with decreasing slope and increasing values of the viewshed parameter. To characterize the map errors, we filter the population of non-glacier land differences to remove points with slopes greater than 20 degrees and viewshed values less than 2 images, to make them representative for glacier areas. Application of the filter decreases the variance of the non-glacier point elevation changes by ~35%. After filtering, the average non-glacier land elevation difference is -3.1 m with a standard deviation of 12.2 m (Table 1).

Table 1 shows error estimations for each region, giving the mean non-glacier land elevation differences, the error for the cumulative geodetic balances (area-weighted average elevation change), and for the volume changes. The mean difference is the bias between maps, which is used to adjust the final elevation change curves. Little bias is apparent in the north and west regions analyzed, while a significant bias exists from Nordenskiöld Central and southwards. This is attributed to ground control point errors used in the creation of the 1936/38 contour maps. The standard deviation about the mean (ε) represents the uncertainty within an individual point elevation change. To propagate the uncertainties into error estimates for volume change and cumulative geodetic balance, a standard error (Equation 3) is applied to each elevation bin,

$$S.E. = \frac{\varepsilon}{\sqrt{N}} \qquad [3]$$

where N represents a measure of the sample size. There is significant spatial autocorrelation for the non-glacier land differences, so simply taking N as the number of digitized contour points leads to error underestimation. Analysis of semi-variograms revealed that spatial autocorrelation exists at distances of up to ~500 m, which translates into 4 uncorrelated measurements per km^2. Conservatively, we assume that only 1 uncorrelated measurement occurs within 1 sq. km., and as

such, N becomes the area (in km^2) of each elevational bin (i.e. the number of measurements in an elevation bin). Volume change error (ε_V) is then the summation of the standard errors multiplied by the hypsometry of each region:

$$\varepsilon_V = \sum_i S.E._i \cdot A_i \qquad [4]$$

Similarly, the error associated with the area-average elevation change (ε_B) is simply the volume change error divided by the average of both areas, A. This approach emphasizes the reduction in error that occurs through the summation of large spatial areas while accounting for the spatial autocorrelation.

Table 1: Non-glacier point elevation difference statistics for 7 regions. The mean difference is the systematic bias used to adjust elevation change curves. The standard deviation (ε) is the individual point elevation accuracies while ε_V and ε_B are the error estimates for volume change and cumulative balance, respectively.

Region	*Mean difference*	ε	ε_V (km^3)	ε_B (m)
Brøggerhalvøya/Oscar II Land	-0.24	8.23	0.63	1.63
Prins Karls Forland	-1.66	9.87	0.39	4.10
Nordenskiöld West	0.46	11.93	0.70	2.95
Nordenskiöld Central	-4.67	13.17	1.12	2.71
Heer Land	-4.83	11.61	1.53	1.38
Nathorst	-2.87	11.60	1.14	2.44
Wedel Jarlsberg Land	-6.50	12.49	2.27	1.12
Total	**-3.13**	**12.22**	**3.64**	**0.77**

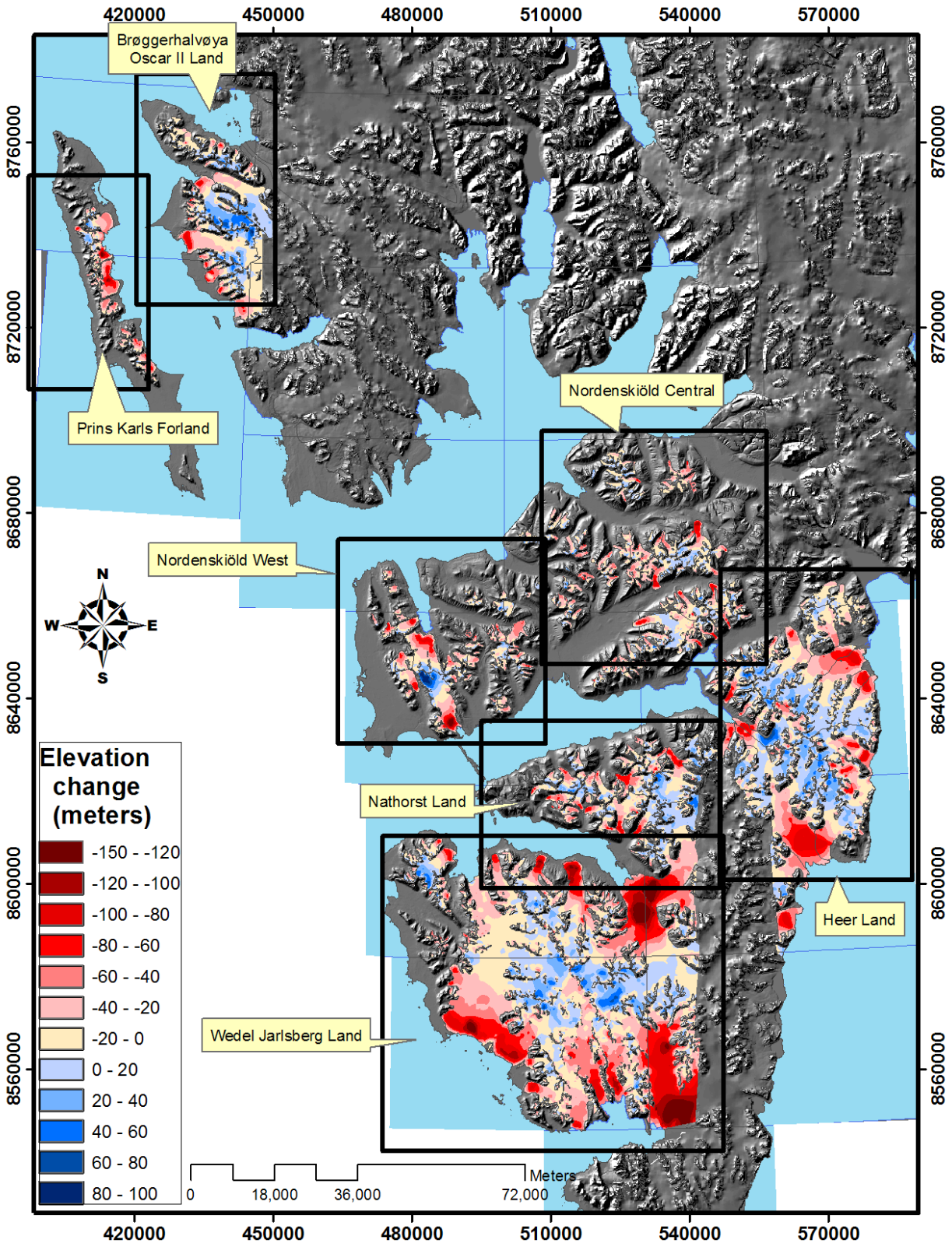

Fig. 3: Elevation change map over parts of Svalbard (1936/38 – 1990) showing the divisions of the 7 regions used in this analysis. The grid references are WGS84, UTM zone 33 North.

Results

Western Svalbard

There are mostly small valley glaciers in Brøggerhalvøya, Oscar II Land, and Prins Karls Forland (Fig. 3), totaling about 520 km^2 (1936/38). The glaciers of Brøggerhalvøya/Oscar II Land are generally polythermal cirque glaciers (Liestøl, 1988), whereas piedmont glaciers dominate Prins Karls Forland (Hagen and others, 1993). Some larger glaciers, Uversbreen, Comfortlessbreen, and Aavatsmarkbreen, are included within the analysis. However, the viewshed parameter for these areas shows that the photographic aerial coverage is very poor, so that some of the difference data are removed. The well-studied glaciers Kongsvegen and Kronebreen are not included as the 1990 DEM coverage does not extend to these regions yet.

Brøggerhalvøya/Oscar II Land experienced a 12 % glacial area decrease while Prins Karls Forland experienced a 30% glacier area decrease (Table 2). All glaciers of the regions are retreating, with a maximum of 100 and 145 m frontal thinning for Brøggerhalvøya/Oscar II Land and Prins Karls Forland, respectively. Many of the smaller glaciers have experienced elevation losses across the entire surface of the glacier, including all of Prins Karls Forland (Fig. 4). A trend toward glacier thickening at the upper elevations is apparent moving eastward within the regions.

The hypsometric (area-altitude) distribution for Brøggerhalvøya/Oscar II Land is greatest between 250 and 550 m.a.s.l., with the 54 year average ELA (position where the elevation change curve approaches zero) at 350 m (Fig. 5a). The greatest hypsometric weight controlling the mass balance of the region therefore is at a high enough altitude to maintain accumulation and firn. Prins Karls Forland, on the other hand, has most of its glaciated area at lower altitudes (50-250 m), with the entire elevation change curve below zero (Fig. 5a). The glaciers of Prins Karls Forland are generally downwasting, with an annual geodetic balance 3 times more negative than Brøggerhalvøya/Oscar II Land. The latter may be attributed to its more coastal location, as well as having a lower hypsometric distribution making the region more sensitive to temperature increases.

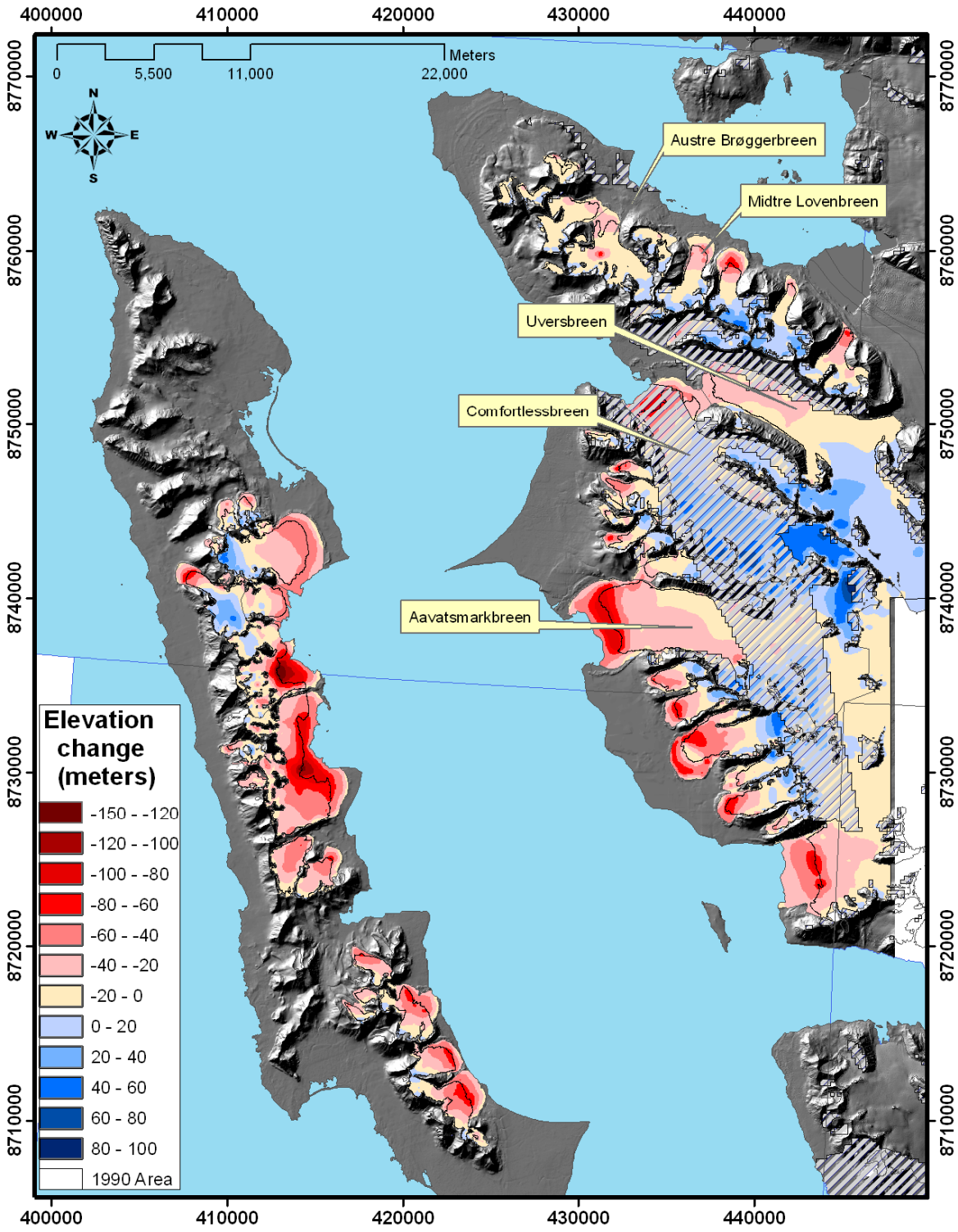

Fig. 4: Elevation change map of northwest Svalbard: Brøggerhalvøya/Oscar II Land (east) and Prins Karls Forland (west). The shaded region indicates areas where the viewshed parameter is 0 or 1, which were removed from the analysis.

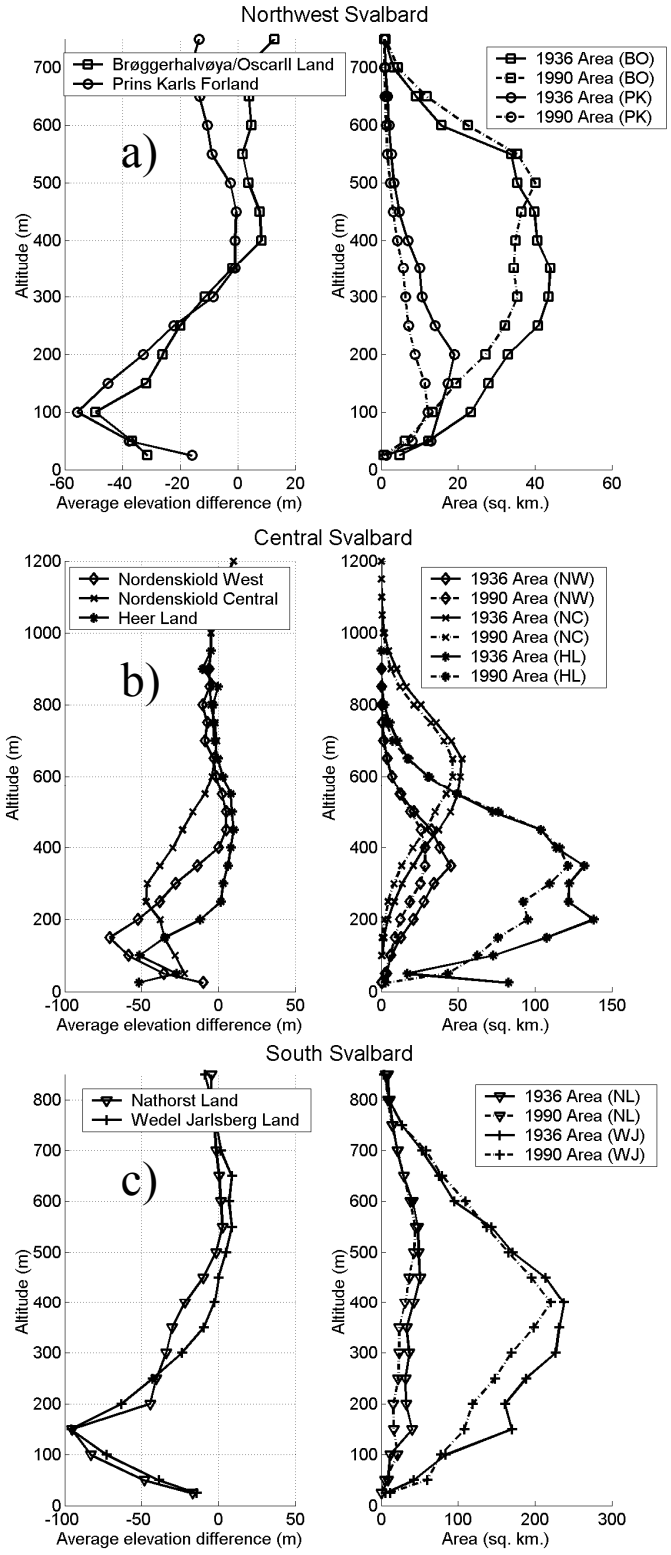

<u>Fig. 5</u>: Elevation change curves and hypsometry for a) Northwest Svalbard: Brøggerhalvøya/Oscar II Land (BO) and Prins Karls Forland (PK); b) Central Svalbard: Nordenskiöld West (NW), Nordenskiöld Central (NC) and Heer Land (HL); c) South Svalbard: Nathorst Land (NL) and Wedel Jarlsberg Land (WJ).

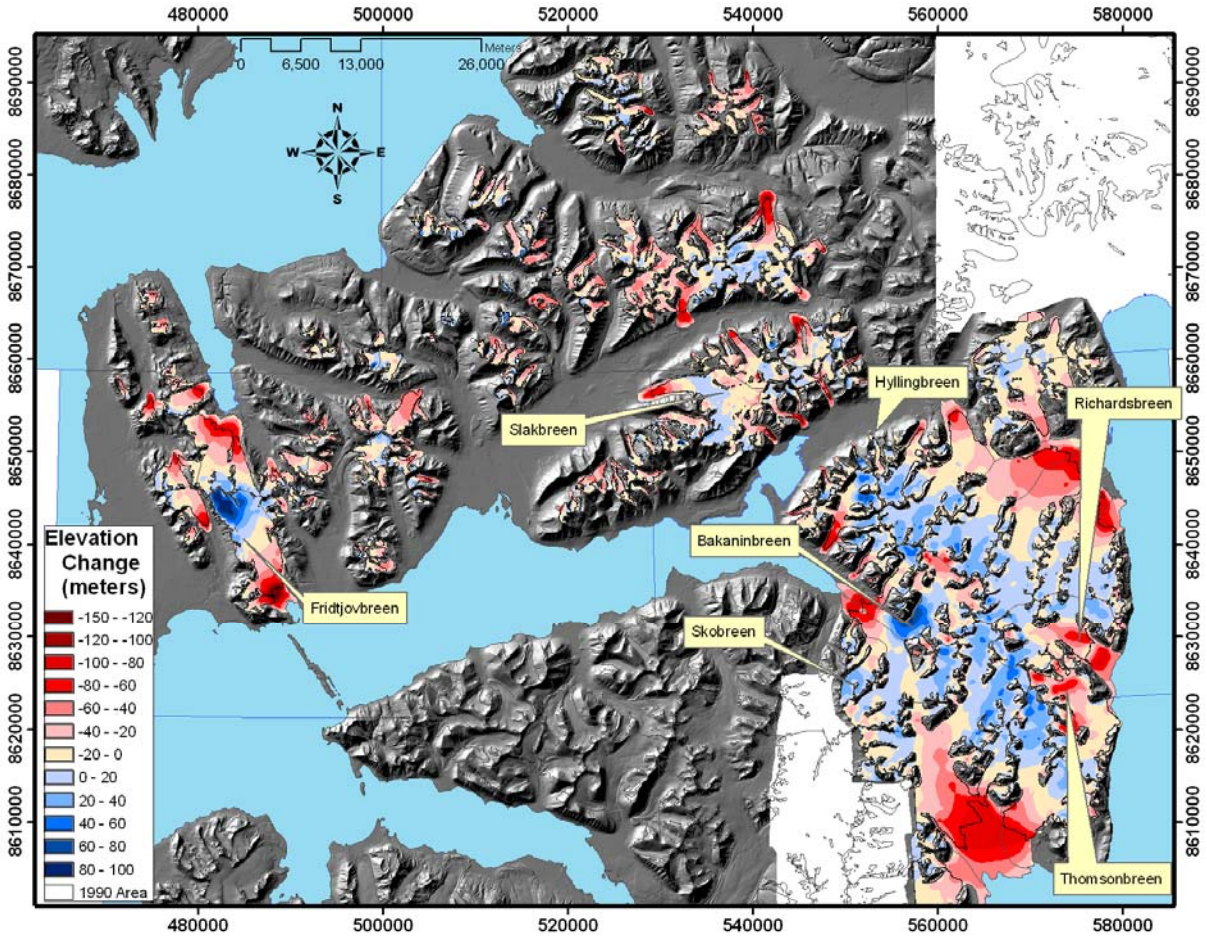

Fig. 6: Elevation changes in Central Svalbard (Central and West Nordenskiöld and Heer Land Regions). Note that the east coast experienced significant elevation increases and 5 of the 8 glaciers that surged (pre and post 1990) occur in this region.

Central Svalbard

Central Svalbard is characterized by relatively high precipitation at the coasts and the drier conditions inland (Winther and others, 1997). This is apparent when looking at the distribution and size of glaciated areas; the east coast (Heer Land) is highly glaciated, 68%, while Nordenskiöld Central and West consist of 19% and 18% glaciers, respectively. The east coast also consists of ice caps and outlet glaciers while Nordenskiöld Central and West contain mainly small valley and cirque glaciers.

Nordenskiöld West decreased in glacial area by ~25% while the majority of glaciers in the region have decreased in elevation across their surfaces, including the larger Grønfjordbreen. Fridjovbreen is the only glacier with significant elevation increases. It is a surge-type glacier, however, that recently surged in 1995 (Murray and others, 2003), five years after the end of the elevation change period (1936-1990) in this study. We note that the clear trend of glacial build-up

from 1936/38 to 1990 (Fig. 6) confirms the relative accuracy of the estimated changes from these two maps.

Nordenskiöld Central has similarly decreased in glacial area by ~20%. Slight elevation increases occur on the 2 larger ice fields containing Slakbreen and Drønbreen. Heer Land glacier areas decreased by ~15%, where all glaciers have retreated from their 1936/38 positions despite the fact that some glaciers surged. Nonetheless, interior areas show significant elevation increases (Fig. 6), which can be attributed to westward-moving winter low pressure systems that deposit the largest snow amounts (Winther and others, 1998). The annual geodetic balance of -0.16 m a^{-1} is the least negative out of all the regions in this study.

Analysis of the elevation change curves (fig. 5b) leads to two conclusions about the glacial (and climatic) regionality of Central Spitsbergen. First, Nordenskiöld Central has the highest ELA at ~850 m.a.s.l, implying a drier climate than the other two regions. Second, the elevation change gradient is steepest for Heer Land, in comparison to the other two regions of central Svalbard, inferring more dynamic glacial behavior since steeper mass balance gradients indicate greater mass turnover (Østrem and Brugman, 1991). In fact, all glaciers on Heer Land show elevation increases in their upper regions, while 5 glaciers have surged before and after 1990.

There is ample evidence of the geometric effects of surging in Heer Land. Surging glaciers are characterized by long quiescent and short surge phases. During the quiescent phase, the accumulation area increases in elevation while the ablation area decreases. The short surge period is characterized by rapid mass flow of ice down glacier resulting in elevation decreases in the accumulation area and increases in the ablation area.

Bakaninbreen surged in the late 1980s (Murray and others, 1998), leading to a distinct pattern seen in Fig. 6. The central part of the glacier experienced increases of up to 100 m, coinciding with the location of the surge termination just downstream of the 90-degree bend in the glacier (Murray and others, 1998), while the accumulation area of the glacier decreased in elevation from the transfer of mass during the surge. Thomsonbreen and Hyllingbreen display a similar surge pattern, with elevation decreases in the upper regions, and increases in the lower regions. The pattern is not as distinct as on Bakaninbreen, since the Thomsonbreen surge occurred from 1950-1960 and the Hyllingbreen surge from 1970 -1980 (Hagen and others, 1993), allowing some elevational adjustment in the decades before the 1990 DEM was created. Richardsbreen, a tidewater glacier in 1936/38, shows the largest decreases at the front with increases at the upper

elevations, another example of surge-glacier build-up. Richardsbreen later surged sometime between 1990 and 2002 (Svalbard Topographic Map Series: C10 Braganzavågen; 2006). Most recently, Skobreen surged in 2004-2005, while the 1936/38 – 1990 changes show similar build-up patterns.

Table 2: Area, volume change, and mass balances for the 7 regions. All estimates are given in ice equivalent units.

Region	*1936 Area (km^2)*	*1990 Area (km^2)*	*1936 % glacier area*	*Percent Area change*	*Volume Change (km^3)*	*Cumulative Balance (m. ice)*	*Annual Balance (ma^{-1})*
Brøggerhalvøya/ Oscar II Land	409	357	51%	-13%	-3.91	-10.21	-0.19
Prins Karls forland	111	77	15%	-31%	-3.23	-34.24	-0.63
Nordenskiold West	271	202	18%	-25%	-4.88	-20.64	-0.38
Nordenskiold Central	456	367	19%	-20%	-5.75	-13.98	-0.26
Heerland	1201	1011	62%	-16%	-9.46	-8.55	-0.16
Nathorst Land	527	409	39%	-22%	-11.68	-24.98	-0.46
Wedel Jarlsberg Land	2147	1903	66%	-11%	-47.12	-23.27	-0.43
Total	**5123**	**4325**	**47%**	**-16%**	**-86.03**	**-18.21**	**-0.34**

Southern Svalbard

The southernmost regions receive the largest amounts of precipitation on Svalbard (Winther and others, 1997), and also contain the largest glaciated area analyzed in this study. The glacier area on Nathorst Land decreased 22%, where the majority of ice loss stems from one large tidewater glacier, Doktorbreen. Elevation decreases of up to -150 m are evident on most glaciers of the area, and most glaciers experience slight increases at higher altitudes. No apparent surges can be seen in Fig 7.

Wedel Jarlsberg Land contains the largest ice area within this study, and consists mainly of ice caps and outlet glaciers with few small valley glaciers. Glaciated area decreased by 11%, with large elevation losses at the fronts of the outlet glaciers, while the upper elevations thickened. The elevation increases also suggests a potential surge-build up, especially on Polakkbreen, Finsterwalderbreen, and Amundsenisen. The elevation change pattern on Amundsenisen is similar to more recent changes measured from 1991 to 2001 (Hagen and others, 2005), although surface lowering on the southern parts of the glacier seem to be smaller during 1936/38-1990 period. One post-surge is apparent on Hessbreen, which is known to have surged in 1974 (Hagen and others, 1993). Recherchebreen surged in 1948, although this is not apparent in Fig. 7.

Elevation decreases occur in both the accumulation and ablation areas, thus the glacier has not (and maybe will not) adjusted to pre-surge altitudes.

The elevation change gradient (Fig. 5c) of Wedel Jarlsberg Land is similar to Nathorst Land, with large decreases between 100 and 200 m a.s.l., approaching zero at ~500 m.a.s.l.. A difference between the two regions lies in the hypsometry, where most of the glaciated area lies lower for Wedel Jarlsberg Land than that of Nathorst Land. The elevation change curve for Nathorst Land is slightly more negative than that of Wedel Jarlsberg land, and consequently, the annual geodetic balance for Nathorst Land is slightly more negative than that for Wedel Jarlsberg Land.

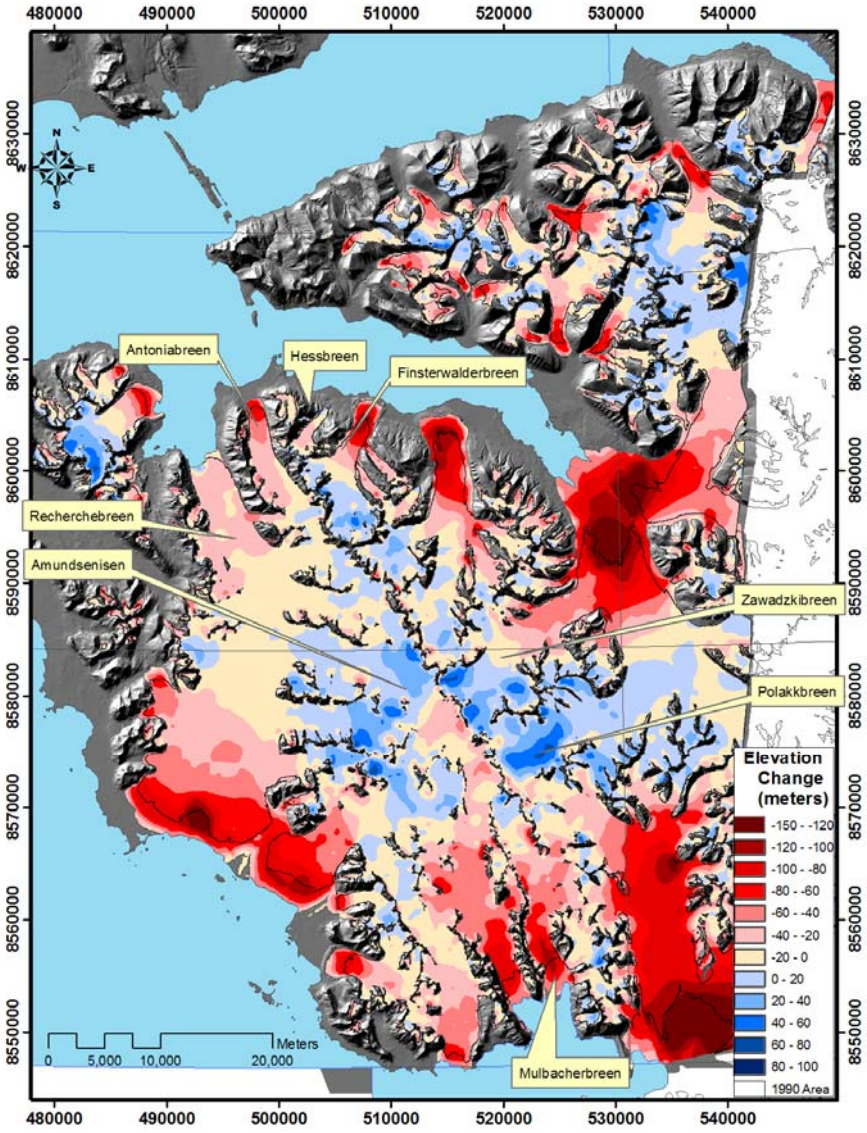

Fig. 7: Elevation change map of South Svalbard (Nathorst Land and Wedel Jarlsberg Land), 1936 to 1990.

Discussion

The use of older topographic maps for elevation data remains difficult due to the limited accuracy of the early epoch. The first proper topographic maps of Svalbard were created with oblique aerial photographs, and were tied by ground control points that were determined through triangulation from Longyearbyen (central Svalbard). The large scale biases (Mean differences in Table 2) within the non-glacier point elevation differences are attributed to ground control point errors. Local datum variations also exist within the topographic map series that can be attributed to the variation in flight lines as well as the overall topographic coverage of a particular area.

Special consideration is required when using non-glacier elevation differences to quantify errors such that statistics are representative of the glacial areas. Two parameters, slope and viewshed ('image viewability') are related to the error associated with the 1936/38 topographic maps, and are used to filter out both unrepresentative non-glacier elevation differences as well as bad data over glaciers. Moreover, as glacier elevation difference points are averaged over altitude bins, it is reasonable to assume that the errors will be minimized based upon the area of that particular bin. Spatial autocorrelation of older contours can be assessed using semi-variograms, which for the 1936/38 topographic maps show there is spatial autocorrelation up to a distance of ~500 m. By conservatively assuming that one measurement every square kilometer is uncorrelated, we believe the errors presented in Table 1 accurately express the minimization of errors in volume change and geodetic balance estimations derived from these maps.

Care must be used when determining the hypsometric elevation change averages (Δh from equation 1) from contour points. In this study, contour points extracted from the original digitization tend to be more numerous towards the edges of the glacier (due to the curvature of the contour). Long term elevation changes on the edges of a shrinking glacier are also slightly smaller than those in the center. Simply averaging contour points, therefore, creates underestimated (and unrepresentative) averages for each elevation band. Others have found that pixel averages are relatively independent of the interpolation procedure used (e.g. Andreassen, 1999) where the same underestimated trend between contour point averages is found. This emphasizes the importance in having a representative (elevation change) average for the areas from which they derive.

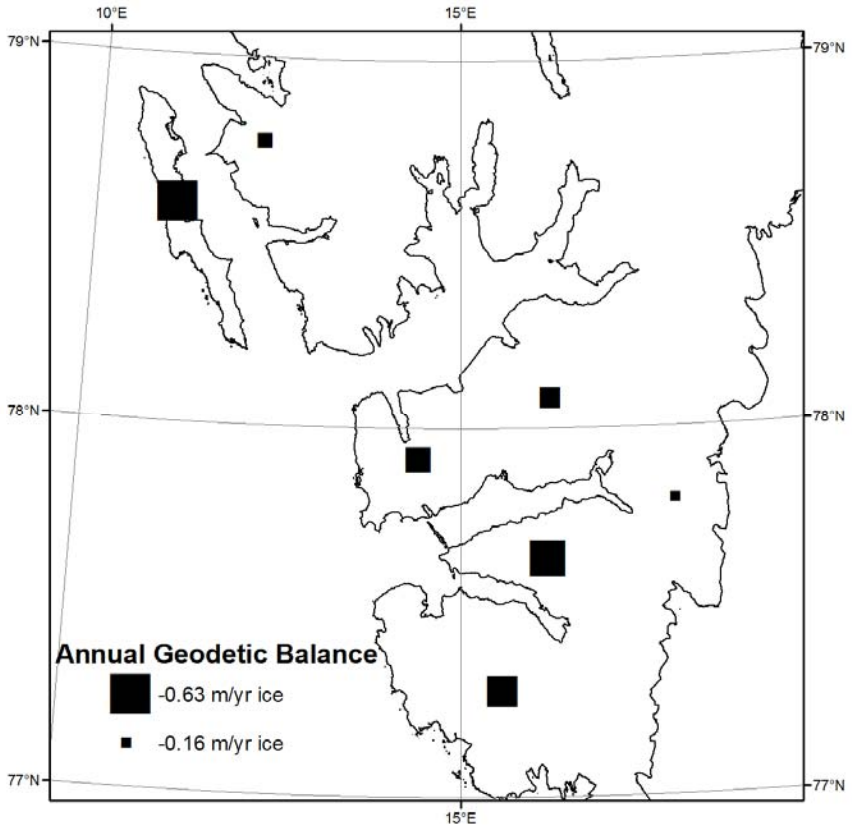

Fig. 8: Annual geodetic mass balances for the 7 regions. The most negative mass balances occur in the south and west, while less negative balances occur on the east coast and inland regions.

In the 54 year period (1936/38 – 1990), Svalbard glaciers have lost large amounts of ice, while the inner regions of the larger ice caps and fields show elevation increases. There is marked climatic regionality within Svalbard, clearly seen from the spatial variability in the relative percentage of glaciated area, as well as from the long-term geodetic balances implied by the volume changes (Table 2).

The regionality of the geodetic balance (Fig. 8) can be directly related to topography, and to climatic patterns that tend to influence Svalbard with moisture-bearing low-pressure system from the southeast (Hagen and others, 1993). Prins Karls Forland has the most negative annual geodetic balance of the regions, which results from its coastal location as well as having most of its glacial area at lower altitudes. Brøggerhalvøya/Oscar II Land, despite being situated only ~25-30 km east of Prins Karls Forland, has the 2nd least negative geodetic balance, which is attributed to a higher hypsometry as well as a more inland location. Similarly, Central Nordenskiöld has a small geodetic balance due to its interior location (drier) and higher altitude hypsometry. The

coastal regions in central Svalbard, Heer Land and Nordenskiöld West, have varying geodetic balances despite having more similar precipitation regimes than that of Central Nordenskiöld. The east coast, however, experiences more accumulation as more winter precipitation comes with easterly winds than westerly winds (Winther and others, 1997). The more negative geodetic balance of Nordenskiöld West reflects the affect of warm westerly weather systems, similar to that of Prins Karls Forland. The less negative balance of Heer Land implies a potential dominance of winter on the net balance of the east coast of Svalbard. Southern Svalbard has the most negative geodetic balances of all the regions analyzed. Nathorst Land has a slightly more negative geodetic balance than Wedel Jarlsberg Land, reflecting its location being protected from the east and south from winter storms.

Most of the regions show elevation decreases at low altitudes and increases at higher altitudes (except Prins Karls Forland). Heer Land, in particular, shows the most drastic pattern of elevation increases at higher altitudes. Five glaciers in this region have surged between 1936 and 1990 while the rest of the glaciers in the region show marked elevation increases. This is the same patterns observed during surge build-up. Nathorst Land did not have any surging glaciers in the period 1936-1990, although elevation increases are significant upon three connected glaciers (Parbreane, Svalbreen, Rokkbree) suggesting mass build up. Wedel Jarlsberg Land has had two past glacier surges (Hessbreen and Recherchebreen) during the study period, while 3 glaciers show signs of surge build-up (Polakkbreen, Zawadzkibreen, and Amundsenisen). It is not completely clear whether the elevation increases are caused by precipitation increases (Raper and others, 2005) or from slow dynamic responses (Hagen and others, 2005). The elevation change patterns and surge history of this study imply a more dynamic influence that may be controlled by climatic weather patterns.

Hagen and others (2003a & 2003b) estimated the annual mass balance of Svalbard to between -0.12 and -0.27 m a^{-1} (w. eq.), based upon data from the late 1960s to about 2000. Assuming a density of 0.9 kg/m^2, the estimated annual geodetic balances for the regions analyzed in this study is -0.30 m a^{-1} (w. eq.). The north and northeastern regions of Svalbard are presumably more in balance than the south and western regions, and thus this estimate may be slightly too negative for the entire Svalbard archipelago. Nonetheless, this estimate is in agreement with previous Svalbard estimates and represents a longer term average (1936-1990) for the central and southern regions of Svalbard.

Bamber and others (2005) estimated the average rates of thinning over the period 1996-2002 by averaging elevation differences without (hypsometric) weights for 3 glaciers in Wedel Jarlsberg Land. Their annual thinning rate estimate of -0.47 m a^{-1} for the period from 1996 to 2002 is slightly more negative than our geodetic balance estimate for the region from 1936 to 1990 (-0.43 m a^{-1}).

However, the averaging methods for the latter estimates are different and the coverage is limited within the flight line estimates. Therefore, we take the same points as in Bamber and others (2005) to determine elevation changes for three periods (Period I: 1936-1990; Period II: 1990-1996; Period III 1996-2002) for three glaciers in Southern Svalbard (Table 3). Mean annual elevation changes are obtained from an unweighted average as the point distributions are more heavily weighted towards the larger ice masses (Bamber and others, 2005). Average thinning rates are given for the individual glaciers as named in Bamber and others (2005), but emphasis is placed on the entire southern Svalbard estimate.

Southern Svalbard has experienced an increased thinning rate through the three time periods. The rate of thinning has doubled between the Periods I and II, and tripled between Periods II and III (Table 3). The profiles points are not representative for the entire Wedel Jarlsberg Land, which is apparent since the mean annual thinning rates derived from the profiles (-0.07 m a^{-1}) is much smaller than the annual geodetic balance for Wedel Jarlsberg Land (-0.43 m a^{-1}) for Period I. This discrepancy emphasizes the differences between geodetic balance estimations (area-weighted) and annual thinning rate estimates from center-line profiles.

Table 3: Mean and standard deviations (st. dev.) of *dh/dt* point estimates over 3 glaciers in Southern Svalbard between 1936-1990, 1990-1996, & 1996-2002. Profiles from Bamber and others (2005).

	1936 - 1990		*1990 - 1996*		*1996 - 2002*		*Number of*
Glacier	*mean*	*st. dev.*	*mean*	*st. dev.*	*mean*	*st. dev.*	*points*
Antoniabreen	0.08	0.13	-0.32	0.83	-0.52	0.07	33
Rechercherbreen	-0.01	0.29	0.04	0.47	-0.46	0.21	74
Mulbacherbreen	-0.46	0.54	-0.54	0.62	-0.56	0.08	23
Southern Svalbard Points	**-0.07**	**0.37**	**-0.16**	**0.64**	**-0.49**	**0.17**	**130**

Conclusion

In this study, we use old topographic maps made from oblique aerial photographs to study glacier elevation changes over a long time interval (54 years). Non-glacier land elevation differences are used to quantify the errors associated with the glacial elevation changes, while slope and viewshed (the number of aerial photographs that provide coverage of a particular point) are shown to be related to these differences. The viewshed parameter helps to remove poorly visible data points where contours may be schematic rather than derived from photogrammetry. Slope is used to create representative statistics for quantifying elevation errors over glaciers. By averaging over large areas, the errors can be greatly reduced. If careful assessment of the non-glacier land elevation differences is undertaken, older topographic maps from oblique aerial photographs provide useful glaciological information and, as in this study, provide a baseline from which modern elevation change estimates can be compared.

Svalbard glaciers (for the regions analyzed) have been retreating and losing mass in the period 1936-1990, with a 16% area decrease and a total volume change of -86.03 ± 3.64 km^3 (1.59 km^{3}a^{-1}). There is a distinct regionality to the elevation change patterns, which can be attributed to variations in topography (hypsometry) and climatic regime. Many of the regions in Svalbard experience elevation increases at the upper altitudes, which has been attributed to increasing precipitation (Raper and others, 2006) or to dynamics (Hagen and others, 2006). Finally, in southern Svalbard, mean annual thinning rates from three consecutive time periods show that that the rate of thinning has increased dramatically since 1990.

Acknowledgements

We would like to thank the Norwegian Polar Institute for providing office space, computer facilities, and data for the completion of this project. Special thanks to the Mapping Department that assisted incredibly with technical support and acquisition of the data. Acknowledgements to T. Murray and J. Bamber for providing useful comments and suggestions that greatly improved the manuscript.

Chapter 4

Modern glacier geometry and elevation changes (1936 – 1990 – 2004)

Introduction

Modern elevation change estimates provide an independent approach to *traditional* mass balance measurements for understanding glacier changes in relation to climate (Haakensen, 1986; Østrem and Haakensen,1999; Krimmel, 1999). Recently, the acquisition of elevation data over glaciers has become more efficient through digital photogrammetric techniques as well as increase use of differential GPS (dGPS) and laser altimetry (Eiken and others, 1997; Hagen and others, 2005; Krabill and others, 1999,2000; Bamber and others, 2005; James and others, 2006). In *Chapter 3*, older topographic maps coupled with a modern digital elevation model (DEM) derived past estimates of glacier elevation changes and their transformation to geodetic mass balance data. In this chapter, modern elevation changes derived from differential GPS and LIDAR altimetry data are compared to the older period changes (Chapter 3) to document glacial fluctuation on Svalbard during the past seventy years. In 2005, four glaciers in northwest Svalbard were profiled using differential GPS creating two elevation change time intervals. In 1996 and 2002, NASA's airborne LIDAR altimetry instrument was flown over Svalbard which allows three elevation change time intervals to be analyzed.

Data

An overview of the glaciers and data forms used is provided in Table 1. The earliest data are topographic maps from the photographic aerial surveys of 1936/38 made by the Norwegian Polar Institute (NPI). Maps created from vertical aerial photographs in 1966 are used in some areas where the 1936 maps do not exist. The errors have been addressed in Chapter 2; accuracy and precision is limited due to the technology available at the time, to the relatively high flying height, and to problems resulting from low contrasting glacial areas which make contour placement difficult. Chapter 3 describes the conversion from map data into long term elevation

Table 1: Overview of the glaciers and data used to create the time periods from which elevation changes and volume changes are estimated.

Glacier	1936 maps	1966 maps	1990 DEM	1995 DEM	1996 NASA profile	2002 NASA profile	2005 dGPS profile	Period I	Period II	Period III
Northwest Svalbard										
Midtre Lovenbreen	X		X				X	1936-1990	1990-2004	
Austre Lovenbreen	X		X				X	1936-1990	1990-2004	
Uversbreen	X	X	X				X	1936(66)-1990	1990-2004	
Kongsvegen		X		X			X	1966-1995	1995-2004	
South Svalbard										
Antoniabreen	X		X		X	X		1936-1990	1990-1996	1996-2002
Mulbacherbreen	X		X		X	X		1936-1990	1990-1996	1996-2002
Rechechebreen	X		X		X	X		1936-1990	1990-1996	1996-2002

and volume changes. It is shown that errors associated with volume changes and mass balances are reduced by the integration over large spatial areas.

Digital elevation models (DEM) created from vertical aerial photographs (taken in late summer) using a modern photogrammetric workstation (NPI) provides elevation surfaces from 1990 and 1995. The aerial photographs of 1990 (1:50000) covers large areas over Svalbard; however, the DEM is incomplete over Kongsvegen and thus a higher resolution DEM based on 1995 aerial photographs (1:30000) is used. The 1990 DEM has a resolution of 20 meters and a general horizontal accuracy of ±2-3 meters. The 1995 DEM has a resolution of 5 meters and a horizontal accuracy of ±1-2 meters.

During the spring 2005, dGPS profiles were acquired over four glaciers in the vicinity of northwest Svalbard. Kinematic dGPS is collected using two survey grade recievers, one moving rover that is towed behind a snow-mobile (see Eiken and others, 1997), and a fixed reference station. The reference station is located no further than a distance of 30 km from the kinematic profiles. An in-depth study on the accuracy and application of dGPS on glaciers in Svalbard (Eiken and others, 1997) concluded that an accuracy of ±10 cm can be achieved when at least 5 satellites are available with good geometry (PDOP<5) and less than a 3 second logging interval is used. A 1 second logging interval is used and the post-processed profile points are filtered for satellites and good geometry.

Elevation profiles over southern Svalbard acquired using NASAs Automatic Topographic Mapper 3 (ATM), a laser altimeter with a nominal vertical accuracy of ~10 cm (Krabill and others, 2000). The profiles were measured in May 1996 and 2002, so the measured glacier elevations include the end of winter snow depths.

Glacier descriptions

The two small glaciers of this study (< 10 km^2), Midtre and Austre Lovenbreen, are located adjacent to Ny Ålesund in Kongsfjorden, north-west Svalbard (Fig 1). Midtre Lovenbreen contains the longest continuous high arctic mass balance series with traditional measurements beginning in 1967. The glacier has been losing mass and retreating since 1967, with a mean annual net balance of -0.34 m w.e. and only 5 positive balance years out of 27 (Lefauconnier and others, 1999). Austre Lovenbreen is of a similar size and type of glacier located adjacent to Midtre Lovenbreen (Fig 1).

Kongsvegen is the largest studied glacier of the area and spans the highest altitudes. It is a polythermal surge-type glacier (Liestøl, 1988) consisting of a relatively thick warm ice layer (Björnsson and others, 1996) with the last documented surge in 1948 (Hagen and others, 1993). Presently, it is believed to be in a quiescent phase, building up to a new surge (Melvold and Hagen, 1998; Hagen and others, 1999; Hagen and others, 2005). Traditional mass balance measurements exist from 1987, with an annual average balance of +0.11 m w.eq. from 1987 to 1997 (Lefauconnier and others, 1999). Good correlation found between the net balances of Kongsvegen and Austre Brøggerbreen allowed a reconstruction of the net balance back to 1967 where an average net balance of +0.04 m. w.eq. is estimated for the period from 1967 – 1994 (Melvold and Hagen, 1998).

Uversbreen is a medium sized glacier located adjacent to Kongsvegen (Fig 1). The area is half the size of Kongsvegen and nine times larger than Midtre and Austre Lovenbreen. The glacier spans the same area-altitude distribution of the two smaller glaciers. No mass balance or velocity measurements are available. Ground penetrating radar profiles over the central region showed that of the cold ice layer is much thicker than that of Kongsvegen (Björnsson and others, 1996).

Methods

The Period I changes are compared to modern estimates over four glaciers in Northwest Svalbard and along two profiles in south Svalbard. For northwest Svalbard, the dGPS profiles are spatially representative, that is, elevation points are located both along the center line and along the edges; therefore, geodetic annual balances are estimated. The NASA altimetry profiles (Bamber and others, 2005) are center line estimates of elevation change and do not contain

spatially representative data. Geodetic balances are therefore not estimated, instead mean elevation changes are provided.

For Period I estimates, the 1936 (66) contour points are converted from European Datum 1950 to WGS 1984 to make them comparable to the 1990 DEM. Elevations from 1990 are extracted at contour points and further analyzed using a hypsometric method (see Chapter 1 and 3). Elevation change maps are created using an iterative finite difference interpolation technique (Hutchinson, 1989).

Period II changes are derived in a similar manner by comparing the recent profiles (dGPS and LIDAR) to the 1990 (95) DEM. Ellipsoidal elevations from the profiles must be converted to geoid heights, so they are comparable to the DEMs; a constant geoid ellipsoid difference based on an average of 2-3 reference stations in the local vicinity is used. Although a spatially variable conversion factor is preferential, a constant should not introduce a systematic bias greater than ~0.2-0.3 m.

For northwest Svalbard, spatially representative dGPS profiles acquired in spring 2005 provide elevation points and snow depths, through probing at a distance interval of 100-500 meters (Fig. 1). Snow depth maps for 2005 are spatial interpolations (Hutchinson, 1989) of the individual snow measurements. Subtracting snow depths from the 2005 elevations yields the 2004 summer surface. The 2004 surface is then more directly comparable to the 1990 summer surface (DEM).

Total volume change is calculated by taking the average elevation change within individual altitude bands multiplied by the glacier hypsometry (see chapter 3, eq. 2). The hypsometry from the map with the larger glacier area is used. Elevation change curves for Period I are determined through pixel averaging of the interpolated elevation change surfaces. Period II curves are estimated by averaging dGPS points within the elevation bins. As the points are fairly well distributed spatially, there is little difference between the point and pixel averages.

In forming the average elevation change, we divide total volume change by the average of old and new areas (eq. 7, chapter 1). For Austre Lovenbreen and Kongsvegen, the 2004 area is not available. Therefore, Period II estimates are derived using only the original area (1990 or 1995), and the balance calculations underestimate the actual balance. These particular glaciers are retreating where the older area is larger than the average, making geodetic balances less negative.

Fig. 1: Snow depth maps from 2005 over the four northwest glaciers with dGPS profiles, snow depth points, and 1990 contours.

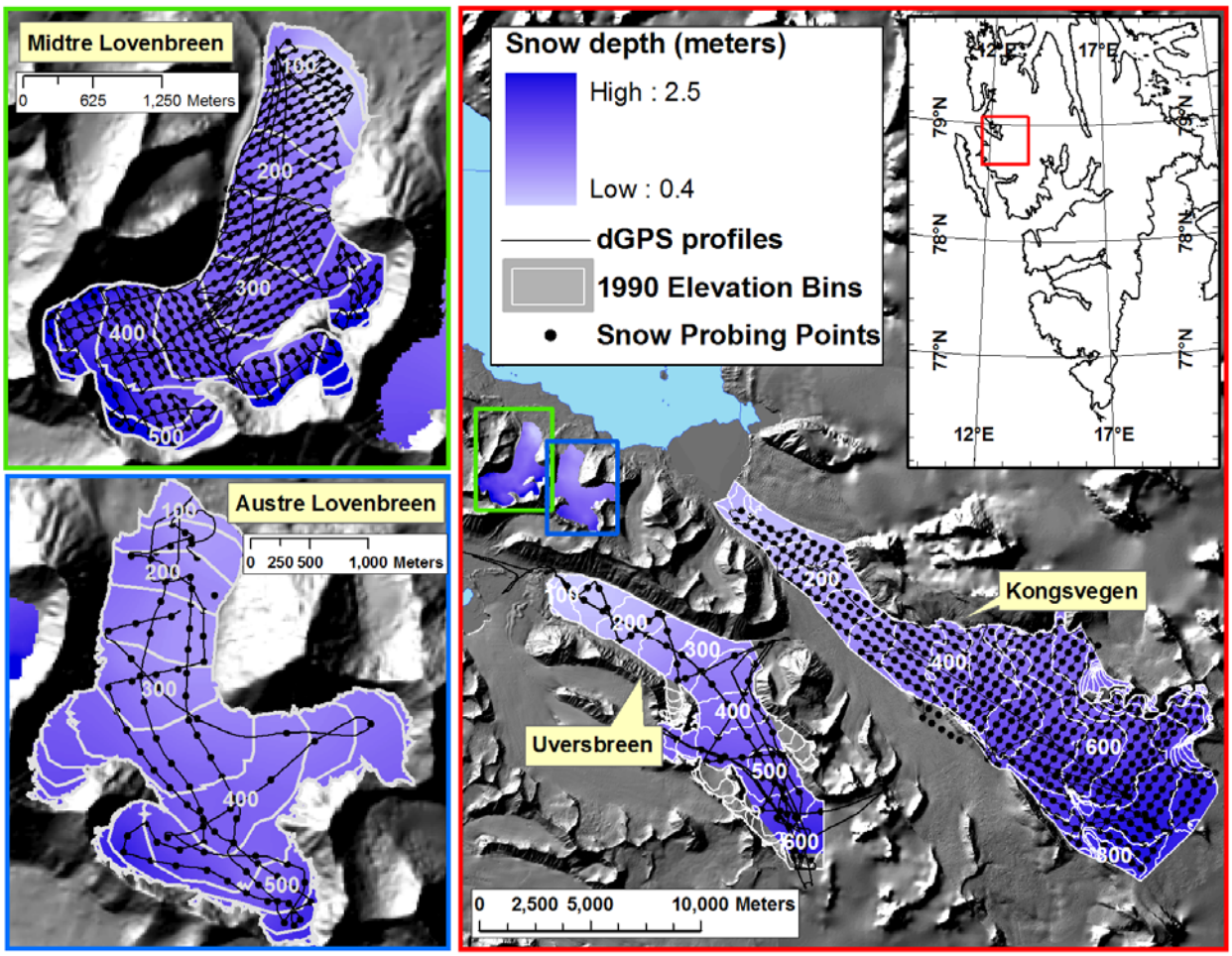

Conversely, if the glacier were advancing, the use of an older area, less than the average, overestimate geodetic balances. In addition, Period I volume changes are not estimated for Uversbreen as the data do not come from a single map year; the lower elevation contours are from 1936 while the higher contours are from 1966.

Two important considerations are that of density conversion and the timing of elevation acquisition. Elevation changes are not converted into water equivalent; all numbers are in ice equivalent. A variable water equivalent conversion can be used if the elevation of the snow line during the time of data acquisition is known (Krimmel, 1999), or through a weighted average by the relative area percentage of the ablation, accumulation, and firn areas (Sapiano and others, 1998). For glaciers with high-mass turnover and large ablation rates, the timing of data acquisition should be corrected for additional emergence and ablation that occurs if the

acquisition date is before the end of summer (Andreassen, 1999; Cox and March, 2004). For Period I, both surfaces are for the end of the summer while the long time interval minimizes the importance of any potential adjustments. During Period II for northwest Svalbard, the 2004 summer surface is derived by subtracting measured snow thicknesses while the 1990 DEM is a summer surface. However, the NASA profiles of southern Svalbard are measured in May. So this difference needs to be accounted for as the later period data have an additional snow thickness. This study ignores the difference as no snow depth data exists in the area, and thus estimates contain a systematic bias (the 1996 and 2002 elevations are too high), such that elevation decreases are underestimated and increases overestimated.

Errors

The accuracy of the Period I estimate is discussed in detail within Chapter 2, where it is found that the largest error source is associated with misplaced contours. The error is minimized in volume change estimates through integration over large areas. When analyzing changes over individual glaciers, the error is not greatly reduced due to the smaller areas. Additionally, only a few airphotos from the same flight line are used. Non-glacier elevation differences are used to get a handle on the errors associated for each individual glacier. Points located over slopes greater than 20 degrees are removed as significant vertical errors result from horizontal errors over steep slopes. For Midtre and Austre Lovenbreen, the resulting points consist of those in front of the glacier. For the larger Uversbreen and Kongsvegen, low-sloped nunatak tops are included to provide a more representative estimate of the bias between the maps. The error estimations for the volume change and the annual geodetic balances are derived through the methods described in the *Errors* of Chapter 3 and presented in Table 2.

The GPS profiles result in high accuracy elevation data. The largest uncertainty arises from converting from ellipsoid to geoid heights, which could lead to a systematic shift in the elevation changes. The error associated with an elevation change point (ε) is estimated through a root mean square of the accuracies associated with the 1990(95) DEM and the dGPS points. The DEMs are considered to contain a general accuracy of 3 meters. The dGPS points were conservatively estimated to contain an accuracy of 2 meters which incorporates random elevation errors (±0.5 m), random errors resulting from the snow depth subtraction (±0.5 m), as well as

potential systematic errors (±1 m). The resulting transformation into volume change and annual geodetic balance errors is presented in Table 2.

Table 2. Error estimates for the Northwest Glaciers. The mean difference is the bias used to adjust the changes, ε is the error within an individual elevation change point, ε_V is the volume change error and ε_B is the error in the annual geodetic balance.

	Period I: 1936(66) - 1990(5)				Period II: 1990(5)-2004		
Glacier	Mean difference	ε	ε_V (km^3)	ε_B (m)	ε	ε_V (km^3)	ε_B (m)
Midtre Lovenbreen	-2.1	4.72	0.04	0.13	3.6	0.03	0.37
Austre Lovenbreen	6.7	9.04	0.08	0.24	3.6	0.03	0.36
Uversbreen	-0.4	9.68	-	-	3.6	0.09	0.12
Kongsvegen	-1.0	7.97	0.36	0.10	3.6	0.16	0.15

Results

Northwest Svalbard

Midtre Lovenbreen lost ~0.12 km^3 of ice since 1936. The rate of area decrease was ~0.03 km^2 a^{-1} during Period I and ~0.02 km^2 a^{-1} during Period II (Table 3). The elevation change curves (Fig 3) demonstrate the entire glacier is thinning more rapidly during Period II and is generally down-wasting (Fig 2). The annual geodetic balance for Period II (-0.55 m a^{-1}) is more than double that of Period I (-0.23 m a^{-1}). For Austre Lovenbreen, the area decreased by 28% during the early epoch from 7.53 to 7.42 km^2. An area for 2004 is not available, and thus Period II geodetic balances are underestimates. During Period I, the front thinned ~1 m a^{-1} while slight increases are seen in the upper cirque regions (Fig. 2). During Period II the entire glacier loses elevation (Fig 3). Austre Lovenbreen experienced a volume loss of -0.09 km^3 and -0.03 km^3 ice with annual balances of -0.25 and -0.44 m a^{-1} ice equivalent for Periods I and II, respectively. Similar to Midtre Lovenbreen, the geodetic balance for Austre Lovenbreen has nearly doubled between the two time periods.

During Period I, Kongsvegen retreated by ~4 km and lost approximately 0.77 km^3 of ice (Table 3). The front averaged elevation losses of 1.8 m a^{-1} (Fig 3) with maximum thinning rates at the center line of 2-2.5 m a^{-1}. The accumulation area experienced maximum and average increases of ~1.5 m a^{-1} and 0.5 m a^{-1}, respectively. Melvold and Hagen (1998) compared the same 1966 maps with dGPS center line profiles obtained in 1991 to determine that the front was

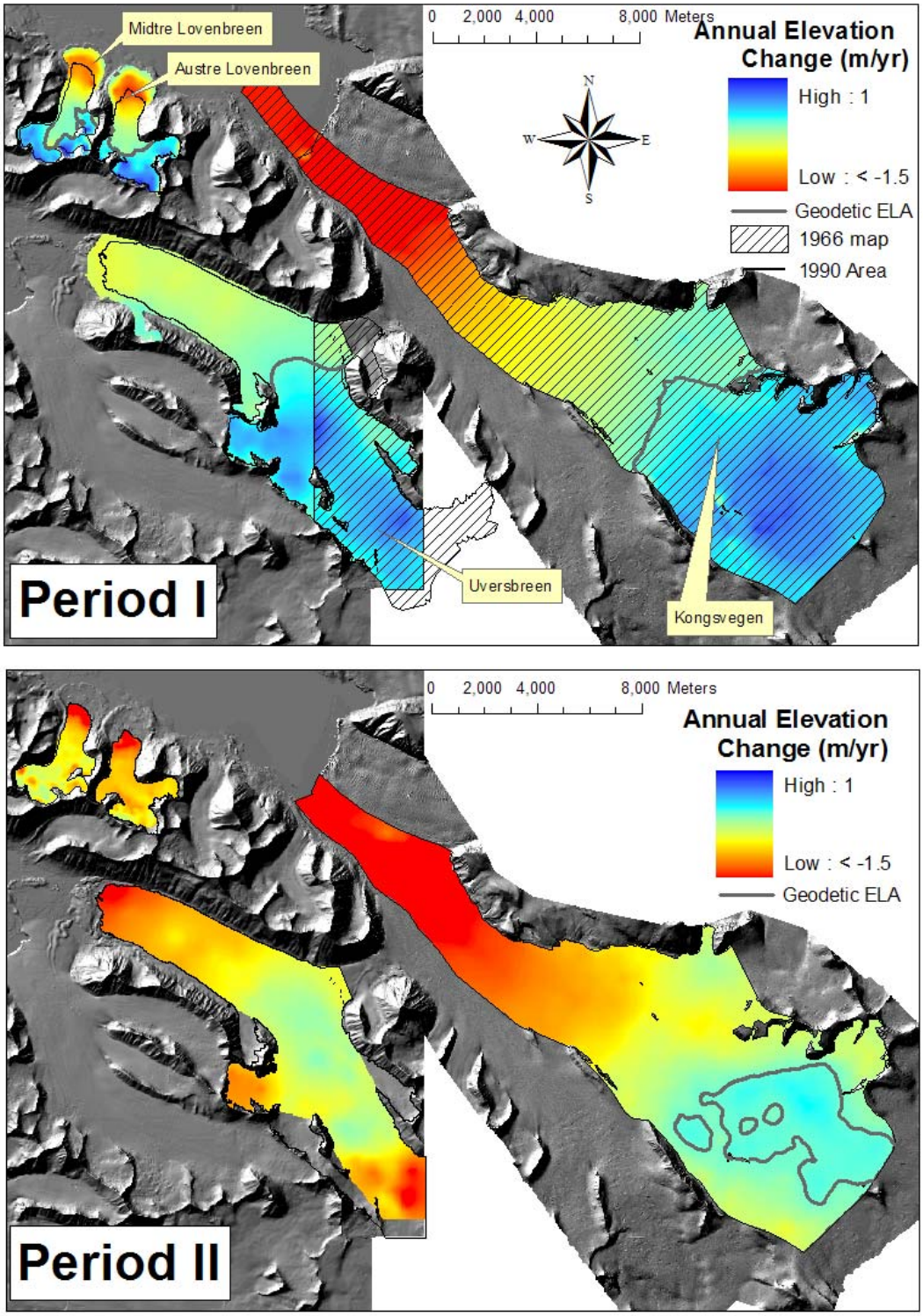

Fig. 2: Elevation changes of the 4 glaciers of northwest Svalbard. The period I changes (top) include 1936-1990 differences over Midtre and Austre Lovenbrenn, 1966-1995 differences over Kongsvegen. The lower altitudes for Uversbreen are from 1936-1990 while the upper altitudes are from 1966-1990. Period II is from 1990-2004 for Uversbreen, Midtre and Austre Lovenbreen, and from 1995-2004 for Kongsvegen.

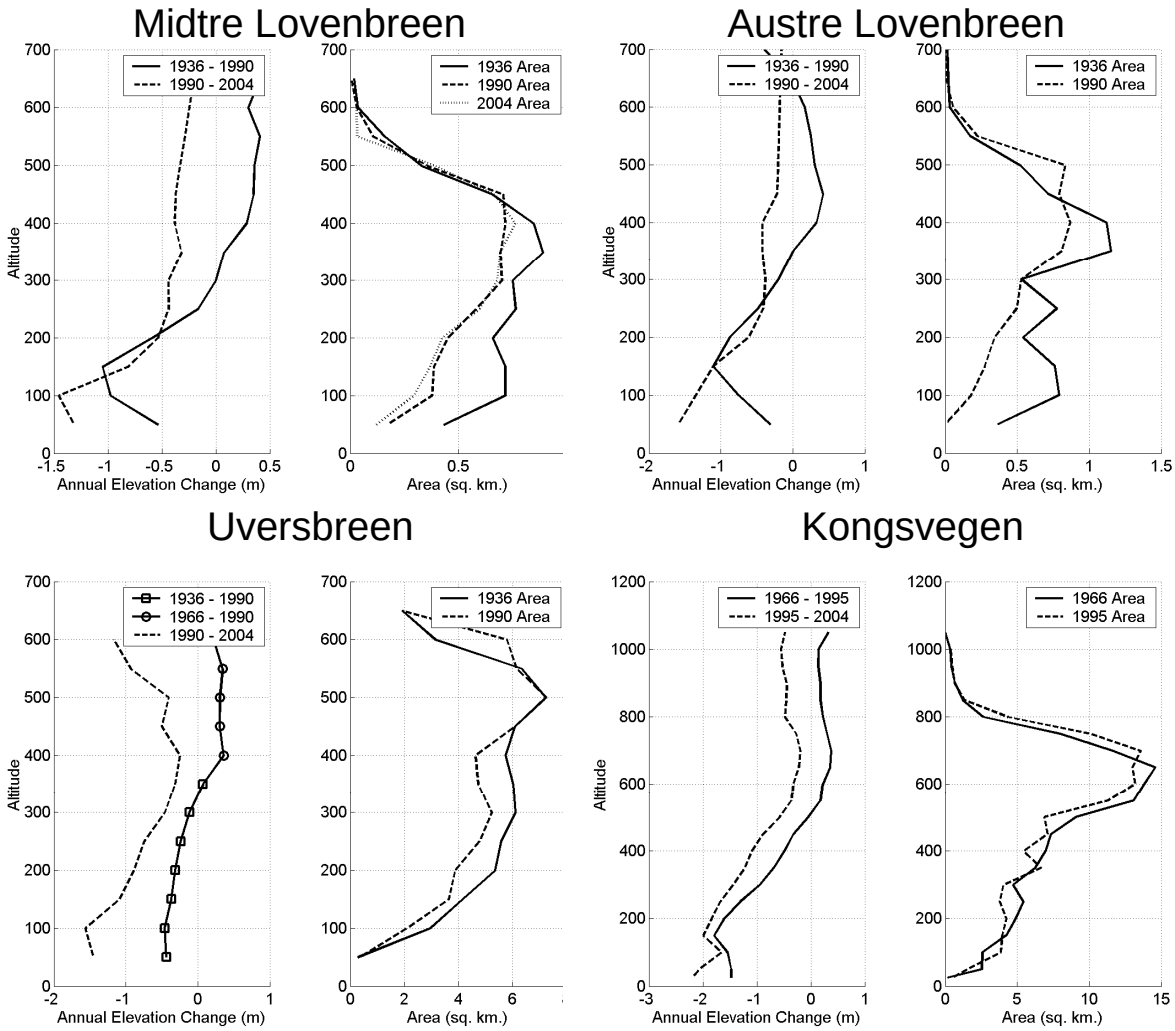

<u>Fig. 3:</u> Elevation change curves and hypsometry of four northwest Svalbard glaciers for Period I and II. The Period II curves are all shifted to the left (more negative) from the Period I curves implying more rapid thinning during Period II.

thinning by up to 2.5 m a^{-1} while the upper glacier was increasing ~0.75 m a^{-1}. The difference between the two studies is that center line estimates (Melvold and Hagen, 1998) represent the maximum changes, while hypsometrically average elevation changes are slightly lower than the maximum. Nonetheless, the slow build-up in the accumulation area is attributed to continual quiescent phase build up despite the significantly negative geodetic balance for Period I. The negative annual average balance does not agree with the reconstructed net balances of Kongsvegen back to 1967, suggesting a weakly positive balance (Melvold and Hagen, 1998).

During Period II, the front had averaged thinning rates of 2 m a^{-1} while the accumulation area experienced, on average, only slightly negative average elevation changes (Fig. 3). The

geodetic ELA migrated considerably up glacier between the two periods (Fig. 2). The area in which elevations increase decreased significantly between Period I and Period II. Similarly, Hagen and others (2005) found smaller upbuilding from 1996-2004 (0.2-0.3 m a^{-1}) as compared to 1992-1996 (0.5-0.7 m a^{-1}) from center line profiles.

The average elevation change curve is more negative in Period II than in Period I with a geodetic balance which is more than three times as negative in Period II compared to Period I. The Period II balance is slightly underestimated as only the older, larger, area is used in eq. 7 of chapter 1. More importantly, the Period II balance may be excessively negative as losses in the upper glacial regions are assumed to consist entirely of ice. The assumption of ice equivalent density ignores firn loss and the potential of internal accumulation where decreases at higher altitudes may be explained by firn densification. Although the magnitude of loss is most likely overestimated, the more negative geodetic balance during Period II agrees with the increasing negative annual mass balance measured on Kongsvegen since 1998 (pers. comm. Kohler, 2006).

For Uversbreen, it is difficult to estimate a volume change and geodetic balance due to the very different initial map years. The earliest epoch maps are composed from vertical photographs taken in 1936 for the lower altitudes (<350 meters) and 1966 for the upper altitudes. The glacier experienced small decreases from 1936 to 1990 at the front where thinning is less than on the smaller glaciers. Average increases of ~0.5 m a^{-1} are experienced at upper altitudes from 1966 to 1990 (Fig 3), similar to that of Kongsvegen.

During Period II, elevation changes are entirely below zero for all elevation bands (Fig. 3). The elevation change pattern seen in Fig 2 shows that the upper altitudes experienced surface lowering similar to that at the front of the glacier, while the central part of the glacier experienced close to zero change. One possible explanation is that a dynamical event may have occurred in the upper regions, with transport of mass to the central region through a "mini-surge". An alternate hypothesis is that an observed surge on neighboring Osbornebreen (Rolstad and others, 1997) affected the upper altitudes of Uversbreen with ice transported in the opposite direction. This seems unlikely as the accumulation area of Uversbreen is a considerable distance, divided by numerous nunataks, from Osbornebreen. A third explanation may be that of firn densification, however, the magnitudes of losses required at upper altitudes through densification are unreasonably large.

In summary, these four glaciers of northwest Svalbard experience negative volume changes and geodetic balances. The geodetic balance for the two smaller glaciers is similar to that of the larger Kongsvegen during Period I although the time periods for the smaller glaciers extend farther back in time. During Period II, elevation changes and annual geodetic balances are more negative than for Period I. The difference in balances from Period I to Period II is more extreme on Kongsvegen than that of the smaller glaciers implying a larger, possibly more complex, response of larger glaciers on Svalbard to the changing climate. However, Kongsvegen is a surge type glacier which may play a role in the observed pattern of elevation changes.

Table 3: Area, volume changes, and annual geodetic balances of the four glaciers in northwest Svalbard for Period I (1936-1990/5) and Period II (1990/5-2004).

	Area (km^2)			*Volume Change (km^3 ice)*		*Annual Geodetic Balance (m ice/yr)*	
Glacier	***1936***	***1990***	***2004***	***36-90***	***90-04***	***36-90***	***90-04***
Midtre Lovenbreen	7.00	5.31	5.07	-0.08	-0.04	-0.23	-0.55
Austre Lovenbreen	7.53	5.42	-	-0.09	-0.03	-0.25	-0.44
Uversbreen	61.15	56.82	-	-	-0.54	-	-0.89
Kongsvegen	120.70	116.05	-	-0.77	-0.74	-0.22	-0.71
Total	**196.38**	**183.60**		**-0.94**	**-1.35**		

South Svalbard

Southern Svalbard was surveyed by NASA's LIDAR profiler in May 1996 and 2002 (Bamber and others, 2005). Average elevation changes between flight lines analyzed for three glaciers correspond to areas from which the 1990 DEM (NPI) is compiled. The exact points were taken from Bamber and others (1995) to perform the analysis which is originally presented in the Discussion of Chapter 3. This section will briefly address the comparison of those points within three time periods; Period I: 1936-1990, Period II: 1990-1996, and Period III: 1996-2002. Large variability exists between the elevation change points, especially from 1990 to 1996. Therefore, the original NASA flight lines from 1996 are compared to the 1990 DEM and to the Period I changes to examine the large variability seen between 1990 and 1996.

The points from Bamber and others (2005) consist of 300 meter, along track, averages. This was done to minimize the affect of surface roughness (random errors) and crevasse migration on the individual point elevation changes. Two points were placed adjacent to each other in the accumulation area to more heavily weight the upper areas in the unweighted averaging scheme. To compare the older time period with these points, Period I elevation

changes are averaged over a diameter of 300 meters, extracted to the point dataset, where the mean results in an average annual dh/dt estimate.

Results are presented in Table 4, and emphasis is placed upon the entire southern Svalbard estimate as the points associated with Bamber and others (2005) do not spatially represent the glaciers for which they are named. In fact, the points associated with Antoniabreen are not located over the glacier at all, but over an adjacent cirque region of Recherchebreen.

Table 4: Annual dh/dt averages (unweighted) for points used in Bamber and others (2005).

	Period I 1936-1990		Period II 1990-1996		Period III 1996-2002		
Glacier	**mean**	**st. dev.**	**mean**	**st. dev.**	**mean**	**st. dev.**	**Number of points**
Antoniabreen	0.08	0.13	-0.32	0.83	-0.52	0.07	33
Rechercherbreen	-0.01	0.29	0.04	0.47	-0.46	0.21	74
Mulbacherbreen	-0.46	0.54	-0.54	0.62	-0.56	0.08	23
Southern Svalbard Points*	**-0.07**	**0.37**	**-0.16**	**0.64**	**-0.49**	**0.17**	**130**

The rate of thinning for southern Svalbard has doubled from Period I to Period II, and nearly tripled from Period II to Period III. Period II thinning rates are underestimated as the 1996 profile was acquired at the end of winter while the 1990 DEM is from the end of summer; i.e. 1996 elevations contain snow thicknesses that decrease by the end of the summer. Nonetheless, similar thinning trends are apparent in the northwest region where annual geodetic balances have also become more negative. A difficulty in comparing the northwest geodetic balance estimates with this south Svalbard estimate is whether the unweighted estimating procedure properly represents the hypsometry for southern Svalbard. Additionally, the center line points may not be spatially representative for the edges of the glacier.

Table 4 also shows the large elevation change variation during Period II as compared to Periods I and III. The 300 meter averaging scheme used for the points in Table 4 hides local variation making spatial analysis and interpretation of the point dataset difficult. Therefore, the original 1996 NASA profile elevations are analyzed spatially (Fig. 4) to better visualize the changes. Since the 1996 profile was acquired at the end of winter when snow depths are at a maximum, the 1996 profile is too high as compared to the 1990 summer surface. Therefore, elevation decreases during Period II are underestimated, while elevation increases are overestimated. No attempt to adjust the data is done, implying that the elevation changes do contain a small systematic bias.

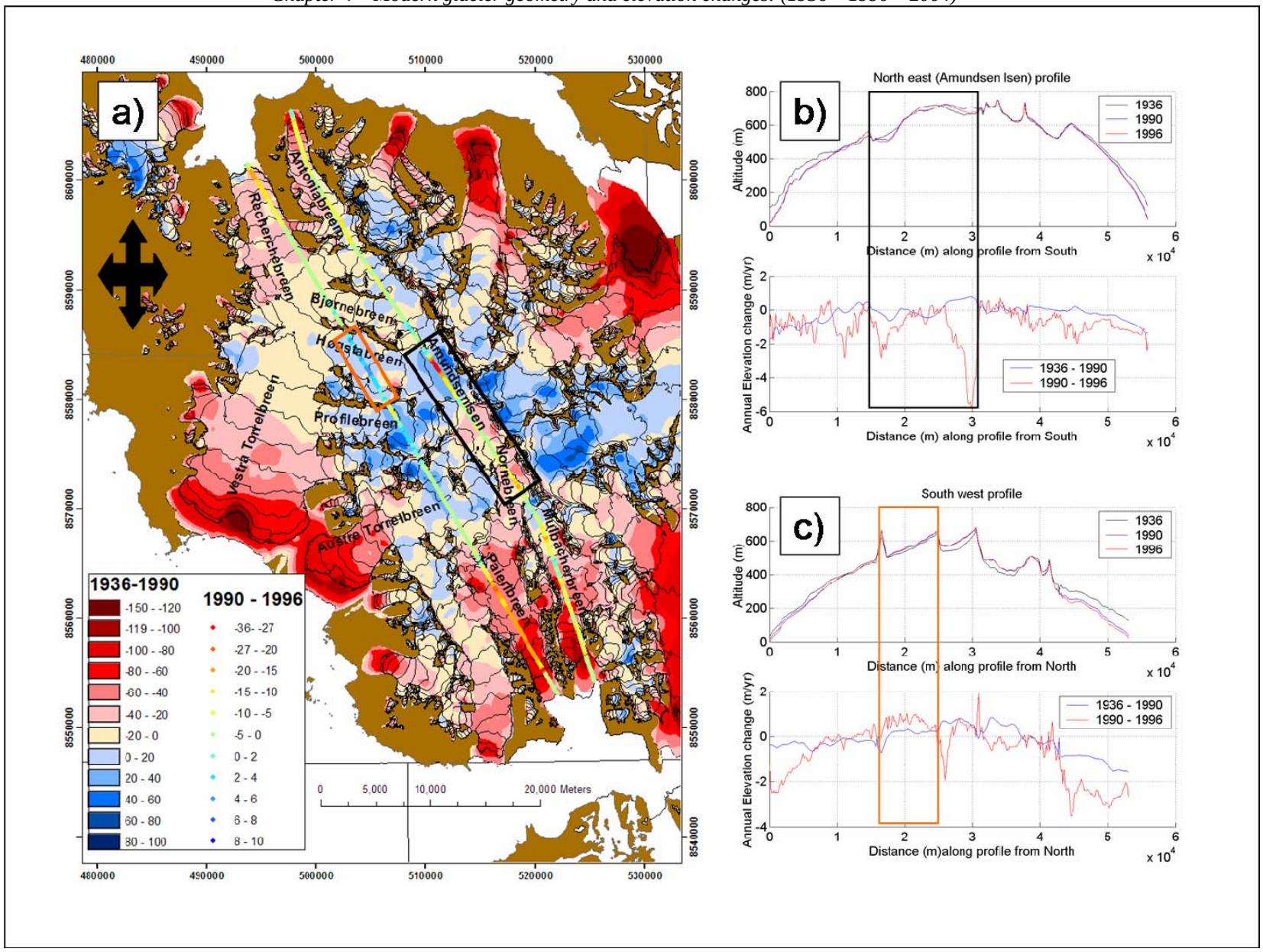

Fig. 4: (a) 1936-1990 elevation change map of Wedel Jarlsberg Land with the 1990 – 1996 profile elevation changes.
(b) The northeast distance elevation profile covering Amundsenisen (top) along with the annual elevation changes (bottom).
(c) The southwest distance elevation profile (top) and the annual elevation changes (bottom).
The boxed insets in figs. 4b and 4c correspond to the colored boxes in fig. 4a.

The general pattern is losses at the glacier snouts, and variable increases and decreases in the upper areas (Fig 4). The rate of frontal thinning (the beginning and end of the profiles) is more negative during Period II than Period I, especially on the southwest profile covering Recherchebreen and Paeirlbreen (Fig. 4c). More elevation change variability exists for the outlet glaciers of the northeast profile during Period II (Fig. 4b). Antoniabreen shows annual thinning rates of ~0.5 and ~1 m a^{-1}, for Period I and II, respectively. Mulbacherbreen presents a complex negative signal (Fig. 4b) during Period II that either may indicate a surge (upper altitudes experienced decreases of up to 3 m a^{-1} while the lower elevations show a noisy signal of elevation decreases), or reflect the location of the flight line which is positioned close to the valley sides.

Amundsenisen, covered by the northeast profile, experiences a varying pattern of elevation changes during Period I (Fig 4a and 4b), dominated by elevation increases (~0.5 m a^{-1}) towards the north and slight decreases (~0-0.5 m a^{-1}) in the south. During Period II, extreme decreases (~6 m a^{-1}) occur on the north part of the ice cap while slight decreases (~0-2 m a^{-1}) continue to occur on the south part of the ice cap. The pattern suggests a gradual buildup of the north part of Amundsenisen during the long 54 year Period I, with a large dynamical event occurring during the short 6 year Period II that resulted in losses of 36 meters.

Nornebreen connects the southern portion of Amundsenisen to Paierlbreen. There are relatively small changes (-0.5-0 m a^{-1}) during Period I and larger decreases (up to -3 m a^{-1}) during Period II. The location of the extreme decreases during Period II coincides with the presence of large crevasses noted in 1991 by Hagen and others (2005). Whether the extreme decreases of Nornebreen are related to those of Amundsenisen is not clear. However, patterns on Høgstabreen, a glacier draining the northern part of Amundsenisen into the confluence of Vestre Torrelbreen and Rechecherbreen, suggest small thickening (0.2 m a^{-1}) during Period I with larger thickening (0.5-1 m a^{-1}) during Period II. An interpretation of this spatial pattern of elevation changes is that the ice cap of Amundsenisen migrated northwards from Nornebreen during Period I with a type of mini-surge during Period II that transported ice into the adjacent Høgstabreen.

The southwest profile does not cover one particular glacier, but cover the fronts of Recherchebreen and Paierlbreen and crosses tributary glaciers of Bjørnebreen, Høgstabreen, Profilebreen, and Austre Torrelbreen. Thinning rates at the fronts of the outlet glaciers are larger for Period II than Period I with decreases of 3 m a^{-1} and 2.5 m a^{-1} on Paierlbreen and Rechecherbreen, respectively. The rates of thinning for the glacier fronts of the southeast profile

are also greater than those for the northeast profile. The accumulation area for Austre Torrellbreen experienced increases (~0.5-0.7 m a-1) during Period I and decreases of 0.5 m a^{-1} during Period II. The pattern between increases and decreases of the two periods correspond (see Fig 4c, 3.2 – 3.7 * 10^4 m). Profilebreen generally experienced elevation increases close to 1 m a^{-1} during Period I and II. However, a small region towards the north experiences large elevation decreases (~2 m a^{-1}) during Period II. The elevation of Bjørnebreen, a tributary of Recherchebreen, remains relatively stable within all epochs.

In summary, the thinning rates at the front of the outlet glaciers are larger during Period II than for Period I, and are also larger on Recherchebreen and Paierlbreen (Fig 4c) than on Antoniabreen and Mulbacherbreen (Fig 4b). The upper altitudes consist of a mixed elevation change signal of increases and decreases that seem to be related to dynamical events affecting Amundsenisen, Nornebreen, Høgstabreen, Mulbacherbreen, and a small section of Profilebreen.

Discussion

Glacier surface elevation changes provide an independent approach towards analyzing the mass balance and variations of the glacier surface through time. A single point elevation change upon the glacier is both a function of climate and dynamic changes. Climatically, the glacier surface elevation changes in response to varying accumulation and ablation. Dynamically, the elevation changes through submergence and emergence of ice as well as to large-scale surge events which create extreme changes. The relationship between elevation change in terms of both climate and dynamics is defined in equation 7 of chapter 1. Assuming steady state dynamics, emergence and submergence of ice is equal when integrated over the entire glacier surface.

A glacier is rarely in steady state, however. For a non-surging glacier, the dynamical response of a glacier is slow in relation to the climatic forcing (Johannesson, 1989) such that a time lag exists between dynamic adjustments due to varying climate. Therefore, the assumption of steady state dynamics generally holds when integrating long term elevation changes over the entire surface, as the magnitudes of the elevation changes are much larger than the ice fluxes (Paterson, 1994).

A surging glacier, however, experiences a rapid dynamic response in relation to the slower climatic forcing; a different situation as that described by Johannesson (1989).

Nonetheless, conservation of mass implies that integration of the changes over the entire surface results in the dynamical terms canceling in equation 2. The difficult question is to assess the degree to which a large scale dynamical event (surge) has on the interpretation of annual elevation changes and geodetic balances in relation to climate.

Elevation data (contour maps, DEMs, and elevation profiles) across a glacier surface represent a snapshot of the surface at a time. The difference between two glacier surface 'snapshots' is the volume change of the glacier within the time period (assuming bedrock beneath the glacier has not changed), independent of the history behind those changes, whether climatically or dynamically driven.

Elseberg and others (2001) and Harrison and others (2001) attempt to differentiate the climatic and dynamic components of the mass balance by introducing the concepts of a *reference* ("*climatic*") surface and *conventional* surface mass balance. The concept is built upon response time theory from Johannesen and others (1989) such that Harrison and others (2001) derive a functional relationship between area and volume changes that specifies dynamic behavior. This relation combined with the statement of conservation of mass results in a simple approach to understanding glacier response to climate. A reference surface mass balance is the mass balance performed over the original area coupled with two adjustment parameters that account for the area and volume changes (geodetic balances). The cumulative reference surface mass balance in their study is more negative than the conventional due to the recession of the terminus which reduces the size of the ablation area bringing the glacier closer to equilibrium, and the surface lowering which shifts the balance into a more negative regime. Previous studies demonstrate that the conventional (traditional) mass balance may not always reflect trends in climate, and that "by removing the effects of changing surface configuration on mass balance, reference surface balances are more closely related to climatic trends" (Elseberg and others, 2001).

The previous discussion emphasizes the notion of the geodetic volume change as derived from two snapshot glacier surfaces in time and its independence from the factors that cause the changes. In a simple retreating glacier, where dynamics are less important, the geodetic balance can easily be explained by climatic variations of ablation and accumulation. For larger glaciers, especially on Svalbard, geodetic volume change and balance analysis is complicated by surges. After a surge, more ice is available for melt in the ablation area while submergence in the accumulation area is reduced. The glacier surface therefore slowly re-builds back to a quasi-

equilibrium position in response to the surge (the quiescent phase). During the quiescent phase, the surface mass balance, which reflects the climatic variables of accumulation and ablation, remains similar; however, the drastic elevation changes caused by the surge may slightly affect the meteorlogical variables associated with mass balance as they are typically functions of altitude (Oerlemans and Hoogendoorn, 1989). Nonetheless, the fact that ice fluxes decrease dramatically after a surge suggest that the surface mass balance and geodetic balance should be similar in this post-surge period.

Volume change estimates and associated geodetic balances can be interpreted by climatic changes assuming steady-state response time theory of Johannesson (1989). A surge occurring close to the elevation change time period, however, greatly complicates the signal, and thus consideration of dynamical events is critical in relating elevation and volume changes of Svalbard glaciers solely to climatic factors.

The Dynamic signal

Analysis of the elevation changes presented is complicated by numerous surge and surge-like events. For example, Kongsvegen surged in 1948; the elevation change map (Fig. 2) for Period I shows the typical quiescent phase build up. The front of the glacier has retreated by over 4 km since the surge during Period I. The Period II changes however show that the area of buildup is decreasing, while the entire hypsometrically averaged elevation change in the accumulation area is negative. This may be explained in part by firn loss and/or densification, but nonetheless implies that buildup is slowing more recently, similar to findings by Hagen and others (2005). Whether the elevation signal in Period II is typical for the end of the quiescent phase is difficult to say without looking at glacier velocities. Another possibility is that the signal presented in Period II is the result of climate with increased temperatures shifting the ELA up glacier, and additional melt at higher altitudes is causing firn loss and internal accumulation responsible for the elevation losses in the accumulation area.

Uversbreen may have experienced a near equilibrium mass balance from 1936 to 1990 since frontal thinning is lower than that of the smaller glaciers Midtre and Austre Lovenbreen (Fig 2). Thickening from 1966 to 1990 is similar to that experienced on Kongsvegen (Fig 2). The elevation increases in the accumulation area during Period I suggest potential build up of a surge-type glacier. Period II changes look remarkably like a mini-surge, with the accumulation

area decreasing in elevation similar to the front, and the central regions remaining close to zero. If the pattern is indeed a surge, then it appears to have progressed half way down the glacier before stopping at the center of the glacier. Part of the reason the "mini-surge" may not have reached the front of the glacier is the presence of a relatively thick cold layer (Björnsson and others, 1996). If bedrock freezing is occurring at the front, the connection between frontal ice and the underlying rock may be strengthened, hindering basal slippage. Moreover, the proposed central glacier surge termination corresponds with the location of a glacier damned lake, setevatnet (Liestøl, 1977), and therefore, potential hydrological linkages between the surge and the lake merit further thought.

The southern region (Wedel Jarlsberg Land) elevation changes are rife with surges as well, complicating the interpretation in relation to climate. Recherchebreen surged in 1948 although a detectable signal is not apparent in the elevation change maps of Period I (Fig 4a). Reduced elevation changes are however seen with less ice loss at the front of the glacier than on neighboring glaciers and an accumulation area with slightly negative values implying that the glacier has not completely re-built to the pre-surge geometry. During Period II the frontal thinning rate is more negative and the confluence with Bjørnebreen shows slight increases. This suggests that the glacier may still be rebuilding up to its pre-surge surface geometry.

Since 1990, a major dynamical event seems to be associated with Amundsenisen, one that affects the adjacent Nornebreen and Høgstabreen (Fig 4a). During Period I, the dome of the Amundsenisen ice cap seems to have migrated northwards (Fig 4b) before spilling out through Høgstabreen during Period II, as inferred from the extreme decreases over Amundsenisen (Fig 4b) and associated increases over Høgstabreen (Fig. 4c). Additionally, large decreases over Nornebreen could be a result of the sudden elevation decrease over Amundsenisen. The events then explain the large variability seen in the Period II estimates (Table 4), although snowfall variation could also be a factor. In addition, a chaotic pattern of elevation decreases is apparent on Mulbacherbreen during Period II. This is either explained by the flight line which is situated close to the valley side or by a surge during Period II.

The Climatic signal

The previous discussion emphasizes the difficulty in relating elevation changes to past climate. The elevation change signal depends on the time period over which it is measured, as a

long time interval gives a low temporal resolution snapshot of the surface geometry changes. Short term dynamic events, such as a surge, can have a large effect on the surface geometry. Nonetheless, according to conservation of mass, the geodetic balance estimations from volume changes are independent of ice dynamics.

Of course, errors are larger for estimates of geodetic balances, especially over individual glaciers in northwest Svalbard as compared to the regional geodetic balances estimated in Chapter 3. The Period II geodetic balances for the northwest glaciers (except Midtre Lovenbreen) are underestimates of the actual balance as a single area was used in the estimation rather than an average of the area. In addition, assuming constant density (i.e. all elevation changes are the results of ice loss/gain rather than snow or firn) can influence the geodetic balance estimations. For the Period I changes, assuming constant density does not affect the geodetic balance calculation significantly due to the magnitude of the changes and the length of the time interval (54 years). During Period II, however, assuming constant density may not hold for the upper elevations, especially on Kongsvegen and Uversbreen. The upper elevations of these glaciers can be affected by short term precipitation variations, as well as variations in the rate of snow/firn densification.

For the four northwest Svalbard glaciers analyzed, a significant increase in the thinning rate is experienced between Period I and Period II. For the smaller glaciers, Midtre and Austre Lovenbreen, it is easy to relate this change directly to climate as almost no firn layer presently exists implying that water inputs into the glacier are diminishing where ice is basically downwasting, as the elevation change curves show (Fig. 3).

For Midtre Lovenbreen, traditional mass balance measurements exist since 1967. The mean annual net mass balance from 1967 to 1988 is estimated to be -0.41 m a^{-1} ice equivalent (Hagen and Liestøl, 1990). The annual geodetic balance from 1936 to 1990 is lower (-0.23 m a-1) suggesting that the mass balance was closer to equilibrium pre 1967. This is in agreement with a more extensive geodetic study of Midtre Lovenbreen which shows that the rate of glacier thinning has increased significantly since the 1960s (Kohler and others, submitted).

For Kongsvegen, the Period I changes are a typical reflection of quiescent phase build up of a surge-type glacier despite the fact that the volume change and annual geodetic balances are negative. During Period II, although elevation increases do occur in the upper altitudinal interior of the glacier (Fig 2), the hypsometrically weighted elevation change averages of the upper

regions is negative overall. The annual geodetic balance is 3.5 times more negative during Period II than Period I. This is inferred as a climatic signal of the glacier, although elevation losses in the accumulation area may be partly due to the general process of firn densification and/or firn loss rather than ice loss. If this is the case, the geodetic balances are in fact too negative. A concrete means of testing this is to model the density increase required to give the observed elevation changes. The magnitude of losses in the accumulation area (0.5 m a^{-1}) are rather large to be solely explained by densification.

For Uversbreen, both the elevation change curves (Fig 3) and geodetic balances (Table 2) are more negative during Period II than Period I, despite experiencing the surge-like event during Period II. It is seen that the center part of the glacier remains close to zero where the lower and upper regions experience ice losses. Granted that firn loss and the process of firn densification cannot be ruled out, it seems that the volume change and geodetic balance signal is dominated by climate, while the apparent surge adds low resolution noise into the signal. This glacier therefore suggests that surging may in fact be independent of the overall climatic signal seen through geodetic volume changes.

Despite the fact that the Period II geodetic balances are generally underestimated on three glaciers (due to the use of a single area from 1990/95), they are significantly more negative than the Period I estimates. The Period II geodetic balances of the two smaller glaciers are approximately double those of Period I. The larger Kongsvegen experiences a Period II geodetic balance 3.5 times more negative than Period I. This may suggest that the larger glaciers of Svalbard have a more extreme response to a changing climate than that of the smaller glaciers.

For southern Svalbard, thinning rates also increase since 1990 though large dynamical events affect the shorter time intervals since 1990. For these regions, geodetic balances were not able to be estimated as profiles are not spatially representative of the glaciers in the region. Nonetheless, a doubling in the unweighted average *dh/dt* estimates is experience between Period I and Period II and a 7 fold increase between Period I and Period III. Analysis of the entire profile from 1996 show that major dynamical events during Period II explain much of the variability in *dh/dt* estimates as compared to Period I and III. Nonetheless, it is difficult to interpret the variations due to the short time interval of only 6 years which could also be affected by precipitation variations. In addition, the comparison of the early spring surface (the 1996 profile)

with a late summer surface (1990 DEM) incorporates a systematic difference that should be accounted for.

Summary

In this chapter, modern elevation change estimates are compared to the baseline estimates of Chapter 3. For both northwest Svalbard and southern Svalbard, the glaciers are thinning (losing elevation) at a faster pace since 1990. In some instances, it is difficult to determine whether climate or dynamics is affecting the elevation change signal. It is thought that the dynamical events that occur within the time intervals have a small effect on the overall climatic signal of volume changes and associated geodetic balances. For northwest Svalbard, despite surges occurring on Kongsvegen and Uversbreen, the elevation change curves and geodetic balances since 1990 are much more negative than that of the earlier period. For southern Svalbard, unweighted average *dh/dt* estimates imply an increasing thinning rate since 1990 though, the different times of the data acquisition and the large scale variations in dynamics makes interpretation difficult. In summary, both the northwest and southern Svalbard glaciers are losing mass faster more recently, but upper altitudes show a complex signal that is difficult to attribute solely to climate due to the close coupling between glacial history, temperature, precipitation, ice fluxes, and firn densification.

"The change was well summed up in a declaration published after a meeting of scientists from the four great international global research programmes in 2001 which said:

> The earth system behaves as a single, self regulating system, comprised of physical, chemical, biological, and human components. The interactions and feedbacks between the component parts are complex and exhibit multi-scale temporal and spatial variability.

This indeed is Gaia."

From *The Revenge of Gaia* by James Lovelock

Chapter 5

Conclusions and future work

Glaciers and ice masses are very important components of the earth system both in terms of global water storage and as climate indicators. Land ice contains enough water to raise sea level 69 meters (Church and others, 2001). Although the majority of this water is tied up in Greenland and Antarctica, the smaller glaciers and ice caps have the potential to release the most water over the next century (Dyurgerov and Meier, 1997). Moreover, glaciers are a complex reflection of the present climate as the mass balance is a function of temperature and precipitation, and an elongated past climate in the form of glacier geometry and front positions. In this manner, glaciers can be thought of as a climatic memory of a particular location during a defined past.

Recent predictions from global climate models indicate warming temperatures linked to the rise of greenhouse gases in the next 100 years (ACIA report, 2005). The response of the earth system to climate change is, however, complicated by the coupling between air and sea temperature, ocean and atmospheric circulation patterns, sea and land ice extent, and many more (Houghton and others, 2001). Svalbard is a climatically sensitive area located at the distal end of the warm North Atlantic current responsible for redistributing global energy from the tropics to the arctic. Svalbard glaciers and ice masses may therefore experience a rapid response to a change in climate (Hagen and others, 2003a).

In this study, a significantly long time record of Svalbard glaciers is presented in the form of elevation and volume changes. Older topographic maps from 1936/38 are compared to the 1990 DEM to estimate 54 year volume changes from ~5000 km^2 of glaciers. The elevation change signal is dominated by significant frontal thinning with slight increases at higher altitudes. For all areas studied, volume losses are observed averaging ~1.59 ± 0.1 km^3a^{-1} ice with an average annual geodetic balance of -0.30 m a^{-1} w.eq. This generalized volume loss signal coincides with the step-like warming in Svalbard since the end of the Little Ice Age in the 1920s (Nordli and Kohler, 2003).

The glaciers and ice masses are divided into 7 geographically distinct regions. Significant regional variability exists within the annual geodetic balances (Chapter 3, Fig. 8) which is

attributed to the glacial hypsometry (area-altitude distribution) as well as common climatic weather patterns. The most negative balances occur in the south and the west coasts while the least negative is seen on the east coast and inlands.

Regional snow scale studies (Winther and others, 1998; Sand and others, 2003) indicate that the east coasts and southern regions of Spitsbergen receive the largest amounts of winter precipitation while northern and interior areas remain relatively dry. The largest frequency of winter and spring cyclones in the circum-arctic occurs within the Svalbard/Barents Regions (Serreze and Barry, 1988) and storms generally strike Svalbard from the east-southeast (Hagen and others, 1993; Humlum and others, 2003). Therefore, the presence of the least negative geodetic balance on the east coast (Heer Land) seems to be a result of the relatively high winter accumulation. This is in contrast to mass balances on the west coast of Svalbard which are best correlated to summer temperatures (Lefauconnier and Hagen, 1990; Lefauconnier and others, 1999).

The largest pattern of elevation increases is apparent on the east and south coasts. The glaciers of Heer Land, in particular, all show elevation increases at higher altitudes unless the glacier has surged in the recent past. Whether the elevation increase pattern is linked to increases in precipitation with time (Bamber and others, 2004; Bamber and others, 2005; Raper and others, 2005), or from a slowed dynamic response (Melvold and Hagen, 1998; Hagen and others, 2005) is not clear. In general, synoptic activity has increased significantly during the past 40 years (Serreze and others, 2000), which may be increasing snow deposition to the east coast. If this is the case, then, the ice flux of these glaciers on the east coast have not completely adjusted to the increased mass input.

In summary, during the 54 year time interval, the west and south coasts have the most negative mass balances, presumably due to the affect of the warm ocean currents that run along the west coast of Spitsbergen and warming temperatures. The east coast of Svalbard is showing less volume losses and larger elevation increases possibly linked to increases in arctic synoptic activity. The regional variability documented in long term geodetic balances suggests that climatic changes is not only increasing the mass loss, but also affecting the dynamics and ice fluxes of glaciers in Svalbard.

More recently, a modern elevation change interval was created by comparing differential GPS measurements and LIDAR altimetry profiles to the 1990 DEM. Although these change measurements contain higher precision and accuracy than the changes estimated from the older topographic maps, the assumptions involved with constant density and photographic timing have a larger influence due to the shorter time interval. Nonetheless, volume changes continue to be negative in this time interval for the northwest glaciers. The geodetic balances imply a doubling in the thinning rate for the smaller glaciers, and a more complicated response for the larger glaciers. Similarly, modern average *dh/dt* estimates in southern Svalbard show thinning rates 4-5 times that of the early period. Although not directly addressed in this study, the enhanced thinning rates is presumably linked to increased temperatures with the glacier fronts thinning more than 1 m a^{-1} more than that of the early estimates.

A major uncertainty in these estimates lies in the assumption of constant density in which elevation losses at upper altitudes are thought to consist entirely of ice. Research on the effects of firn densification in a changing climate is crucial in understanding elevation changes on glaciers and ice sheets. Studies indicate a large temperature dependency upon the densification rate of firn (i.e. Arthern and Wingham, 1998; Wingham, 2000; Zwally and Jun, 2002). The elevation losses at the top of Kongsvegen and Uversbreen could thus be related to firn loss and/or enhanced densification, which would result in geodetic balances for the most recent period being overestimated (i.e. too negative). Research aimed towards estimating firn layer variations is thus imperative to understand glacier changes in relation to climate. Ground penetrating radar (GPR) coupled with shallow ice coring could be useful in determining this component.

Elevation changes transferred into volume changes and geodetic balances present a complex signal that is both associated with climatic fluctuations and dynamical events. Sometimes, it is difficult to separate these components and care must be used when relating geodetic balances to climate. A prime example is that of Kongsvegen, which experienced a surge in 1948. The average annual elevation change rates from 1966 to 1995 reflect those of quiescent phase build up after the surge. Nonetheless, the surge seems to be a longwave component of the volume change signal where the larger influence reflected is that of climate, i.e. the geodetic balance is still negative despite quiescent phase build up. In addition, Uversbreen seemed to experience what looks like a mini-surge between 1990 and 2004 in which the upper altitudes decreased in elevation as much as the lower elevations, while the middle elevations remained

close to zero. Nonetheless, in comparing the elevation change curves from the older and more recent periods, a significant negative shift is apparent, which seems to be the overall climatic signal, despite the effect of a mini surge. Lastly, large variation is seen in the NASA profiles over Wedel Jarlsberg land between 1990 and 1996. Despite the fact that the 1990 surface is from summer, while the 1996 is from spring, and the time interval is only 6 years, the magnitude and pattern of the changes imply dynamical influences. These dynamical influences must be accounted for when interpreting glacier elevation changes into a climatic signal.

In summary, two general conclusions result from this thesis. First, a great wealth of information arises from documenting glacier elevation changes over a large spatial area, and over a long time interval. The difficulty arises when the estimated volume changes are to be related to climate as this requires assumptions of constant density and steady state dynamics. Modelling the surface changes within the time interval can reveal answers to whether these assumptions are valid. For Svalbard, some regional variability exists within the geodetic balances, which is attributed to climatic patterns that affect the east and west coasts differently. These patterns must be accounted for when relating mass balances to climate.

The second conclusion is that the glaciers of Svalbard are losing ice volume at a faster rate more recently which can be attributed to a changing climate. The large scale synoptic patterns in atmospheric and oceanic circulation, and possibly temporal changes associate with them, is leading to increased thinning at the glacier fronts and slight increases at higher altitudes. While the volume change signal is dominated by a climatic component, the dynamic component of the signal complicates the interpretation. Climate change is not only affecting glacier surface change in the form of temperature, but also in the form of precipitation. These changes progress through the glacier creating complicated dynamic patterns. Nonetheless, the present glacial-climate signal is that of increased volume loss.

References

Arctic Climate Impact Assessment (ACIA). 2005. Cambridge University Press, New York.

Andreassen, L.M. 1999. Comparing traditional mass balance measurements with long-term volume change extracted from topographical maps: a case study of Storbreen glacier in Jotunheimen, Norway, for the period 1940-1997. *Geografiska Annaler* **81A**, 467-476.

Andreassen, L.M., H. Elvehøy and B. Kjøllmoen. 2002. Using aerial photography to study glacier changes in Norway. *Annals of Glaciology* **34**, 343-348.

Arendt A.A., K.A. Echelmeyer, W.D. Harrison, C.S. Lingle, V.B. Valentine. 2002. Rapid wastage of Alaska glaciers and their contribution to rising sea level. *Science* **297,** 382-386.

Arthern R.J. and D.J. Wingham. 1998. The natural fluctuations of firn densification and their effect on the geodetic determination of ice sheet mass balance. *Climatic Change* **40**, 605 – 624.

Bamber J., W. Krabill, V. Raper, J. Dowdeswell. 2004. Anomalous recent growth of part of a large Arctic ice cap: Austfonna, Svalbard. *Geophysical Research Letters* **31**(12), doi: 10.1029/2004GL019667.

Bamber J., W. Krabill, V. Raper, J.A. Dowdeswell, J. Oerlemans. 2005. Elevation changes measured on Svalbard glaciers and ice caps from airborne LIDAR data. *Annals of Glaciology* **42**, 202 – 208.

Bader, H.1954. Sorge's Law of densification of snow on high polar glaciers. *Journal of Glaciology*, **2**(15), 319-323.

Björnsson, H., Y. Gjessing, S.E. Hamran, J.O. Hagen, O. Liestøl, F. Pálsson., B.Erlingsson. 1996. The thermal regime of sub-polar glaciers mapped by multi-frequency radio-echo soundings. *Journal of Glaciology* **42**(140), 23 – 32.

Björnsson, H. 1998. Hydrological characteristics of the drainage system beneath a surging glacier. *Nature* **395**, 771 – 774.

Cambell, James B. 2002. *Introduction to Remote Sensing, third edition.* London: The Guilford Press.

Church, J. A., J. M. Gregory, P. Huybrechts, M. Kuhn, K. Lambeck, M. T. Nhuan, D. Qin, and P. L. Woodworth. 2001. Changes in Sea-Level, in *IPCC Third Scientific Assessment of Climate Change*, edited by J. T. Houghton, Y. Ding, D. J. Griggs, M. Noguer, P. J. van der Linden, X. Dai, K. Maskell, and C. A. Johnson, pp. 639–694, Cambridge University Press, Cambridge.

Cox, L.H. and R.S. March. 2004. Comparison of geodetic and glaciological mass-balance techniques, Gulkana Glacier, Alaska, U.S.A. *Journal of Glaciology* **50**(170), 363 – 370.

Davis C.D. 2002. *Statistics and Data Analysis in Geology*. 3rd Ed. New York: John Wiley and Sons.

Davis C.H., C.A. Kluever, B. Haines. 1998. Elevation Change of the Southern Greenland Ice Sheet. *Science* **279**, 2086.

Dowdeswell J.A., R. Hodgkins, A.M. Nuttall, J.O. Hagen, G. Hamilton. 1995. Mass balance change as a control on the frequency and occurrence of glacier surges in Svalbard, Norwegian High Arctic. *Geophysical Research Letters* **22**(21), 2909 – 2912.

Dowdeswell J.A. and 10 others, 1997. The mass balance of circum-arctic glaciers and recent climate change. *Quaternary Research* **48**, 1-14.

Dyurgerov, M. B., and Meier, M. F., 1997a: Mass balance of mountain and subpolar glaciers: a new global assessment for 1961–1990. *Arctic and Alpine Research* **29**, 379–391.

Dyurgerov, M. B., and Meier, M. F., 1997b: Year-to-year fluctuations of global mass balance of small glaciers and their contribution to sea-level change. *Arctic and Alpine Research* **29**, 392–402.

Echelmeyer and 8 others. 1996. Airborne surface profiling of glaciers: a case-study in Alaska. *Journal of Glaciology* **42**(142), 538-547.

Eiken, T., J.O. Hagen, K. Melvold. 1997. Kinematic GPS survey of geometry changes on Svalbard glaciers. *Annals of Glaciology* **24**, 157 – 163.

Elseberg D.H., W.D. Harrison, K.A. Echelmeyer, R.M. Krimmel. 2001. Quantifying the effects of climate and surface change on glacier mass balance. *Journal of Glaciology* **47**(159), 649-658.

Etzelmüller B., G. Vatne., R.S. Ødegård., J.L. Sollid. 1993. Mass balance and changes of surface slope, crevasse and flow pattern of Erikbreen, northern Spitsbergen: an application of a geographical information system. *Polar Research* **12**(2), 131 – 146.

Finsterwalder, R. 1954. Photogrammetry and glacier research with special reference to glacier retreat in the eastern Alps. *Journal of Glaciology* **2**(15), 306-314.

Fountain A.G. and A. Vecchia. 1999. How many stakes are required to measure the mass balance of a glacier? *Geographiska Annalar* **81A**(4), 563 – 572.

Haakensen, N. 1986. Glacier mapping to confirm results from mass-balance measurements. *Annals of Glaciology* **8**, 73 – 77.

Hagen J.O. and O. Liestøl. 1990. Long-term glacier mass-balance investigations in Svalbard, 1950 – 1988. *Annals of Glaciology* **14**, 102 – 106.

Hagen J.O., O. Liestøl, E. Roland, T. Jørgensen. 1993. Glacier atlas of Svalbard and Jan Mayen. Norwegian Polar Institute, Meddelelser Nr. 129. Oslo.

Hagen J.O., K. Melvold, T. Eiken., E. Isaksson, B. Lefauconnier. 1999. Mass balance methods on Kongsvegen, Svalbard. *Geografiska Annalar* **81A**(4), 593 – 601.

Hagen J.O., K. Melvold, F. Pinglot, J.A. Dowdeswell. 2003a. On the net mass balance of the glaciers and ice caps in Svalbard, Norwegian Arctic. *Arctic, Antarctic, and Alpine Research*, **35**(2), 264-270.

Hagen J.O., J. Kohler, K. Melvold, and J.G Winther. 2003b. Glaciers in Svalbard: mass balance, runoff, and freshwater flux. *Polar Research* **22**(2), 145-159.

Hagen J.O. and N. Reeh. 2004. *In situ* measurement techniques: land ice. *In* Mass Balance of the Cryoshpere. Cambridge University Press, New York.

Hagen, J.O., T. Eiken, J. Kohler, K. Melvold, 2005. Geometry changes on Svalbard glaciers: mass-balance or dynamic response? *Annals of Glaciology* **42**, 255 – 261.

Hamilton G. and J.A. Dowdeswell. 1996. Controls on glacier surging in Svalbard. *Journal of Glaciology* **42**(140), 157 – 168.

Harrison, W.D., D.H. Elsberg, K.A. Echelmeyer, R.M. Krimmel. 2001. On the characterization of glacier response by a single time-scale. *Journal of Glaciology* **47**(159), 659 – 664.

Houghton J. T., Y. Ding, D. J. Griggs, M. Noguer, P. J. van der Linden, X. Dai, K. Maskell, C.A. Johnson (eds). 2001. *Climate Change 2001. the scientific basis. Contribution of Working Group I on the third assessment report of the Intergovernmental Panel on Climate Change.* Cambridge University Press, Cambridge.

Humlum, O. 2002. Modelling late 20th-century precipitation in Nordenskiöld Land, Svalbard, by geomorphic means. *Norsk Geografisk Tidsskrift* **56**, 96-103.

Humlum O, A. Instanes, J.L. Sollid. 2003. Permafrost in Svalbard: a review of research history, climatic background and engineering challenges. *Polar Research* **22**(2), 191 – 215.

Hutchinson, M.F. 1989. A new procedure for gridding elevation and stream line data with automatic removal of spurious pits. *Journal of Hydrology* **106**, 211-232.

James, T.D., Murray, T., Barrand, N.E., Barr, S.L. 2006. Extracting photogrammetric ground control from Lidar DEMs for change detection. *The Photogrammetric Record* **21**(116), 1-17.

Jansson, P. 1999. Effect of uncertainties in measured variables on the calculated mass balance of Storglaciären. *Geografiska Annalar* **81A**(4), 633 – 642.

Jiskoot H., P. Boyle, T. Murray. 1998. The incidence of glacier surging in Svalbard: evidence from multivariate statistics. *Computers and Geosciences* **24**(4), 387 – 399.

Jiskoot H., T. Murray, P. Boyle. 2000. Controls on the distribution of surge-type glaciers in Svalbard. *Journal of Glaciology* **46**(154), 412 – 422.

Johannesson, T., Raymond, C.F., Waddington, E. 1989. Time-scale for adjustment of glaciers to changes in mass-balance. *Journal of Glaciology* **35**, 355-369.

Kamb, B. 1987. Glacier surge mechanism based on linked-cavity configuration of the basal water conduit system. *Journal of Geophysical Research* **92**(B9), 9083 – 9100.

Kleinbaum, D.G., L.L. Kupper, K.E. Muller, A. Nizam. 1998. *Applied regression analysis and other multivariate methods.* 3rd ed. London, Brooks/Cole Publishing co.

Kohler, J., T. James, T. Murray, C. Nuth, O. Brandt, N. Barrand, H.F. Aas, A. Luckman. Recent acceleration of sea level contribution from glaciers on Svalbard. Submitted to *Geophysical Research Letters.*

Krabill and 8 others. 1999. Rapid thinning of parts of the southern Greenland ice sheet. *Science* **283**, 1522 – 1524.

Krabill and 9 others. 2000. Greenland ice sheet: high-elevation balance and peripheral thinning. *Science* **289**, 428 – 430.

Krimmel, R.M. 1989. Mass balance and volume of South Cascade Glacier, Washington 1958-1985. *In* Glacier Fluctuations and climatic Change. J. Oerlemans (ed.), 193 – 206.

Krimmel, R.M. 1999. Analysis of difference between direct and geodetic mass balance measurements at South Cascade Glacier, Washington. *Geografiska Annalar* **81A**, 653 – 658.

Lefauconnier B. and J.O. Hagen. 1990. Glaciers and climate in Svalbard: statistical analysis and reconstruction of the Brøggerbreen mass balance for the last 77 years. *Annals of Glaciology* **14**, 148 – 152.

Lefauconnier B. and J.O. Hagen. 1991. Surging and calving glaciers in eastern Svalbard. *Norsk Polarinstitutt Meddelelser*, 116.

Lefauconnier B., J.O. Hagen, J.B. Ørbæk, K. Melvold, and E. Isaksson. 1999. Glacier balance trends in the Kongsfjorden area, western Spitsbergen, Svalbard, in relation to the climate. *Polar Research* **18**(2), 307 – 313.

Liestøl, O. 1988. The glaciers of the Kongsfjord area, Svalbard. *Norsk geog. Tidsskr.* **42**, 231-238.

Liestøl, O., 1977. Setevatnet, a glacier dammed lake in Spitsbergen. Norsk Polarinstitutt, *Årbok.*

Lliboutry, L. 1974. Multivariate statistical analysis of glacier annual balances. *Journal of Glaciology* **13**(69), 371 – 392.

Melvold, K. and J.O. Hagen. 1998. Evolution of a surge-type glacier in its quiescent phase: Kongsvegen, Spitsbergen, 1964-95. *Journal of Glaciology* **44**(147), 394 – 404.

Murray T., J.A. Dowdeswell, D. Drewry, I. Frearson. 1998. Geometric evolution and ice dynamics during a surge of Bakaninbreen, Svalbard. *Journal of Glaciology* **44**(147), 263-272.

Murray T., A. Luckman, T. Strozzi, A.M. Nuttall. 2003. The initiation of glacier surging at Fridjovbreen. *Annals of Glaciology* **36**, 110-116.

Murray T., T. Strozzi, A. Luckman, H. Jiskoot, P. Christakos. 2003. Is there a single surge mechanism? Contrasts in dynamics between glacier surges in Svalbard and other regions. *Journal of Geophysical Research* **108**(B5), 2237, doi:10.1029/2002JB001906.

Nordli, P.Ø. and J. Kohler. 2003. The early 20th century warming. Daily observations at Green Harbour, Grønfjorden, Svalbard. *Rapport Klima* 12, 20 p.

Oerlemans J., and N.C. Hoogendoorn. 1989. Mass-balance gradients and climatic change. *Journal of Glaciology* **35**(121), 399 – 405.

Østrem G. 1986. Repeated glacier mapping for hydrological purposes: water power planning. *Annals of Glaciology* **8**, 135 – 140.

Østrem G., and M. Brugman. 1991. Glacier mass-balance measurements: a manual for field and office work. *NHRI Science Report* No. 4. Environment Canada.

Østrem G., and N. Haakensen. 1999. Map comparison of traditional mass-balance measurements: Which method is better? *Geografiska Annaler* **81A**, 703-711.

Paterson W.S.B. 1994. *The physics of glaciers. Third Edition.* Oxford, etc. Elsevier.

Paterson W.S.B. and N. Reeh. 2001. Thinning of the ice sheet in northwest Greenland over the past forty years. *Nature* **14**, 60-61.

Pinglot J.F., M. Pourchet, B. Lefauconnier, J.O. Hagen, E. Isaksson, R. Vaikmäe, K. Kamiyama. 1999. Accumulation in Svalbard glaciers deduced from ice cores with nuclear tests and Chernobyl reference layers. *Polar Research* **18**(2), 315 – 321.

Pinglot J.F., J.O. Hagen, K. Melvold, T. Eiken, C. Vincent. 2001. A mean net accumulation pattern derived from radioactive layers and radar soundings on Austfonna, Nordaustlandet, Svalbard. *Journal of Glaciology* **47**(159), 555 – 566.

Pinglot J.F. and 13 others. 2003. Ice cores from Arctic sub-polar glaciers: chronology and post-depositional processes deduced from radioactivity measurements. *Journal of Glaciology* **49**(164), 149 – 158.

Raper V., Bamber J, and Krabill W. 2006. Interpretation of the anomalous growth of Austfonna, Svalbard, a large Arctic ice cap. *Annals of Glaciology*. **42.**

Rasmussen, L. A. 2004. Altitude variation of glacier mass balance in Scandinavia. *Geophysical Research Letters*. vol. 31, L13401 doi:10.1029/2004GL020273

Rasmussen, L. A. and L. M. Andreassen. 2005. Seasonal mass balance gradients in Norway. *Journal of Glaciology*. **51**(175), 601 – 606.

Rolstad, C., J. Amlien, J.O. Hagen, B. Lundén. 1997. Visible and near infrared digital images for determination of ice velocities and surface elevation during a surge on Osbornebreen, a tidewater glacier in Svalbard. *Annals of Glaciology* **24**, 255 – 261.

Sand K., J.G. Winther, D Maréchal, O. Bruland, K. Melvold. 2003. Regional variations of snow accumulation on Spitsbergen, Svalbard, 1997-99. *Nordic Hydrology* **32**(1/2), 17 – 32.

Sapiano, J.J., W.D.Harrison, K.A. Echelmeyer. 1998. Elevation, volume and terminus changes of nine glaciers in North America. *Journal of Glaciology* **44**(146), 119-135.

Serreze M.C., and R.G. Barry. 1988. Synoptic activity in the arctic basin, 1979-85. *Journal of Climate* **1**, 1276 – 1295.

Serreze M.C., J.E. Box, R.G. Barry, J.E. Walsh. 1993. Characteristics of Arctic synoptic activity, 1952-1989. *Meteorology and atmostpheric physics* **51**, 147 – 164.

Serreze M.C. J.E. Walsh, F.S. Chapin III, T. Osterkamp, M. Dyurgerov, V. Romanovsky, W.C. Oechel, J. Morison, T. Zhang, R.G. Barry. 2000. Observational evidence of recent change in the northern high-latitude environment. *Climatic Change* **46**, 159 – 207.

Svalbard Topographic Map Series: C10 Braganzavågen. 2006. 1:100 000. Tromsø, Norsk Polarinstitutt.

Tobler, W. R. 1970. A computer model simulation of urban growth in the Detroit region. *Economic Geography*, **46**(2), 234-240.

Wingham, D.J. 2000. Small fluctuations in the density and thickness of a dry firn column. *Journal of Glaciology* **46**(154), 399 – 411.

Winther J-G., O. Bruland, K. Sand, Å Killingtveit., Maréchal D. 1998. Snow accumulation distribution on Spitsbergen, Svalbard, in 1997. *Polar Research* **17**, 155-164.

Wolf, Paul R. 1983. *Elements of photogrammetry.* London: McGraw-Hill, Inc.

Zwally H.J. and L. Jun. 2002. Seasonal and interannual variations of firn densification and ice-sheet surface elevation at the Greenland summit. *Journal of Glaciology* **48**(161), 199 – 207.

Appendix

A.1: Geodetic Transformation

The first step in comparing two maps is to determine whether the geographic reference systems, that is, the datums and projection are the same for both maps. A geographical reference system is a three dimensional surface, or model, that defines the earth surface and is comprised of three components, an angular unit of measure, a meridian and a datum, all of which define how the spherical model is positioned relative to the center of earth. Pre-1960 reference systems and datums were generally localized in order to best represent the earth surface in that particular area. After 1960, with increased importance of space exploration and remote sensing, a need for a global reference system arose. This led to the creation of the World Geodetic System (WGS), a fixed global reference system that was first implemented in 1960 and was later updated in 1964, 1972, and 1984. Today, all navigation systems, including the Global Positioning System (GPS), operate within WGS84 reference system. A map projection is the mathematical transformation required to portray a curved earth surface as a flat map. The World Geodetic system utilizes the Universal Transverse Mercator (UTM) map projection, a cylindrical projection that is divided into 60 northern and southern zones of 6° longitude each. The benefit of the system is that the cylinder for each of the 60 zones has a scale error not exceeding 0.1 percent and thus edge distortions are minimized.

The 1936/38 topographic map series of Svalbard (Norsk Polarinstitutt) is referenced in the European Datum 1950 datum within the UTM zone 33 north projection. The 1990 Digital Elevation Model (DEM) is referenced with the modern WGS83 datum within the UTM zone 33 north projection. Thus, the older topographic map series must be converted so that the maps are comparable for elevation change studies.

The best geodetic reference system transformation is a local transformation function that is specifically designed for Svalbard. ESRI ArcGIS© provides global transformations for a number of different datums and projections, with the procedure based upon a 7 parameter function. This transformation is derived from ground control points located over mainland Europe, and thus may contain larger variability when performed on Svalbard.

A local transformation has been created (although not yet published) for Svalbard using 49 ground control points and a 3 parameter function, such that the transformation varies spatially by Northing and Easting (J. Kohler, unpublished). The residuals between the actual coordinates and those derived from this transformation for the 49 control points had

approximately normal distributions centered around zero with standard deviations of 3.141 and 4.044 for Northing and Easting, respectively.

The same control points were transformed from the European Datum coordinates to WGS84 using the ©Esri ArcGIS 7 parameter global transformation. Both residual distributions are approximately normal, although the mean difference for northing and easting is -2.05 and 8.22 meters, respectively. The standard deviations for these distributions are 4.30 and 4.65 for northing and easting respectively. The ArcGIS transformation therefore introduces a slight bias on Svalbard with offsets of 2 meters to the north and 8 meters to the west. As expected, the global transformation is not as accurate as the local transformation, although the variance of the residuals is not much larger than those from the local transformation (Kohler, unpublished manuscript). Nonetheless, the accuracy of the transformation is within the limits of precision for the older topographic maps. In addition, the accuracy is also within the limits of the 1990 DEM pixel resolution. Therefore, the global conversion provided by Esri ArcGIS is sufficient enough for this study.

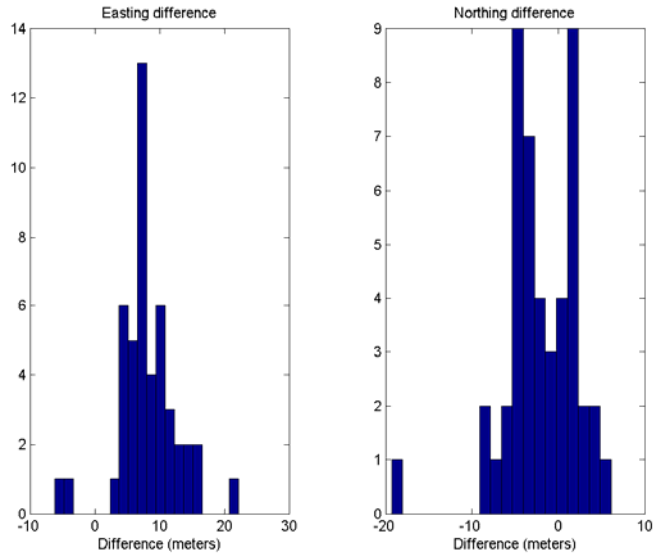

Fig 1: Histograms of the northing and easting residuals. The residuals are the differences between actual ground control coordinates and the transformed ED50-WGS84 coordinates.

Table 1. List of ground control points on Svalbard with the Europeand Datum 1950, actual WGS84, and the transformed WGS84 coordinates along with the residuals between actual and transformed coordinates.

STATION	*ED50 Northing*	*ED50 Easting*	*GCP WGS84-33N Northing*	*GCP WGS84-33N Easting*	*Global WGS84-33N Northing*	*Global WGS84-33N Easting*	*Global WGS84-33N Elevation*	*Residual-Northing*	*Residual-Easting*
Barlaupen	8615928	547018	8615729	546945	8615725	546936	690	9	4
Biskayarhuken	8864925	448713	8864713	448642	8864721	448631	72	10	-8
Bjørnesholmen	8785194	523259	8784986	523187	8784990	523176	51	11	-4
Belcherfjellet	8574437	559330	8574238	559254	8574233	559248	393	7	4
Bohemannflya	8703779	492584	8703578	492507	8703576	492502	97	5	2
Braastadskaret	8532902	766191	8532702	766102	8532699	766108	35	-6	2
Brentskardhaugen	8678768	543878	8678564	543802	8678564	543795	504	7	0
Brimulen	8685211	631947	8685004	631868	8685007	631864	18	4	-3
Centralen	8737838	464370	8737628	464303	8737634	464288	1064	15	-6
Danskøya	8853756	419482	8853544	419411	8853552	419400	111	11	-8
Exilfjellet	8762594	468564	8762386	468488	8762391	468482	1104	6	-5
Fjordnibba	8699749	544588	8699545	544514	8699545	544506	309	8	0
Fosterøyane	8837204	586818	8836996	586747	8837000	586736	117	11	-4
Framslengja	8719512	616064	8719306	615987	8719309	615982	228	5	-3
Gråhuken	8858150	489385	8857941	489311	8857946	489303	38	8	-5
Halvmåneøya	8590919	697437	8590713	697358	8590716	697354	30	5	-3
Hedgehogfjellet	8544070	556612	8543873	556536	8543867	556530	626	6	6
Crozierpynten	8873375	536294	8873167	536222	8873171	536212	62	10	-4
Isispynten	8871788	731593	8871583	731532	8871584	731510	33	22	-1
Kapp Amsterdam	8643487	538871	8643286	538796	8643283	538788	60	7	2
Kapp Koburg	8792405	779622	8792197	779549	8792201	779538	27	11	-4
Kapp Linnè	8666044	467904	8665842	467827	8665841	467822	40	5	1
Kapp Martin	8627668	474967	8627465	474891	8627464	474885	40	7	1
Kapp Mitra	8784695	424392	8784485	424319	8784491	424310	41	9	-6
Kiepertøya	8776483	641213	8776276	641146	8776279	641130	59	16	-3
Kinnvika	8889253	561998	8889044	561925	8889049	561916	35	10	-5
Svarthøgda	8752226	408241	8752019	408168	8752023	408160	139	8	-3
Kofoedodden	8508193	759763	8507987	759695	8507990	759680	32	15	-3
Kræmerpynten	8962691	844940	8962483	844867	8962485	844851	32	16	-3
Longyearbyen-hangar	8686185	511199	8685983	511123	8685981	511117	64	7	1
Lykta Sør	8745749	510364	8745549	510292	8745545	510282	458	10	3
Ny-Ålesund	8763800	434264	8763592	434190	8763596	434182	48	8	-4
Poolepynten	8710091	430627	8709886	430553	8709888	430545	38	8	-2
Velkomstvarden	8863937	476379	8863728	476305	8863733	476297	128	8	-5
Revnosa	8665067	586775	8664865	586697	8664864	586692	44	5	2
Salpynten	8684310	434538	8684107	434462	8684107	434456	57	7	0
Sarstangen	8742007	422918	8741801	422844	8741804	422836	38	8	-3
Slettebu	8606762	508182	8606561	508103	8606559	508100	36	3	2
Sørkappøya	8489349	540034	8489145	539965	8489146	539951	43	13	-1
Storøya	8919117	746189	8918893	746117	8918912	746105	33	12	-19
Teistberget	8702254	590049	8702049	589980	8702051	589967	456	13	-2
Thorkelsenfjellet	8714422	443212	8714217	443137	8714218	443130	451	7	-1
Vermlandryggen	8686568	474742	8686366	474664	8686364	474660	398	5	1
Vesuvaksla	8668685	497523	8668483	497447	8668481	497441	415	6	1
Wagnerfjellet	8786627	484217	8786414	484143	8786423	484135	1123	8	-9
Waly Hetmaskiefjellet	8586906	528090	8586705	528004	8586703	528008	590	-4	1
Annekammen	8746231	456693	8746023	456619	8746027	456611	665	8	-4

A.2: Methods of Estimating Geodetic Volume Changes

Two approaches to estimating glacier volume change from maps and elevation data was presented in Section 1. The *hypsometric* method estimates volume changes (*dV*) by multiplying the average elevation changes (*dz*) by the area (*A*) for each elevation bin (*i*) and subsequent summation over the glacier surface:

$$dV = \sum_i dz_i \cdot A_i$$

dz can either be determined by transforming area changes from old contours (Finsterwalder, 1954), or by averaging elevation change points or pixels over the glacier hypsometry (Arendt and others, 2002). This method, used in Arendt and others (2002) for estimating *dz*, also served as a means for regional spatial extrapolation over Alaska glaciers.

The *grid* method uses gridded digital elevation models (DEMs) to derive a pixel grid of elevation change estimates (Haakensen, 1986; Krimmel, 1989; Etzmuller, 1993). The volume change is derived by summing up the elevation change pixels (h_{i1}-h_{i2}) and multiplying by the pixel resolution (l_p^2):

$$dV = l_p^{\,2} \sum_A (h_{i1} - h_{i2})$$

The grid method has the advantage of containing an even spatial distribution, although DEMs created from old maps may contain artifacts produced by the interpolation procedures.

To compare the methods, all points and pixels that contain viewshed values below 2 are removed and thus the areas are smaller than the total areas in Section 2. Therefore, volume changes (in Fig 1 and Table 1.) are also smaller than those presented in chapter 3. The hypsometric means are derived through two approaches. The first averages the vertices of contour points over the glacier surface (filtered by viewshed below 2). The basis for using vertex points is that they are the original digitizations from contour maps, and inherently contain the resolution of the digitization. Second, points are extracted from contours at a defined distance interval of 100 meters.

The gridding procedure for the elevation change points is an interative finite difference interpolation technique that optimizes contour and spatially sparse elevation data. The technique is a multiresolution interpolation that begins with coarser rasters working down

towards finer resolutions (Hutchinson, 1989). All glacier points are used in the interpolation scheme including those of a low viewshed as they function as boundary conditions for the interpolator. Pixels where the viewshed parameter is below 2 were removed after the interpolation so that the same area is used from which the hypsometric averages represent.

Fig 1: Volume changes as estimated from the hypsometric and grid methods.

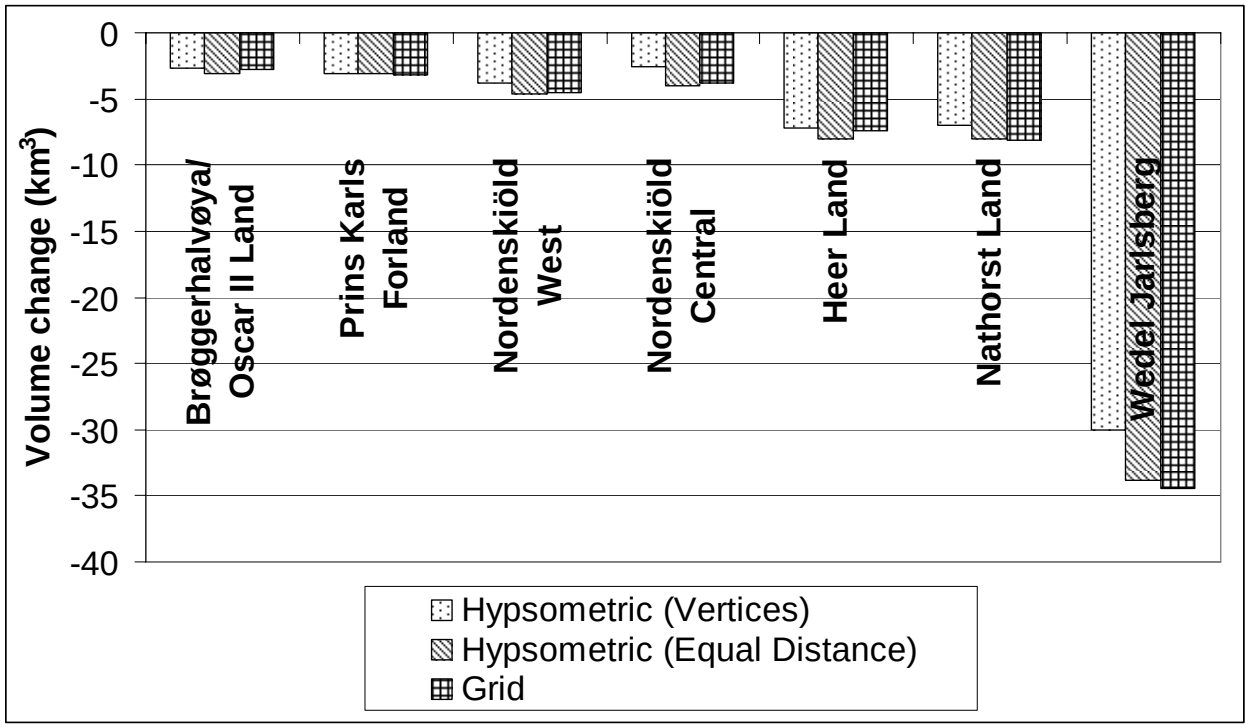

Table 1: Volume changes estimated from the hypsometric and grid methods for the 7 regions

Regions	***Hypsometric Volume Change (vertices)***	***Hypsometric Volume Change (equal distance points 100m)***	***Grid Volume Change***
Brøggerhalvøya/Oscar II Land	-2.62	-3.07	-2.75
Prins Karls Forland	-3.13	-3.07	-3.23
Nordenskiöld West	-3.85	-4.61	-4.57
Nordenskiöld Central	-2.59	-4.01	-3.78
Heer Land	-7.19	-8.05	-7.45
Nathorst Land	-7.03	-7.99	-8.13
Wedel Jarlsberg	-30.01	-33.84	-34.48
Total	**-56.42**	**-64.65**	**-64.40**

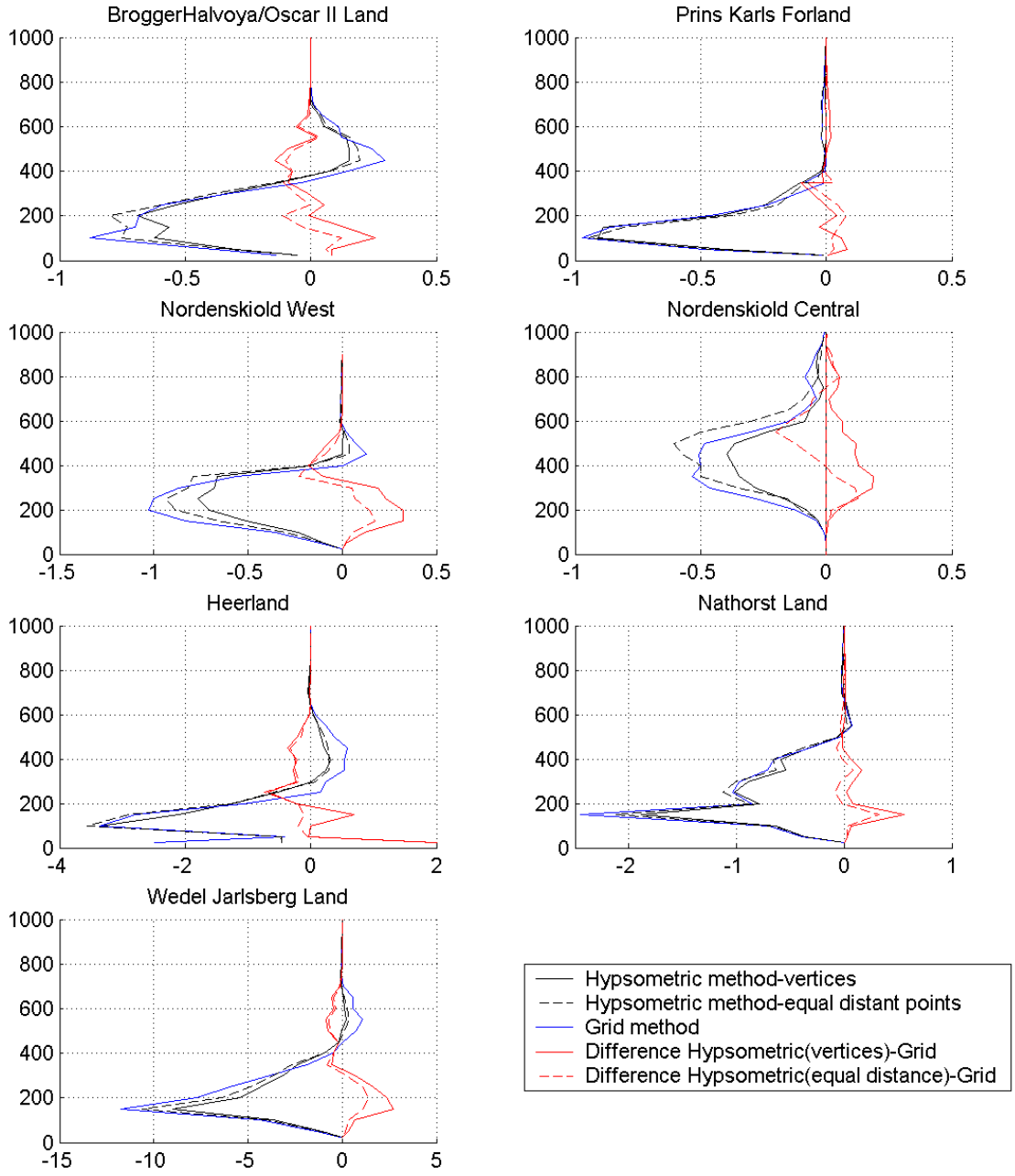

Fig 2: Volume change (x-axis) by elevation (y-axis) and the differences between the two methods for the 7 regions.

Fig 1 and Table 1 display the volume changes as estimated by the various methods. The hypsometric method with vertices underestimates volume changes by 3-31% as compared to the grid method. The volume change as derived from the hypsometric method with equal distance points varies from the grid method by -2 and 11%. The variations in volume change estimates is explained either by unrepresentative average elevation changes for the

hypsometric method or by errors introduced through interpolation. To better understand the variations, volume changes by elevation for each method are presented in Fig 2. For most regions, a trend is inherent where the hypsometric method underestimates both the losses and the gains (i.e. the averages by elevation are pulled closer to 0). It is clear, however, that the hypsometric method using equal distance points provides volume change estimates closer to the grid method. This demonstrates that volume changes derived by the hypsometric method are quite sensitive to the distribution of points along a contour.

It is not reasonable that the grid method would create this systematic trend as a grid inherently places equal area weights over the glacier surface. The grid method, however, introduces data through spatial interpolation. The fact that different interpolators reproduce the same systematic trends in Fig 2 implies that the interpolation is not introducing significant errors. The explanation thus lies behind the representativeness of the contour vertices for each elevation band. Elevation change points closer to the glacier edge experience smaller elevation changes than those at the center of the glacier due to the area loss, especially at the fronts, where 1936 glacier points are located over non-glacier areas in 1990. The elevation differences of these points are inherently smaller than those in the center since ice melted down to bedrock, similar to what occurs at the front of a retreating glacier.

To test this edge effect on the hypsometric averages from contour vertices, points located a distance of 50, 100, and 200 meters were removed, and volume changes estimated. In addition, volume change is estimated through a hypsometric approach using elevation change averages from the equal distance contour points as well as from pixels. Table 2 shows the volume change estimates through these different approaches over the area used in chapter 3. Subsequently, extrapolation is performed over the areas where viewshed is below 2 (unlike the volume changes in Fig 1 and Table 1). The pixel averages for all regions are more negative than using all contour points (as in the grid approach). By filtering points located closer to the glacier edges, the subsequent volume changes become more negative. This results from the fact that the changes along the center of the glacier are larger than those towards the edge. It is also apparent that each region reaches a volume change equivalent to the pixel averages through filtering by different distances (i.e Brøggerhalvøya/Oscar II Land require approximately a distance threshold of 200 meters while Nordenskiold central require just 50 meters). The large variation in the volume changes from filtering express the sensitivity of the hypsometric averages to points located close to the edge. Lastly, the volume changes estimated from the equal distance contour points is more similar to the volume changes through pixel averaging.

Table 2: Volume changes (in km^3) estimated from all contour vertices, the filtered vertices, equal distance contour points, and pixel averages.

Region	Original Vertex pts	50 meter filtered	100 meter filtered	200 meter filtered	Equal Distance pts	Pixel averages
Brøggerhalvøya/ Oscar II Land	-3.23	-3.25	-3.50	-3.86	-3.77	-3.91
Prins Karls forland	-2.80	-3.25	-3.41	-3.63	-3.09	-3.23
Nordenskiold West	-4.18	-5.69	-6.33	-6.85	-4.99	-4.88
Nordenskiold Central	-3.98	-5.83	-6.93	-8.11	-4.91	-5.75
Heerland	-8.82	-9.55	-9.47	-9.19	-9.90	-9.46
Nathorst Land	-10.03	-12.53	-13.97	-15.61	-11.49	-11.68
Wedel Jarlsberg Land	-40.31	-46.57	-48.05	-48.96	-45.60	-47.12
Total	**-73.35**	**-86.67**	**-91.66**	**-96.21**	**-83.75**	**-86.03**

The results of this analysis emphasize the importance of representativeness in estimating glacier volume changes through hypsometric averaging. It is not correct to remove data points close to the glacier edges as these points are actual data. A proper weighting scheme can be devised either by using the length of contour segment lengths as weights or creating points at a defined distance interval. Using contour segment lengths as a weight would not solve the problem completely as the segment lengths do not reflect the glacier area but rather the resolution that they were digitized in. Volume changes from equal distance contour points are more similar to the grid method, but still show slight variation.

Nonetheless, we chose to use pixel averages from the interpolated difference points because the interpolation technique incorporates an equal weighting scheme in the average and uses points close to the glacier edge. The coherency between the volume changes as estimated from equal distance points and pixel averages imply the accuracy of using pixel averages. The one disadvantage is the effect of the interpolation procedure and subsequent creation of data. Andreassen and others (1999) similarly determined that accuracy of volume change estimates through a grid approach is largely independent of the interpolation procedure used. Pixel averages from the interpolation routine, although creating data between contour lines, is more advantageous than using contour points as the effect of spatial representativeness is more important in the hypsometric method than the effect of creating data through interpolation.

A.3: Volume change sensitivity to low contrast in upper glacier areas

Low contrast in upper glacier areas is one of the biggest concerns in using older topographic maps to analyze glacier elevation changes. The low contrasting regions can lead to systematic errors in the accumulation area depending upon the height of the snow line when the photographs were taken. Arendt and others (2002) tested the sensitivity to volume change estimates from the affect, labeled as "floating" contours. In the analysis, the older map contours located 200 meters above the ELA were lowered by 15 meters. The results were that floating contours led to an overestimation of the volume loss (Arendt and others, 2002).

In this analysis, contours located above a hypothetical ELA determined from the original elevation change curveswere lowered and raised by 10 meters where the affect upon the total volume change quantified. The results (Table 1 & 2) indicate that a systematic bias in either direction leads to a 13% difference in the total volume change estimated. If the contours were indeed floating, the volume loss was overestimated, and vice versa if contours were too low.

Table 1: Assessment of floating contours; 1936 contours lowered by 10 meters above ELA.

Regions	ELA	Volume change		Difference
		Original	Adj for floating contours	
Brøggerhalvøya/OscarII Land	450	-3.23	-4.61	-1.38
Prins karls Forland	600	-2.8	-2.87	-0.07
Nordenskiold West	500	-4.18	-4.67	-0.49
Nordenskiold Central	700	-3.98	-4.94	-0.96
Heerland	400	-8.81	-11.746	-2.936
Nathorst	550	-10.025	-11.932	-1.907
Wedel Jarlsberg Land	550	-40.312	-44.438	-4.126
Total		**-73.337**	**-85.206**	**-11.869**

Table 2: Assessment of floating contours: 1936 contours raised by 10 meters above ELA.

Regions	ELA	Volume change		Difference
		Original	Adj for floating contours	
Brøggerhalvøya/OscarII Land	450	-3.23	-1.84	1.39
Prins karls Forland	600	-2.8	-2.74	0.06
Nordenskiold West	500	-4.18	-3.69	0.49
Nordenskiold Central	700	-3.98	-3.01	0.97
Heerland	400	-8.81	-5.89	2.92
Nathorst	550	-10.025	-8.12	1.905
Wedel Jarlsberg Land	550	-40.312	-36.19	4.122
Total		**-73.337**	**-61.48**	**11.857**

Acknowledgements

This entire journey began simply with an email that fell into the right hands. Somehow, I convinced Dr. Jack Kohler (my present supervisor) to meet me for the first time at Oslo Central Stasjon for a cup of coffee in 2004. Jack took a chance, brought me to the Norwegian Polar Institute in Tromsø, and provided a great idea and fantastic opportunity that turned into this Thesis and so much more. With almost no experience in glaciology, I was intrigued by his idea and took on the project in full swing. I cannot thank him enough for the experience and knowledge I have gained during this period.

I spent most of the time with my second supervisor, Dr. Jon Ove Hagen, in the field on numerous far-fetched journeys. On my first field season, he dragged me out to a nunatak overlooking Uversbreen to eat lunch on a fantastic day before snow probing crevasses and finding buried ice. On the next field season, I was lucky enough to accompany him to Hornsund in southern Svalbard to visit the Poles who run a fantastic station, and whom I must thank incredibly for their wonderful hospitality. It was a great 'geotourism tour' with Jon Ove, especially when traversing half of Svalbard only to fall through sea ice 5 km from Svea. I regret we did not get a picture of that situation, as it did look funny. I thank him for those great learning experiences and fruitful advice throughout this period.

I also must thank my colleagues at the Norwegian Polar Institute; Dr. Elisabeth Isaksson for providing great working experiences and opportunities; Ola Brandt for being a great mentor, both in the field, the lab, and so much more; Andrea Taurisano and Harald Faste Aas for giving great advice throughout the project.

Lastly, I would just like to thank my family for always being supportive and helping along the way. I also thank my friends, in Oslo and Tromsø, and special thanks to Dierk and Ann-Live for being so close and supportive through the end of this journey.